

Study on fatigue properties of S45C steel after hybrid surface treatments of  
ultrasonic nanocrystal surface modification and plasma nitriding

Bo Wu

The University of Tokushima

2014

# **Abstract**

for thesis entitled

**Study on fatigue properties of S45C steel after hybrid surface treatments of ultrasonic nanocrystal surface modification and plasma nitriding**

submitted by

**Bo Wu**

for the degree of Doctor of Philosophy

at the University of Tokushima

in January 2014

Surface treatment is an important method to improve fatigue strength and has been used widely in production. The severe surface plastic deformation ( $S^2PD$ ) as a new surface treatment can improve the strength, microhardness, and bring high compressive residual stress into the materials top surface. Especially after this process, the grains in the top surface can be refined into nano-size and show gradient distribution along the deep direction which can provides a super surface properties. With this method, many kinds of  $S^2PD$  were invented and carried out on various metal materials. In this study ultrasonic nanocrystal surface modification (UNSM), as one of  $S^2PD$  methods, was employed on the surface treatment of S45C steel to enhance the fatigue properties.

And a stronger surface layer produced by plasma nitriding combined with UNSM was also studied.

In chapter 1, the S<sup>2</sup>PD method of surface treatment will be stated and also its effect to the fatigue properties, the research about the application of S<sup>2</sup>PD method into the thermal diffusion treatment would be introduced. The research background and purpose of this study also would be introduced.

In chapter 2, the surface process methods and the experimental methods would be introduced. The principle of the UNSM and the plasma nitriding would be described. The characterization methods, such as hardness test, microstructure observation, Nitrogen content measurement, residual stress measurement, surface morphology observation, scanning electron microscopy (SEM), X-ray diffraction (XRD) would be utilized to study the characterization of the surface layer produced in surface treatment. Also the fatigue test and analytical methods would be introduced.

In chapter 3, UNSM was carried out on the surface treatment of S45C steel. The results of surface morphology, roughness, residual stress, and the hardening zone would be shown and a comparison among different UNSM parameters would be taken to discuss the effect of UNSM to the fatigue strength of S45C steel. After the test, we found that for the quenched and tempered S45C steel the best static load is 50 N. As the increase of UNSM strike number, higher compressive residual stress and surface hardness could be obtained. The fatigue strength also could be enhanced, however sub-surface crack between hardening layer induced by UNSM and the basic metal could be observed.

In chapter 4, UNSM has been employed to improve the surface properties of nitriding specimens. The characterization of the top surface layer, such as surface morphology, surface roughness, residual stress and harden surface zone has been test. The results showed little effect of

UNSM to the surface morphology. The residual stress has an opposite reaction as the increase of strike number. For the fatigue results, the fatigue strength has a close relation with the value of residual stress and effect of strike number to the sub-surface cracks was found. For the  $\Delta K_{\text{facet}}$ , an estimated value is close to the average value calculated from the test results.

In chapter 5, the UNSM was brought into the plasma nitriding of S45C steel. After the characterization test, the surface morphology, compound layers were studied and found that UNSM had no influence to the compositions of the nitriding layers. The growth of the thickness for the compound layer was found and the results show that compared with the un-UNSMed sample enhancement of surface hardness, effective nitrogen diffusivity, and fatigue strength were obtained. However a decrease of fatigue limit of UNSMed sample with nitriding 48 h was found induced by the surface defects (small voids) which were produced by prolonged nitriding.

In chapter 6, all the properties of UNSM and plasma nitriding surface treatments were summarized. The characteristics of the different surface treatments were investigated and the fatigue properties were studied. Plasma nitriding still was the best choice for enhancing of the fatigue properties of S45C steel. Though the hybrid surface treatments of ultrasonic nanocrystal surface modification and plasma nitriding was carried out on the surface treatment for S45C steel and some advantages can be found with some process parameters, limitations for the long time of nitriding and high processing density of UNSM hindered the application of these hybrid surface treatments. Especially the surface defects of plasma nitriding with UNSM and the voids in the top surface nanocrystalline layer induced by long nitriding process, all of these defects seriously affected the improvement for the fatigue strength.

# CONTENTS

<b>Chapter 1 Introduction .....</b>	<b>1</b>
<b>1.1 Effect of surface treatment to fatigue properties.....</b>	<b>1</b>
<b>1.2 Severe surface plastic deformation (S<sup>2</sup>PD).....</b>	<b>3</b>
1.2.1 Development of S <sup>2</sup> PD.....	4
1.2.2 Mechanism of S <sup>2</sup> PD .....	6
1.2.3 Properties of materials after S <sup>2</sup> PD treatment .....	7
<b>1.3 Hybrid treatment with S<sup>2</sup>PD nanocrystal surface .....</b>	<b>7</b>
1.3.1 Enhancement of Nitriding .....	8
1.3.2 Other applications .....	10
<b>1.4 Research background .....</b>	<b>10</b>
<b>1.5 Goal and Objectives .....</b>	<b>12</b>
1.5.1 Scope .....	12
1.5.2 Significance.....	13
<b>Chapter 2 Experimental procedures and apparatus .....</b>	<b>14</b>
<b>2.1 Materials.....</b>	<b>14</b>
<b>2.2 Ultrasonic nanocrystal surface modification (UNSM) .....</b>	<b>15</b>
2.2.1 Work principle.....	16
2.2.2 Machining parameters.....	17
2.2.3 Machining process .....	18
<b>2.3 Plasma nitriding.....</b>	<b>19</b>
<b>2.4 Fatigue test.....</b>	<b>20</b>
<b>2.5 Characterization and analysis.....</b>	<b>21</b>
2.5.1 Optical microscope .....	21
2.5.2 Surface roughness analysis .....	21
2.5.3 Hardness test .....	22
2.5.4 Residual stress measurement and X-ray diffraction analysis.....	22
2.5.5 Elemental analysis .....	23
2.5.6 Scanning electron microscopy .....	24
<b>Chapter 3 Effect of Ultrasonic nanocrystal surface modification to S45C steel surface properties .....</b>	<b>25</b>
<b>3.1 Materials Processing .....</b>	<b>25</b>
<b>3.2 Characters of microstructure.....</b>	<b>27</b>
3.2.1 Surface morphology.....	27
3.2.2 Microstructure.....	30
3.2.3 Microhardness .....	32
3.2.5 Residual stress .....	33
<b>3.3 Fatigue properties .....</b>	<b>33</b>
3.3.1 S-N curves.....	33
3.3.2 Fatigue fractures.....	34
<b>3.4 Conclusions.....</b>	<b>38</b>

<b>Chapter 4 Plasma Nitriding S45C steel subjected to ultrasonic nanocrystal surface modification .....</b>	<b>39</b>
<b>4.1 Materials Processing .....</b>	<b>39</b>
<b>4.2 Characters of microstructure.....</b>	<b>40</b>
4.2.1 Surface morphology.....	40
4.2.2 Microstructure.....	42
4.2.3 XRD results .....	43
4.2.4 Microhardness .....	46
4.2.5 Residual stress .....	49
<b>4.3 Fatigue properties .....</b>	<b>51</b>
4.3.1 S-N curves.....	51
4.3.2 Fatigue fractures.....	53
<b>4.4 Effect to the fatigue crack initiations .....</b>	<b>55</b>
<b>4.5 Conclusions.....</b>	<b>58</b>
<b>Chapter 5 Effect of pre-ultrasonic nanocrystal surface modification to plasma nitriding S45C steel .....</b>	<b>59</b>
<b>5.1 Preparation of specimens .....</b>	<b>59</b>
<b>5.2 Characters of microstructure.....</b>	<b>60</b>
5.2.1 Surface morphology.....	60
5.2.2 Microstructure.....	60
5.2.3 XRD results .....	63
5.2.4 Microhardness .....	65
<b>5.3 Effect to nitrogen diffusion .....</b>	<b>66</b>
<b>5.4 Fatigue behavior .....</b>	<b>69</b>
5.4.1 S-N curves.....	69
5.4.2 Fatigue fracture .....	70
<b>5.5 Voids induced by plasma nitriding in nanocrystal surface .....</b>	<b>71</b>
<b>5.6 Conclusions.....</b>	<b>74</b>
<b>Chapter 6 Conclusions .....</b>	<b>75</b>
<b>6.1 Main conclusions.....</b>	<b>75</b>
<b>6.2 Future work .....</b>	<b>77</b>
<b>References.....</b>	<b>78</b>
<b>Acknowledgement.....</b>	<b>83</b>
<b>Publications .....</b>	<b>84</b>

# Chapter 1 Introduction

Metal surface failure is one of the main reasons inducing metal failure, which including materials lose resulted from wear, surface breakage induced by corrosion and fatigue fracture. All of these properties have a close connection with the metal surface properties. Surface enhancement is a method used to improve surface properties (surface roughness, strength[1, 2], abrasion resistance, corrosion resistance [3-5], residual stress [6-9] and fatigue properties [8-16] with many technological means. Compared with other methods, surface treatment is a promising low cost and particularly effective process that can promote the generally properties of metal materials. For fatigue properties, there are many useful surface treatments [8-16] having been studied to aim an efficient method for improving fatigue strength of metal materials, such as nitriding, shot peen and severe surface plastic deformation (which can produce nano-structured surface layer). With these surface treatments the fatigue strength and fatigue life can be enhanced effectively. However, to save energy and shorten the process time, high efficient and quick surface treatment techniques were still the very important future development.

## 1.1 Effect of surface treatment to fatigue properties

For the fatigue properties, a sum of two segments of life for a fatigue crack initiation period and a crack propagate period is used to express the fatigue life of a workpiece. Especially the crack initiation processes dominate the fatigue failure; however crack initiation mechanisms exhibit very complex. There are many factors affecting the fatigue crack initiation, including planar slipbands, grain boundaries, pores, and inclusions, and also the test conditions (temperature, strain, stress and

loading frequency) and environment are the influence factors [17]. As fatigue test cycle exceeds  $10^9$  cycles, many studies found that multiple fatigue limits and sub-surface cracks (fish-eye cracks) inducing by inclusions in interior grains lead the formation of double fatigue limits. There are many studies about the mechanisms of fatigue failure from internal inclusions: 1) hydrogen-assisted fatigue theory, in which fatigue crack initiations were induced by hydrogen concentrations around nonmetallic inclusions [18]; 2) dispersive decohesion of spherical carbide inducing the formation of granular-bright-facet (GBF) [19]; 3) refinement of the grains around inclusions inducing by stress concentration [20]. However the conditions of specimen surface are still the most significant factor for the fatigue behavior. Surface treatment as an enhancing surface properties method to improve fatigue resistance has been developed a long time ago. After surface treatments a characteristic surface topography, an increase in dislocation density and development of compressive residual stress in the near surface regions can be obtained. With the work hardened surface layers and compressive residual stress, the fatigue crack initiation and crack propagate would be inhibited.

For the surface treatment the properties of materials surface layers, fatigue resistance, residual stress and surface roughness, affect fatigue properties. After surface treatment, all three can be modified and more than a single property can affect the fatigue results. Nitriding as one thermo-chemical surface treatment improves fatigue strength by forming nitrides in the top surface layer and compressive residual stress is always induced [15]. Many studies [12, 21] found that little effect of compound layer to enhance fatigue strength. The diffusion region play an important role and as the increase of the depth higher fatigue strength can be obtained [11]. For the shot peen treatment high compressive residual stress can be introduced into surface layer and fatigue threshold  $\Delta K_{th}$  can be enhanced [9]. However as the increase of test loading or test temperatures,

relaxation of compressive residual stress induced by shot peen [7, 22-24] can be presented. So a small role of surface treatment for low-cycle fatigue and useful effect under high-cycle fatigue can be found for metal surface treatment. The change of fatigue cracking source also can be found in many surface treatments: hardening of a surface layer with a smooth surface may induce the sub-surface crack as fatigue crack initiation from the inclusions in metal [12, 25]; however poor surface roughness produced by severe surface destroy may cause stress concentration and decline of fatigue limit [26]. Though surface treatments are an effective method to enhance the fatigue properties of various metals and alloys, various influencing factors must be considered as the complexity of fatigue behaviors with pre-surface treatment, especially for the actual production and processing.

## 1.2 Severe surface plastic deformation (S<sup>2</sup>PD)

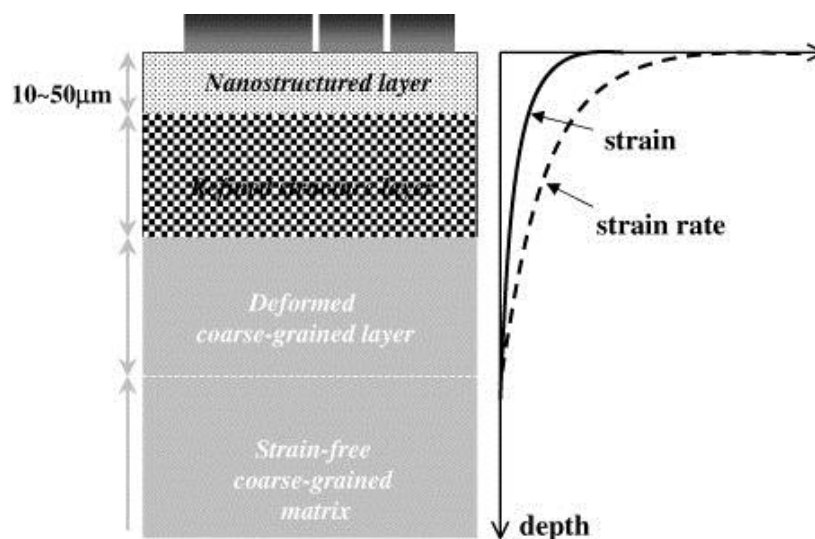


Figure 1-1 Schematic illustration of microstructure characteristics and distributions of strain and strain rate along depth in the surface layer subjected to the SMAT. [27]

Severe surface plastic deformation (S<sup>2</sup>PD), which makes plastic deformation on metal surface in high strain rate and large rate, can refine the toper surface grains into nano-size through slippage

and twinning inside of grains. As one of the effective methods for making nanostructured materials on bulk materials [27], S<sup>2</sup>PD can produce a depth of a nanocrystalline surface layer (from several microns to dozens of micron) and gradual transitions in grain size and strain from the surface to interior can be formed between nano-structured layer and matrix materials (Figure 1-1). An improvement of microhardness, tensile strength, wear resistance, and corrosion resistance and fatigue strength of various materials can be obtained for various materials.

### 1.2.1 Development of S<sup>2</sup>PD

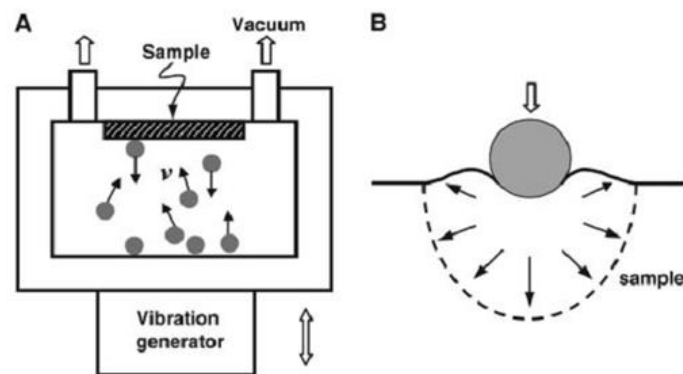


Figure 1-2 Principle of SMAT [28]

S<sup>2</sup>PD process was proposed by Lu [29] as an effective surface treatment of creating nano crystalline on the material's surface in the method of surface mechanical attrition treatment (SMAT). The principle of SMAT was shown in Figure 1-2. Spherical balls, made of different materials (such as steel, glass, ceramics, or other materials), were vibrated by a vibration generator to impact the target materials. After a large number of flying balls in random directions was carried out on the specimen surface at high strain rates, sever plastic deformation and grain refinement were introduced into the toper surface layer. An enhancement of surface layer can be produced and it does not chemically react with the material's surface and does not change the material's chemical

structure.

Many alternative S<sup>2</sup>PD methods have been previously invented and carried out to improve the surface properties of bulk materials, for example, ultrasonic peening (UP) [4], laser shock peening (LSP) [30], surface mechanical attrition treatment (SMAT) [31, 32], ultrasonic shot peening (USSP) [33], ultrasonic surface rolling processing (USRP) [6], surface mechanical grinding treatment (SMGT) [34] (Figure 1-3), and ultrasonic nanocrystal surface modification (UNSM) [25, 35]. Among these techniques, principles of work process vary and different grain refined layer can be produced (for example different surface topography, different depth of processing layer and size of refined grains).

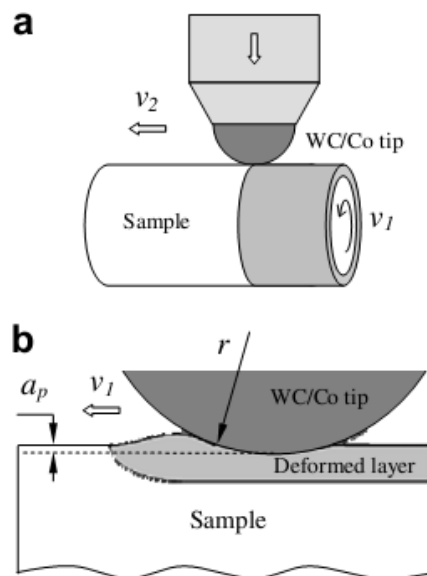


Figure 1-3 Principle of Surface mechanical grinding treatment [34]

All of the S<sup>2</sup>PD-base processes can be regarded as conventional shot peening with different speed and size to repeat impacts of the workpiece surface. So the ball size, speed, and coverage rate or process time were always considered as the key parameters to use to control the processing results [36]. With the bigger balls, deeper of hardening layer, higher surface hardness and smoother surface can be obtained [37]. As the increase of process time, smaller grain size can be produced and

remain in a certain nano-size for the excessive process [38].

## 1.2.2 Mechanism of S<sup>2</sup>PD

The mechanism of S<sup>2</sup>PD has been studied for many years. The necessary and favorable conditions to produce nanocrystalline layers were investigated and considered. So far, many experimental and theoretical investigations showed that amount of strain, strain rate and other deformation factors (low temperature deformation, repetitive or cyclic deformation, multi directional deformation, impurities and/or alloying elements, second phase and hydrostatic pressure) were the favorable conditions to produce surface nanocrystalline [39-42]. With the high strain rate at low temperature a large number of dislocations can be induced within metals and with increase of the amount of strain to 8 [40] lattice rotation was promoted and misorientation angle increased. At last nano-sized grains can be produced on the surface of bulk materials.

With the S<sup>2</sup>PD treatment from various surface treatments, plastic deformation behavior and dislocation activity in metals and alloys can be induced. All of these depend strongly on the lattice structure and the stacking fault energy (SFE). The mechanisms of grain refinement in several metals and alloys have been investigated, including iron (SFE about 200mJ/m<sup>2</sup>) [5, 43, 44], copper (SFE, 78 mJ/m<sup>2</sup>)[45], aluminum (166 mJ/m<sup>2</sup>) [46], and many other materials [6, 37, 47-50]. So the grain refinement mechanism varies as the change of target materials. For iron, the formation and transformation of dense dislocation walls (DDWs) and dislocation tangles (DTs) in original grains are the grain refinement mechanism [44]. Dislocation manipulation and rearrangement, deformation twinning forming nanoscale twin/matrix lamella bundles, and shear banding in the twin/matrix lamellae are the mechanism of the grain refinement for copper [45]. In the refinement of AISI 304

stainless steel planar dislocation arrays and twins, intersection of multidirectional twins leading to grain subdivision and a martensite transformation are the grain refinement mechanism [50]. For the double phase materials the softer phase was refined first and dissolution of second phase were found in many researches [47-49].

### **1.2.3 Properties of materials after S<sup>2</sup>PD treatment**

Many researchers have focused on the characterization and microstructure of the nano-structured layer on the top surface with various S<sup>2</sup>PD and they have studied the mechanical and physical properties, such as wear, corrosion[3], fatigue, strength [1] and thermal stable property. A large number of studies found that with S<sup>2</sup>PD can enhance the fatigue properties [8, 25] and even the fatigue strength or life both can be improved as the hardening surface layer and high compressive residual stress [9, 51]. However some researchers also considered the destroy of specimen surface can induce a decline of fatigue properties [26]. Liu [52] use the SMGT to produce ultrahard and ultrastable nanolaminated structure in nickel. Also the fatigue and wear properties can be enhanced. The structure stability is essential for the application of materials and many researchers have found thermal stability of surface self nanocrystallization for many materials [52-54] and the addition of elements can also increase the temperature of recrystallization[54]. So we can find that S<sup>2</sup>PD is a simple and cost-effective processing technique and potential technological applications can be used in many engineering fields.

### **1.3 Hybrid treatment with S<sup>2</sup>PD nanocrystal surface**

With nanocrystalline produced on the metal surface, many advantaged properties can be

obtained from above introduction. For this layer with gradual distributed refined grains, except nano-sized grains, the materials show peculiar and interesting mechanical and physical properties. With these two characteristics, many surface treatments were introduced to combine with S<sup>2</sup>PD surface treatments. By far a mass of works have been carried out on the thermo diffusion of nanostructured layers produced by S<sup>2</sup>PD.

### 1.3.1 Enhancement of Nitriding

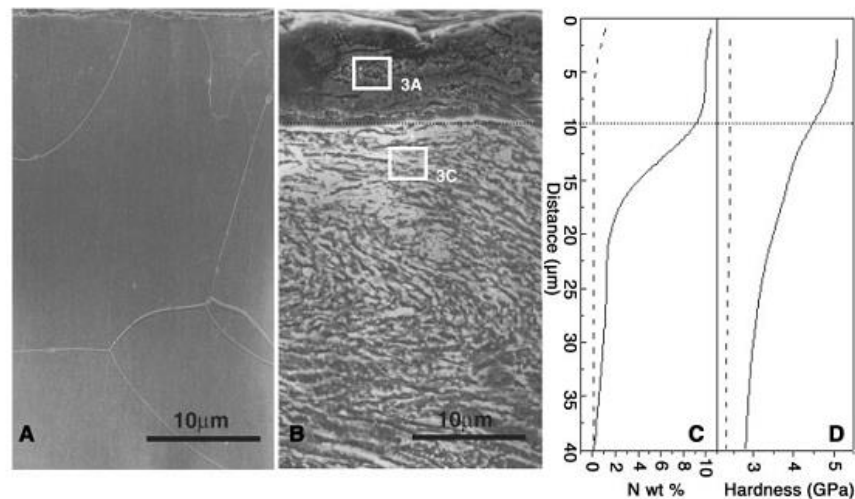


Figure 1-4 Nitriding iron at lower temperatures: cross-sectional observations of (A) an original coarse-grained Fe sample and (B) a SMAT Fe specimen after nitriding at 300 °C for 9 hours (C) nitrogen concentration and (D) microhardness along the depth from the top surface layer in the original Fe sample (dashed lines) and in the treated one (solid lines) [28].

Nitriding, as one of the most widely thermo-chemical surface treatments, can form a composite structure with high hardness and abrasion resistance, corrosion resistance and fatigue properties can be improved significantly. For nitriding results, many process parameters, such as nitriding temperature, time, gas mixture ratio, air pressure and materials composition, can influence the thickness of nitriding layer, depth of diffusion zone and phases of the compound layer [13, 35,

55-57]. However high temperature and long nitriding time consume too much energy and may induce serious deterioration of the processed materials. In order to enhance nitriding efficiency, shorten nitriding time and lower processing temperature, many researches [58-63] have been developed. As nanocrystalline materials processing nano-size grains and a large number of grain boundaries which provide faster atomic diffusion channels than coarse grains, nitriding nanocrystalline has been also considered as one of the enhancing nitriding methods and studied by many researchers [28, 53, 64-71]. Tong et al. [28] reported that in flowing, high-purity ammonia gas (NH<sub>3</sub>) at 300 °C for 9 h an iron plate with pre-SMATed treatment can be nitrided and a continuous compound layer about 10 μm thick was produced. For the specimen with no pre-SMAT treatment no nitrides can be found. He [66] also studied the effect of pre-SMAT to formation of ε-Fe<sub>2-3</sub>N and the results shown that enhancement of nitriding kinetics and lower nitrogen potential needed for the nitrides formation can be obtained due to the numerous grain boundaries in the nanocrystalline Fe. Gu [72] and Tong [73] respectively in their works found that surface nano-structured layer can increase the mass transfer coefficient and thicker compound layer can be obtained. Tong [73] also calculated the effective activation energy for diffusion of nitrogen ( $Q_{\text{eff}}^{\text{N}}$ ) and found that  $Q_{\text{eff}}^{\text{N}}$  in composite nanocrystalline ε-Fe<sub>2-3</sub>N and γ'-Fe<sub>4</sub>N layer is about 54.39 kJ/mol, evidently lower than coarse grain ε-Fe<sub>2-3</sub>N (80.7 kJ/mol) and γ'-Fe<sub>4</sub>N (88.3 kJ/mol). Also the effect of surface nanocrystallization to the composition of nitrides was investigated. In the Lin' research of AISI 321 stainless steel with surface nanocrystallization by SMAT, single S phase could be formed on the specimen surface to avoid the precipitation of CrN at 400 °C. The investigation of AISI 304 austenitic stainless steel with pre-shot peening by Lie [70] also shown a deep region of compound layer and single phase S can be formed at 410 °C and at high temperature of 500 °C the formation

of CrN induced a decrease of corrosion resistance. The effect of temperature to the nitriding surface nanocrystallization results by some researchers [69, 74] demonstrated that high nitriding temperature may weakened the nitriding results of pre-S<sup>2</sup>PD metals comparing with the specimens without pre-treatments, especially for nitrogen composition.

### **1.3.2 Other applications**

In addition to nitriding, many other thermo diffusion treatments (chromizing, nickelizing, aluminizing, galvanizing, boronizing) were also studied by some researchers. Due to the difference of processing temperatures and thermo-chemical reactions, various results would be found. To enhance corrosion resistance and thermal resistance, chromizing is always employed to form a coating on steels. In the research of Wang [53], the diffusivity of Cr in surface nanocrystalline Fe was 4~10 orders of magnitude than in coarse grains within a temperature range of 573~654 K. Lu [75] investigated the effect of processing temperature to chromizing behavior to the nanostructured surface layer on a hot-working tool steel using SMAT. His study showed that at 600 °C a maximum increment of Cr-diffusion depth as the growth of nano-sized ferrite grains with higher temperature. Xiang [76] and Si [77] have studied aluminizing at lower temperature and significantly enhancement could be obtained, however as temperature increases smaller enhancement effect would be found. In boronizing of EN8 steel using SMAT pretreatment [78], not only were the desired case depth and the dense boronized layer achieved but also FeB phase was formed as the decrease of boron potential by pre-SMAT.

## **1.4 Research background**

Ultrasonic nanocrystal surface modification (UNSM), as one of severe surface plastic deformation ( $S^2PD$ ) methods to improve material surface properties, has been used to carry out on many materials treatments [8, 25, 79, 80]. The properties of wear [79, 80], fatigue [8, 25] of materials can be improved as the reason of high surface hardness and compressive residual stress produced by the UNSM treatment. In the study of Cao [8], with the increase of strike number higher fatigue strength can be obtain and small fatigue crack can be restrained as the compressive residual stress produced by UNSM treatment. Suh's study [25] shows that the grain in the top surface zone can be refined into nano-size and the depth of gradual grain refined layer about 100  $\mu\text{m}$  can be produced after UNSM treatment with the applied static force of 100 N. Yasuoka [81] studied effect of different static loading to the fatigue properties of SUS304 austenite stainless steel. They found that the optimum static load for obtaining a high fatigue strength improved by approximately 80% was found to be 90 N and too high static loading (100 N and 110 N) induced a surface layer broken as the formation of strain-induced martensite. Amanov [80] has found that high impact load can get a lower friction and well wear characteristics and smaller nano-grain size can be obtained at the same time. So we can see that the processing parameters (the applied static force, the strike number per  $\text{mm}^{-2}$ , the size of tip ball) can be controlled accurately and all of these parameters have a close connection with the characters of specimen's surface zone after the UNSM treatment. Also the structure of the material receiving surface treatment plays an important role for the formation of microstructure in the surface processing layer. Zhou [82] showed that the SMAT steel sample has a thicker refined layer (with grain size  $< 100$  nm) compared with pure Fe. Cho [49] and Lee [48] found that with more hard phase smaller sized grain can be induced due to the easier formation of dislocation around the hard phase. Plasma nitriding as one of efficient surface hardening methods

has been carried out in the practice product in many fields. Especially for the fatigue properties of materials, the plasma nitriding can produce a super surface as the accuracy control of the nitrogen composition. To avoid stress concentration on the specimen's surface, single phase and thin compound layer are the best choice. The single phase,  $\text{Fe}_4\text{N}$ , which exhibits a better toughness compared with  $\text{Fe}_{2-3}\text{N}$ , is always chosen to enhance the surface properties. At the same time, a thicker diffusion region plays an essential role for enhancement of fatigue strength. By far there are many researches about the enhancement of nitriding by the pre-nanostructured surface [28, 65-70, 72, 74]. Few reports have been found about this hybrid surface treatment for the fatigue properties of metals and long nitriding time processing. In this work, the study of the hybrid surface treatment with UNSM and plasma nitriding was carried out on S45C steel and aims to explore the following issues: 1) the effect of UNSM parameters on the properties of surface nanocrystallization and especially for the fatigue properties of S45C steel; 2) the effect of UNSM to the plasma nitriding S45C steel which has been found that a sub-surface crack induced by inclusions hinders the enhancement of nitriding specimens; 3) With the pre-surface nanocrystallization produced by UNSM and plasma nitriding of the nanocrystalline was carried out and discussed.

## **1.5 Goal and Objectives**

### **1.5.1 Scope**

1. Study on the mechanism of grain refinement during UNSM and effect of different parameters (different strike density and static loading) to the surface properties. The effect of strike density to the fatigue properties and the fractures also was investigated.

2. Plasma nitriding of S45C steel was studied and then UNSM carried out on the plasma nitrided

specimens was also studied to investigate the effect of UNSM to surface properties and fatigue properties of nitriding specimens. Especially the effect of UNSM to the fatigue crack initiation was also studied.

3. The effect of pre-ultrasonic nanocrystal surface modification to the result of plasma nitriding was investigated for 8 h and 48 h. The characterization and microstructure of the plasma nitrided layers of the UNSM specimens were studied. The effect of this hybrid treatment to the fatigue properties of S45C steel was examined and compared with the same nitriding condition.

## **1.5.2 Significance**

1. The effect of UNSM parameters was studied and maximum static loading about 50 N was found for the treatment for S45C steel after quenching and tempering. Grain refinement and enhancement of microhardness, residual stress and fatigue properties was found in this study. A brittle layer about 10  $\mu\text{m}$  and sub-surface crack beneath this layer was found for the U2 specimens.

2. UNSM was applied to plasma nitrided S45C specimens to enhance fatigue properties. Decline of surface residual stress as increasing strike number can be observed. Fatigue limit of nitriding 8 h specimens was improved and no effect on 48 h after UNSM treatment. Fish-eye position was deepened for 48 h specimens and no fish-eye crack for 8 h.

3. Nano-structured surface layers with different grain sizes and depths were nitrided. Thicker compound layer was produced for sample with nano-structured surface layers and nitrogen enrichment was found for nitriding sample with smaller surface grain size. Surface voids were found in nitriding nano-structured surface sample for 48 h and the mechanism was explained through the principle of plasma nitriding.

# Chapter 2 Experimental procedures and apparatus

In chapter 2, the materials preparation, ultrasonic nanocrystal surface modification (UNSM) and plasma nitriding (PN) will be introduced in details. The processes and principles of ultrasonic nanocrystal surface modification and plasma nitriding were also given in the follows. The analysis technique and sample preparation for characterization will be stated.

## 2.1 Materials

In this study, a medium carbon steel S45C shaft was used to investigate the effect of surface treatments. The chemical compositions were 0.45%C; 0.15%~0.35%Si; 0.6~0.9%Mn;  $\leq 0.03\%$ P;  $\leq 0.035\%$ S;  $\leq 0.3\%$ Cu;  $\leq 0.2\%$ Ni;  $\leq 0.2\%$ Cr; balance Fe (in wt.%). To test the fatigue properties with various surface treatments, the specimens were machined into the shape of Figure 2-1.

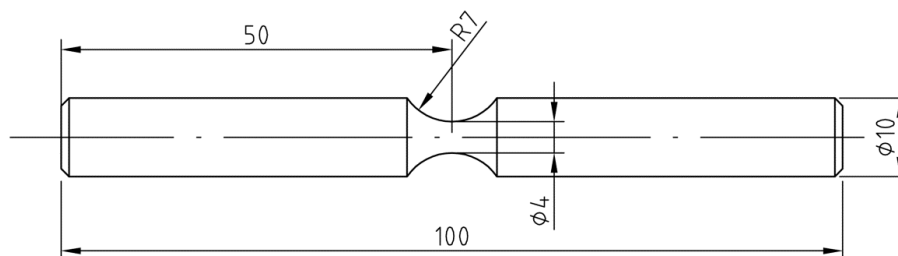


Figure 2-1 Dimension of test specimen for S45C steel.

Quenching and tempering treatments were employed to improve the strength. the investigated region of the specimens were polished with sandpaper from grade 400 to grade 2000 and then processed in a hardened condition (austenitized, 1113 K, 150 min; oil quenched, room temperature; tempered, 773 K, 270 min) to the surface hardness of 31 HRC.

The microstructure of the quenching and tempering specimen was shown in Fig.2-3. The

average grain size is approximately 20  $\mu\text{m}$  and tempered sorbite was obtained after the quenching and tempering treatment. As nital is not used to etch the microstructure, the metallographic structure within the grains cannot be etched clearly and only unclear quenched lath martensite structure can be observed. A transmission electron microscope (TEM) image shows the distribution of the carbides within ferrite grains in Figure 2-4. It can be found that the carbides distribute along the direction of acicular martensite shape.

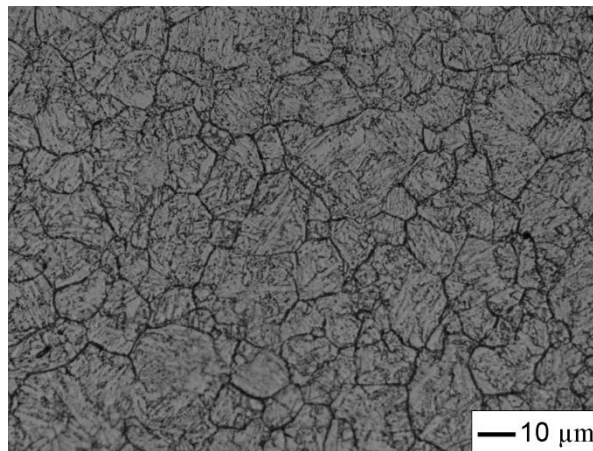


Figure 2-3 Microstructure observation of S45C steel after quenching and tempering.

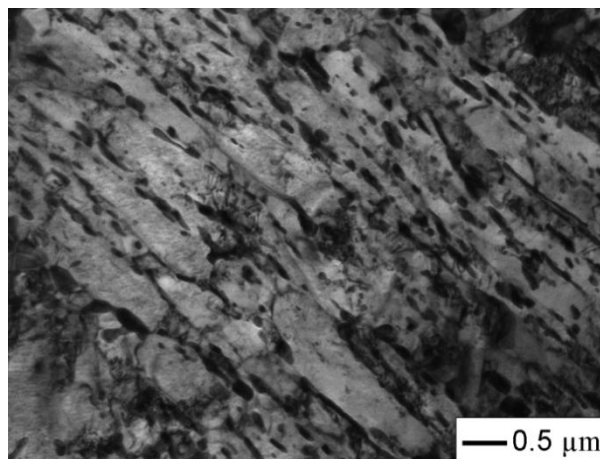


Figure 2-4 Distribution of carbides within ferrite grain.

## 2.2 Ultrasonic nanocrystal surface modification (UNSM)

## 2.2.1 Work principle

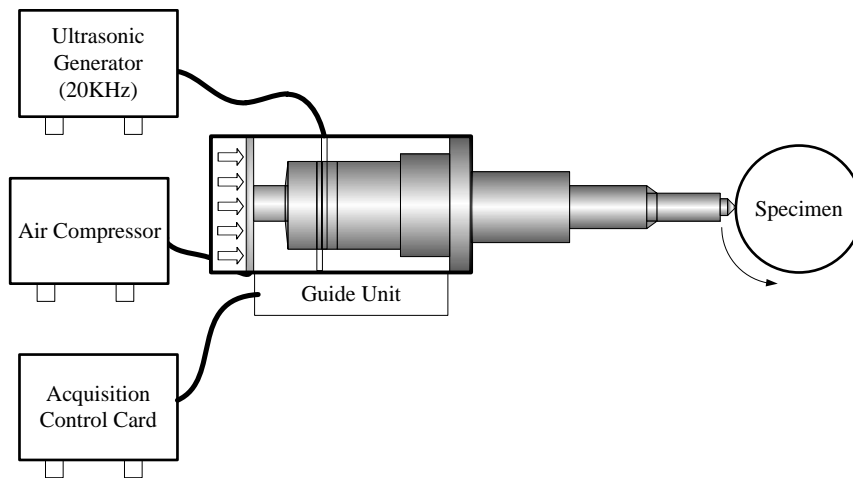


Figure 2-5 Schematic diagram for UNSM

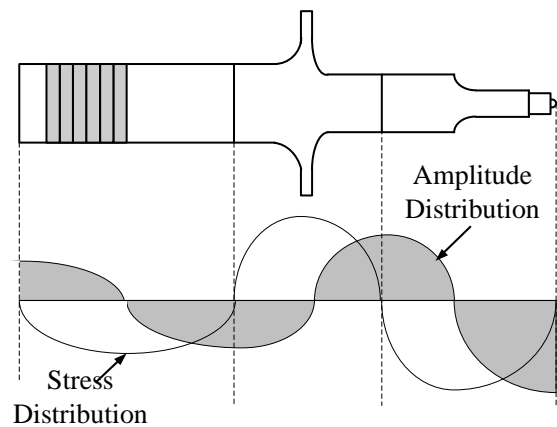


Figure 2-6 Principle of ultrasonic processing

In this study, Ultrasonic nanocrystal surface modification was used to enhance surface properties and obtain gradient changes of grain refinement on specimen surface. Schematic diagram for Ultrasonic nanocrystal surface modification is shown in Figure 2-5. The equipment of UNSM mainly includes ultrasonic generator, air compressor, control card and guide unit. UNSM works basing on an ultrasound transducer which can produce mechanical ultrasonic wave per second, the frequent of several tens of thousands, even millions. As only a few micrometers of amplitude can be generated by ultrasound transducer directly, acoustic horn is frequently employed to obtain an

amplification of amplitude about dozens of micron or several hundred microns. With the amplified mechanical ultrasonic wave, the tip ball was driven onto strike the surface of specimen and severe surface plastic deformation was induced on workpiece.

## 2.2.2 Machining parameters

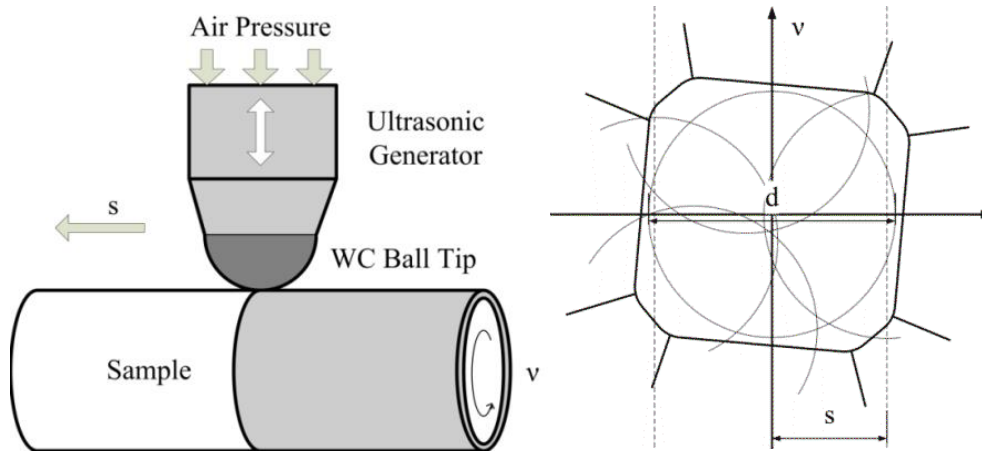


Figure 2-7 Schematic diagram of processing density

A tungsten carbide ball (the diameter: 2.4 mm) was used to strike the surface of samples with thousands of strikes per second and constant pressure. After the UNSM treatment, the original grains of surface layer were refined into nanometer-sized grains with the severe plastic deformation (SPD). This process was obtained through ultrasonic generator (a 30  $\mu\text{m}$  amplitude and 20 kHz) and air compressor devices producing a static force and amplitude of dynamic load. When the TC ball strikes onto the material surface with a rotation sample, a distance (approximately 70  $\mu\text{m}$ ) moves along the horizontal direction. With the linear velocity of the rotation specimen and the feed of main shaft of the strike device (Figure 2-7), the number of strikes to the specimen surface per  $\text{mm}^2$  can be obtained (Equation 2.1).  $N$  is the processing density ( $\text{mm}^{-2}$ ),  $f$  is the work frequency of ultrasound transducer,  $v$  ( $\text{mm/s}$ ) is the moving speed to workpiece surface,  $s$  ( $\text{mm/rev}$ ) is feeding rate,  $R$  ( $\text{rpm}$ ) is the rotating speed of machining tool and  $r$  is the radius of specimen.

$$N = \frac{f}{v*s} = \frac{60f}{R*2\pi r*s} \quad (2.1)$$

### 2.2.3 Machining process

To study the effect of UNSM to the fatigue properties of S45C steel, fatigue specimens were machined following Figure 2-6. During machine tool rotating, ten thousands of impacts were carried on specimen surface with process head. To avoid too hot and induce an oxidation reaction on the surface, cooling liquid was used during machining. And a support was fixed and stand up to the specimen back to prevent bend of the rod specimen as the high force induced by UNSM. The specimen after UNSM treatment is shown in Figure 2-6 and the middle of specimen is the processed region.

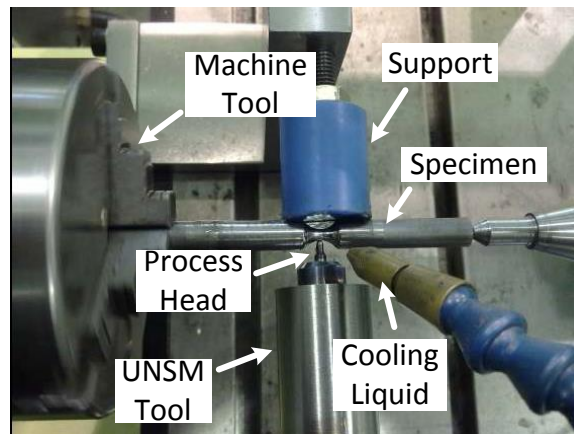


Figure 2-8 Process of UNSM



Figure 2-9 Specimen after UNSM treatment.

## 2.3 Plasma nitriding

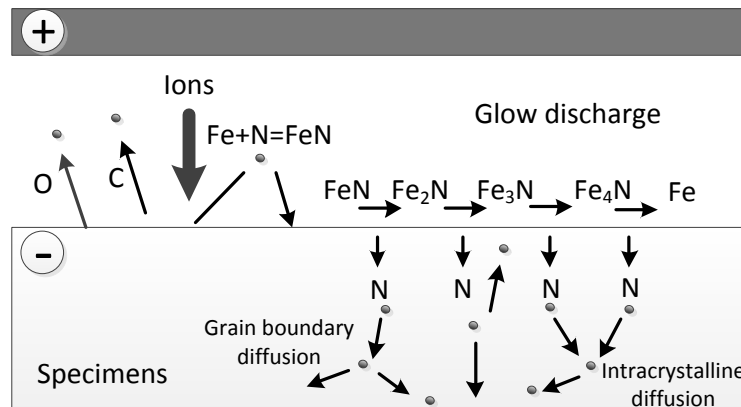


Figure 2-10 Principle of plasma nitriding

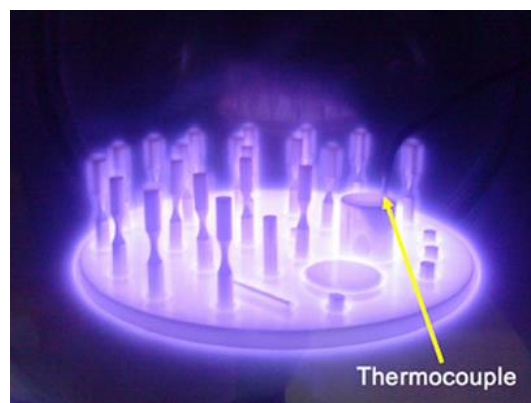


Figure 2-11 Process of plasma nitriding[13]

Plasma nitriding was used to enhance workpiece surface properties to improve fatigue properties of S45C steel in this study. Plasma nitriding as an efficient nitriding treatment and the work principle was shown in Figure 2-10. During plasma nitriding, glow discharge was generated between positive pole and negative pole (specimens). With the gas ionized to positive ions and accelerated in the electric field, ions were sputtered to the specimens' surface. Oxygen, carbon, iron and secondary electron were sputtered from the specimen surface. At the same time the kinetic energy of sputter ion turns into thermal energy and heat the specimen and complex chemical reaction was generated around the negative pole. Compound of iron nitride is formed and decompose ( $\text{FeN} \rightarrow \text{Fe}_x\text{N}$ ). As the

high temperature, a few of nitrogen ions diffuse into the specimen. The process of plasma nitriding is shown in Figure 2-11 and the thermocouple is used to detect the processing temperature and obtain the aim of temperature control.

## 2.4 Fatigue test

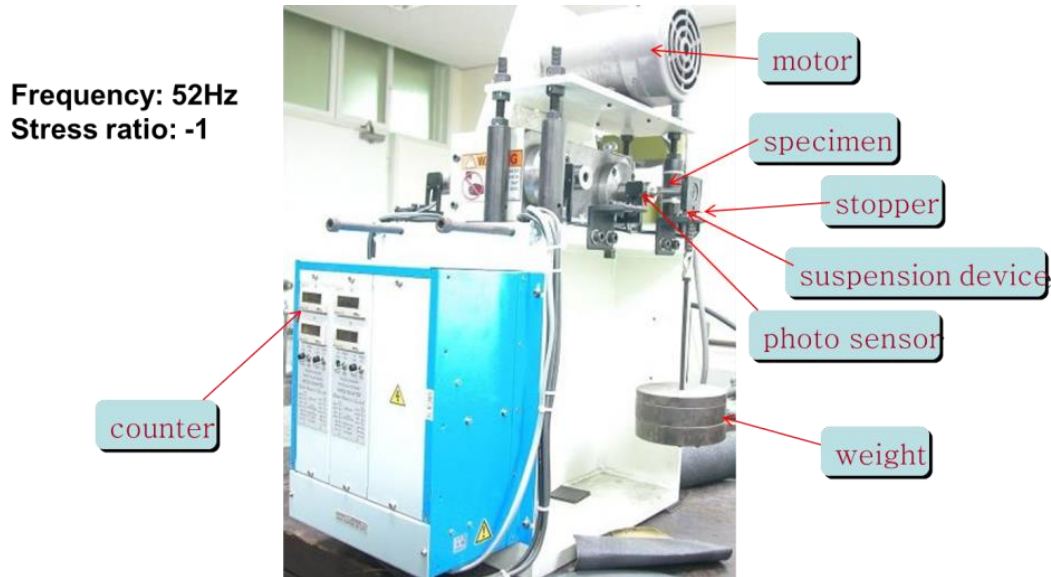


Figure 2-12 Rotating-bending fatigue test machine

To compare the fatigue properties of S45C with different process methods, rotating bending fatigue test was carried out on a dual-spindle rotating bending fatigue test machine (Figure 2-12) in laboratory air atmosphere. In this test, the test frequency was 52Hz and the stress ratio was -1.

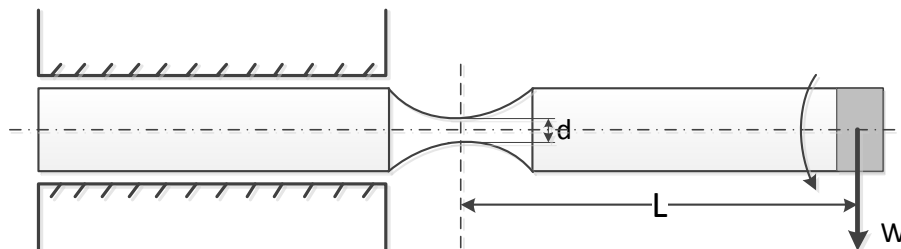


Figure 2-13 Illustration of calculation for the loading force.

$$M = PL = \sigma_0 Z \quad (2.2)$$

$$Z = \frac{\pi d^3}{32}, \quad P = 9.8W, \quad \sigma = K_t \sigma_0, \quad K_t = 1.08$$

The loading force was applied by weights one side of the specimen and the other side was fixed to fatigue test machine (Figure 2-13). The loading stress can be calculated by eq.2.2. In the equation,  $Z$  is the are moment of inertia,  $P$  is the force,  $W$  (kgf) is the weight,  $M$  is the moment of force,  $L$  is the distance between the loading point and the critical section of the specimen ( $L=46.5$  mm),  $\sigma$  is the stress without stress concentration,  $\sigma_0$  is the final loading stress on the critical section of the specimen,  $K_t$  is the stress concentration factor, and  $d$  (mm) is the diameter of the critical section of the specimen. The equation 2.3 can be summarized form the equation 2.2 with the parameters and the final form was equation 2.4. We used this equation to calculate the loading stress from the loading weights.

$$\sigma = \frac{9.8 \times 32 \times WLK_t}{\pi d^3} \quad (2.3)$$

$$\sigma_{(MPa)} = 78W_{(kgf)} \quad (2.4)$$

## 2.5 Characterization and analysis

### 2.5.1 Optical microscope

To examine the surface morphology after surface treatment and the grain-refined layer and the nitriding layer, the cross-section of the all specimens were observed by an optical microscope (Olympus BN2). Before metallographic test, the samples were mechanically polished with the sandpapers (from grade 150 to grade 2000) and then a polish cloth with a liquid suspension of alumina. The saturated picric acid solution was used to etch the specimens in this test.

### 2.5.2 Surface roughness analysis

The effect of the UNSM to the roughness of S45C specimen surface was also test on a contact

surface profiler (ULVAC DEKTAK3). The definition and representation of surface roughness were shown in Figure 2-14 and the parameters, Ra and Rz, were calculated through equation 2.5 and 2.6 by the software.

$$R_a = \frac{1}{L} \int_0^L |y_i(x)| dx \quad (2.5)$$

$$R_z = y_{pmax} + y_{vmax} \quad (2.6)$$

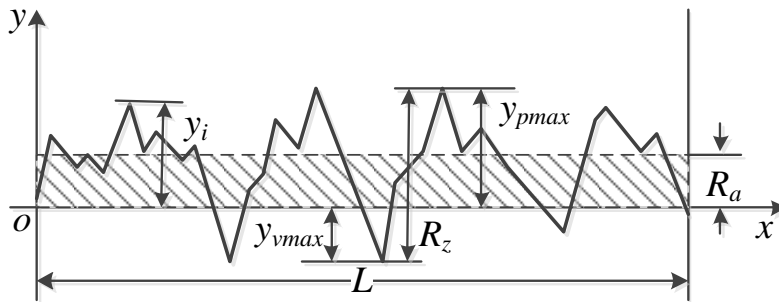


Figure 2-14 The definition and representation of surface roughness

### 2.5.3 Hardness test

The measurement of microhardness of the plastic deformation zone and nitriding layer was carried out on a micro-Vickers hardness tester (MVK-E3, Akashi). To compare the effect of two different process methods, the parameters used in the microhardness test were 50 gf and a duration 15 s.

### 2.5.4 Residual stress measurement and X-ray diffraction analysis

After the treatment, surface residual stress was induced with different mechanisms. X-ray diffraction was used to measure the value of residual stress of all kinds of specimens with a Cr-K $\alpha$  radiation for the long wavelength and deeper penetrating power. The test was carried out on Rigaku XG-4026A1 using the classical  $\sin^2\psi$  method (Using the parameters in Table 2-1). To analysis the

surface layer state of the nano-structure and the compound layer of nitriding samples, Cu-K $\alpha$  was employed to investigate the structure of the surface layer about 5  $\mu\text{m}$  on Rigaku Rint-2000. All the direction of detecting specimen was along the axial direction (Figure 2-15).

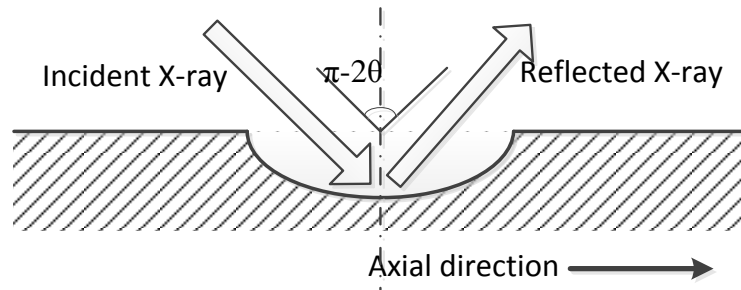


Figure 2-15 The direction of the X-ray test

Table 2-1 Parameters of residual stress test with X-ray

Test equipment	Rigaku PSPC
Radiation	CrK $\alpha$
Test method	Side inclination method
$\sin^2\psi$ (n=7)	0, 0.1, 0.2, 0.3, 0.4, 0.5, 0.6
Voltage	40Kv
Current	30mA
Range of test area	153 $^\circ$ ~159 $^\circ$ ; Fe (221)
Scan speed	0.01 $^\circ$

## 2.5.5 Elemental analysis

The nitrogen content variation along the cross-section of the specimens with the different nitriding duration was measured by an electron probe micro-analyzer (EPMA). The parameters were as follows: accelerating voltage (10 kV); electric current (10  $\mu\text{A}$ ); test diameter (1  $\mu\text{m}$ ); measure interval (2  $\mu\text{m}$ ); and test times (2 times). The specimens were cut and the arrows was the detecting line.

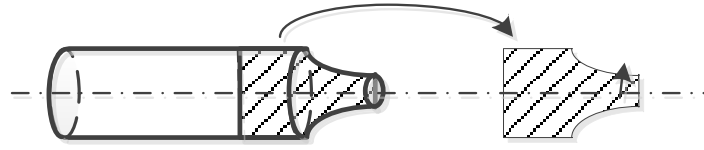


Figure 2-16 The method of nitrogen content detection with EPMA.

## 2.5.6 Scanning electron microscopy

Fractures of the failure specimens were scanned with scanning electron microscopy (S-4700, Hitachi and S-2700, Hitachi). The highest acceleration voltage is 20 kV. The current was set at 10 mA. For there was sub-surface fish-eye crack initiation induced by inclusions, the Energy-dispersive X-ray spectroscopy (EDX) on the same machine was used to detect the composition of the inclusions.

# Chapter 3 Effect of Ultrasonic nanocrystal surface modification to S45C steel surface properties

In this chapter, the quenched and tempered S45C steel was treated by ultrasonic nanocrystal surface modification. S45C steel was processed by UNSM with different technological parameters to improve the fatigue properties. With the surface mechanical treatment, the surface layer of S45C was enhanced with different parameters. The microhardness of cross-section, state of surface layer, fatigue strength and fatigue failure were tested and observed to compare the properties.

## 3.1 Materials Processing

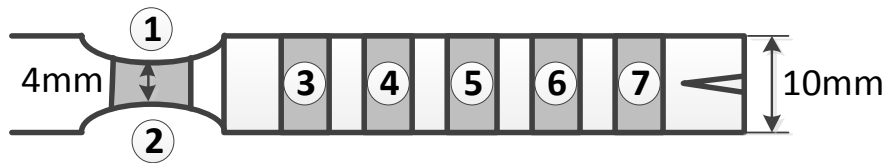


Figure 3-1 Position of UNSM with different parameters.

To choose a maximum static load and obtain a deepest processing zone, different static load (50 N, 60 N, 70 N) were used to process the specimen surface (3~7 in Figure 3-1) and 50 N was chosen with different process densities to test the fatigue properties of S45C steel (1, 2 position of Figure 3-1). The detailed parameters used in this test are shown in Table 3-1.

Table 3-1 Processing parameter of UNSM

Specimens	U1	U2	U3	U4	U5	U6	U7
Pre-treatment	Polished		Un-polished				
Processing Frequency $f$ (Hz)	20000						
Amplitude $A$ ( $\mu\text{m}$ )	30						
Strike Pin Diameter $D$ (mm)	2.4						
Static Loading $F$ (N)	50				70	70	60
Specimens Diameters $r$ (mm)	4	4	10	10	10	10	10

Feeding Rate s (mm/rev)	0.07						
Machine Speed R (rpm)	40	20	40	20	40	20	40
Processing Density N (mm-2)	34000	68000	17000	34000	17000	34000	17000

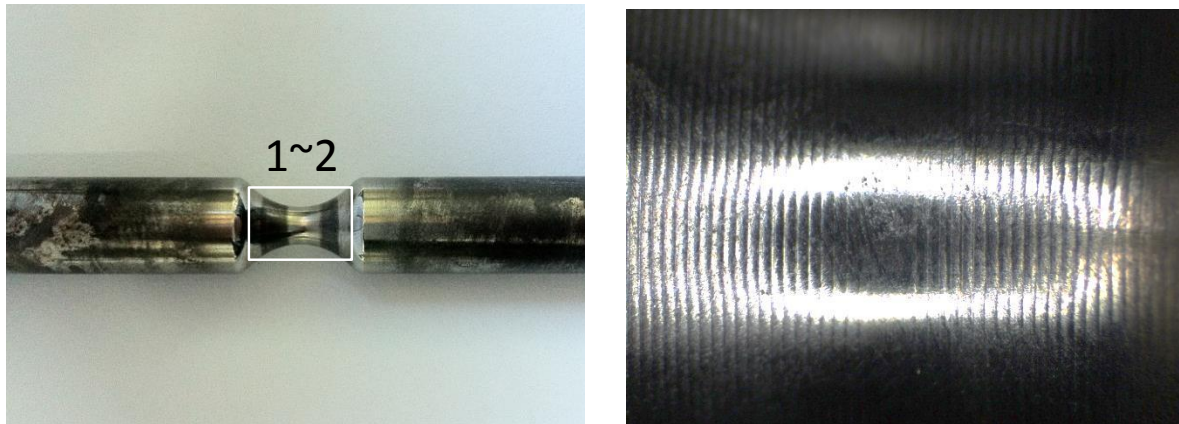


Figure 3-2 Process result of UNSM with parameter 1 and 2.

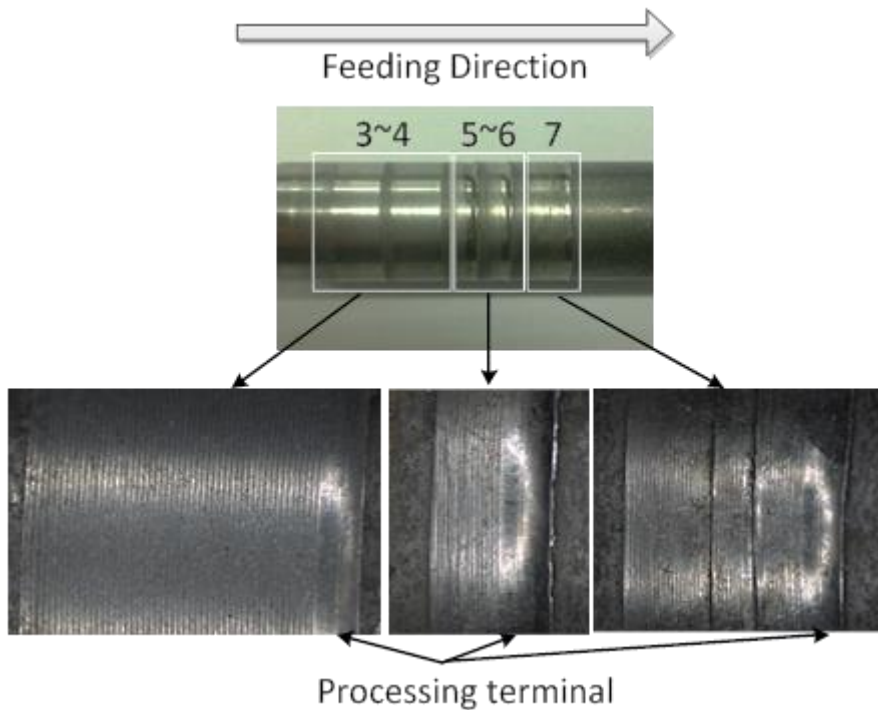


Figure 3-3 Process result of UNSM with parameter 3~7.

The results of specimens after UNSM treatment were shown in Figure 3-2 and Figure 3-3. During process, the static load about 50 N was the best load and under other static load (60 and 70 N) there were vibrations of UNSM system which destroyed specimen surface (Figure 3-3). Force analysis between strike pin and specimen surface was shown in Figure 3-4. The frictional force

between strike pin and specimen surface would increase as the growth of static load. At the same time, the amplitude of ultrasonic process decreased under high static load. This force perpendicular to the striking direction can destroy the resonance produced by the ultrasonic system and UNSM system cannot work in a stable state. So for the quenched and tempered S45C steel the static load 50 N is the maximum force which can be used to improve surface properties.

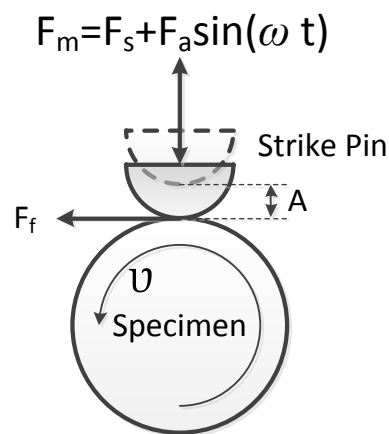


Figure 3-4 Force analysis between strike pin and specimen surface.

## 3.2 Characters of microstructure

### 3.2.1 Surface morphology

The material fatigue properties were sensitive to surface morphology and roughness. Figure 3-5 shows the optical micrograph of samples' surface morphology after UNSM in different process conditions. The results reveal that after UNSM treatments the specimen surface was changed obviously compared with the un-treated specimens on the surface of which many scratches produced during machining can be observed. At the same time the parallel machine marks induced by the UNSM treatments show more apparent as the increasing of processing number. During UNSM process the surface of sample was deformed by repeating strike ball in a short time. And as

the increase of process number the machine marks become clearer and deeper. As the feed rate was 0.07 mm/rev, from the surface morphology results the parallel machine mark width can be measured approximately 70  $\mu\text{m}$ . The result equals to the processing parameters. The surface region between machine marks shows smoother than other region as the reason that the interzonal region is the main active region processed by the strike ball.

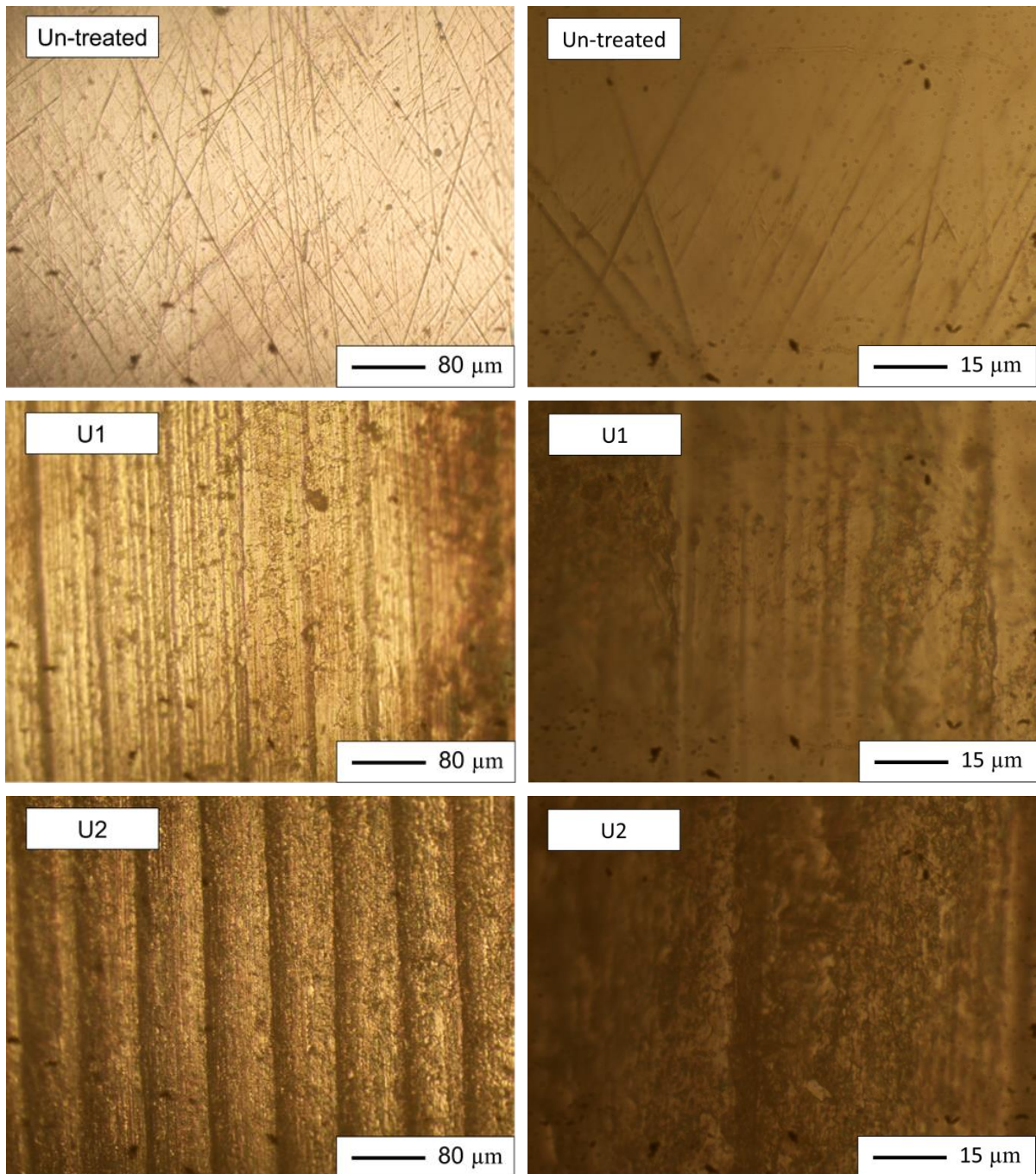


Figure 3-5 The surface morphology of specimens before and after UNSM.

After UNSM treatment the average roughness  $R_a$  was  $0.187 \mu\text{m}$  for U1 and  $0.193 \mu\text{m}$  for U2 and compared with un-treated specimens ( $0.297 \mu\text{m}$ ) the surface roughness has an overall improvement. Combined with the surface morphology results, it can be inferred that at the primary stage sever plastic deformation can improve the surface roughness and remove surface machine marks; however at the later stage overmuch strike number induce the surface deformation and UNSM marks were produced.

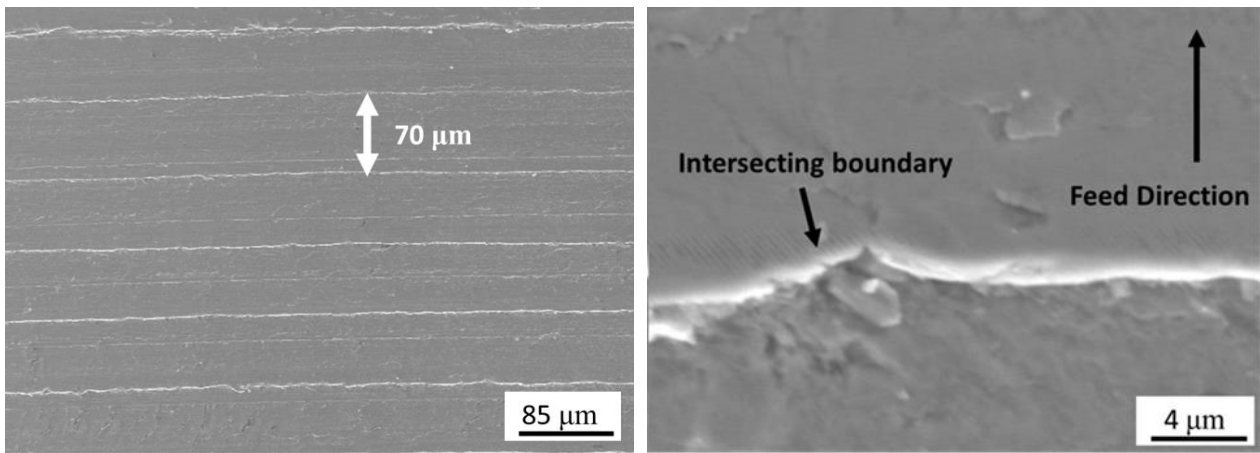


Figure 3-6 The surface morphology of specimens with U1 by SEM.

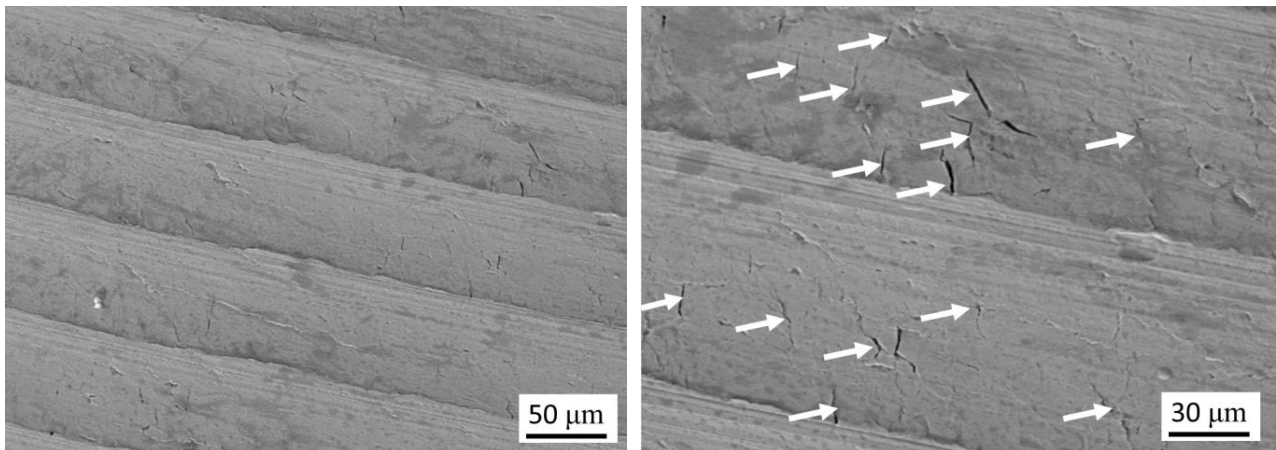


Figure 3-7 The surface morphology of specimens with U2 by SEM (The white arrows are small cracks).

The treated surface of specimens after UNSM also was observed using SEM (Figure 3-6 and 3-7). Intersecting boundaries could be observed obviously for U1 specimens. It is not clear for U2 specimens, however some small cracks were found. This is the reason that too much process

densities induced surface hardening and destroyed the specimen surface.

### 3.2.2 Microstructure

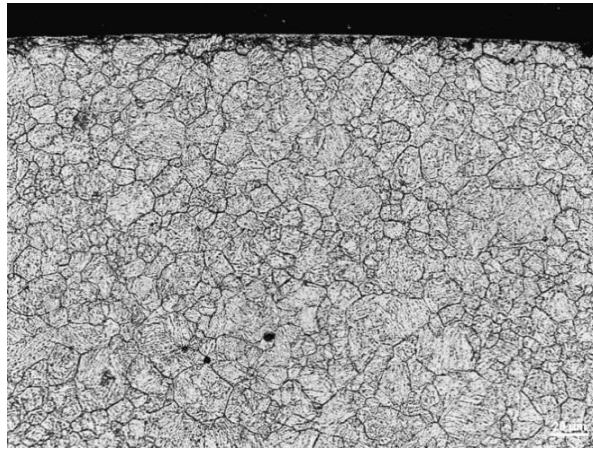


Figure 3-8 The cross-sectional micrographs of the un-treated specimens.

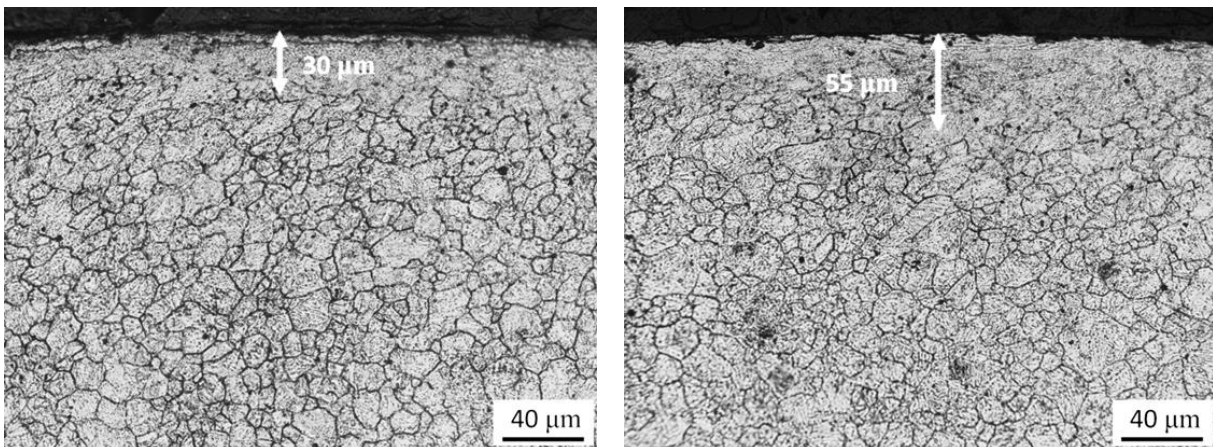


Figure 3-9 The cross-sectional micrographs of UNSMed (U1 and U2) specimens.

Figure 3-8 and 3-9 shows the cross-sectional micrographs of the un-treated, UNSMed (U1 and U2) in different processing conditions. It can be seen that comparing from the un-treated sample's surface there is no difference of the grain between surface and interior zone. After surface treatments, new surface layers were produced in the surface zone. For the UNSMed specimens, grain refined zone and plastic deformation zone were produced by the severe plastic deformation for the repeated striking against the material surface. The UNSM treatment as one of the SSN

methods can promote metal surface grain to refine into nano-size and the microstructural gradient can be obtained on the surface zone of many metal materials [25, 79, 80]. In this test grain-refined gradient also can be produced on the S45C steel surface. As in the top surface zones not only refined grains can be found but also high compress residual stress also existed. This layer was difficult to be etched and to be distinguished. Refined grain and beneath this layer crystal plastic deformation can be found unclearly. From the microstructure images it can be seen that a varied micro-structured layer, the grain of which has been strike into small grain size and is too small to distinguish, about 30  $\mu\text{m}$  was presented for U1 specimens and for U2 samples about 50  $\mu\text{m}$ . As the increasing of strike number the depth of this layer increases. Through X-ray diffraction patterns, the surface structure was scanned and shown in Figure 3-10. The X-ray diffraction patterns shows the typical diffraction patterns of ferrite, a body centered cubic, (110), (210), (211). It can be seen that with the severe plastic deformation, the FWHM value of these diffraction peaks was increase. As the increasing of shocking number, the FWHM value grows. From the relation of grain size with FWHM, we can conclude that not only does the depth of the deformation layer increase with the more striking number, but also smaller grains with the sample's surface zone can be obtained.

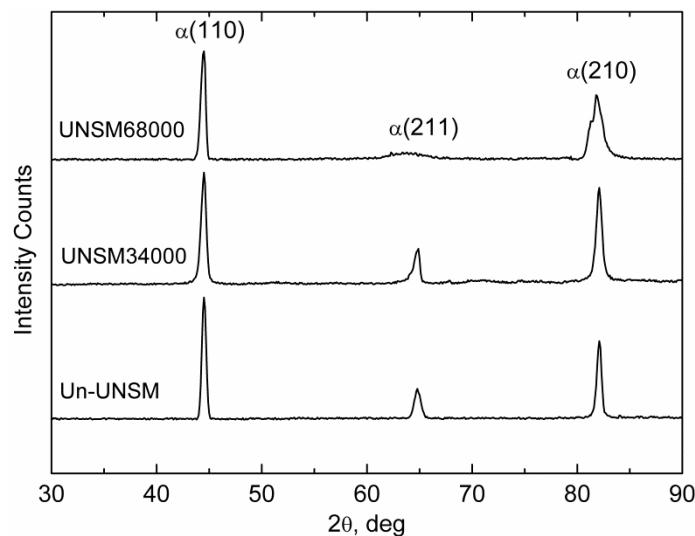


Figure 3-10 The X-ray diffraction patterns of un-treated and UNSMed (U1 and U2) specimens.

### 3.2.3 Microhardness

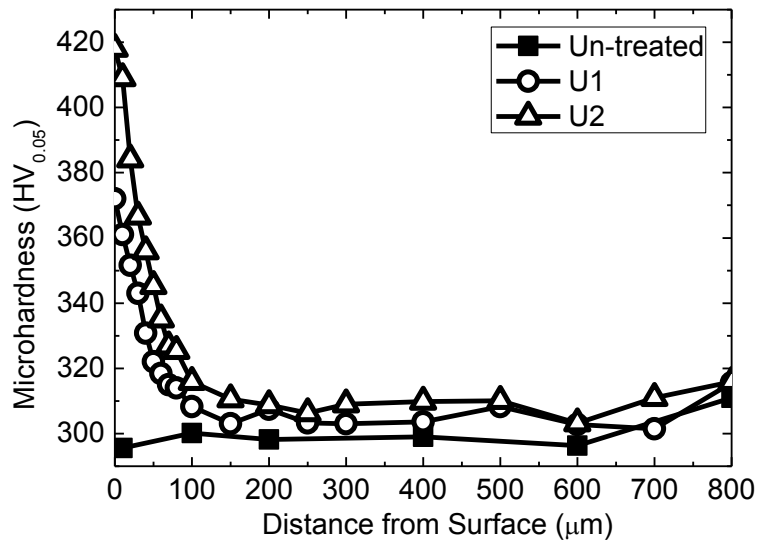


Figure 3-11 The results of microhardness distribution along the cross-section of samples with different treatments.

Figure 3-11 is the results of microhardness distribution along the cross-section of samples with different treatments. The entire test used the 50 gf load to measure the microhardness value. It can be seen that all of the UNSM treatments can enhance the hardness of the materials surface. For the UNSM samples, the microhardness in the top nanostructured layer is 372 Hv for U1 sample and 418 Hv for U2 sample. And then they decrease gradually with the depth down to 300 Hv (the basic material) at 100 μm for U1 and 200 μm for U2. The materials surface was subjected to a severe plastic deformation induce a grain refinement. With the UNSM treatment, increased number of grain boundaries as the refined grains and the generation of high density dislocation with strain hardening restrict the dislocation motion and render the material harder and stronger. Along the increase of the depth, the effects introduced by UNSM weaken, so the hardness decreases to the value of basic material hardness. The state of surface deformation zone has a close relation with the parameters of S<sup>2</sup>PD (ball size, ball speed, direction of shot impact and process times) [46, 83], and as the increasing of ball size, ball speed and process times deeper refined layer can be obtained. In

this study the same results that deeper refined layer was also found for the U2 sample compared with the U1 sample.

### **3.2.5 Residual stress**

Through X-ray diffraction the residual stress near the surface layer (about 20  $\mu\text{m}$ ) can be detected. For the un-treated sample, this value is about -217 MPa. After UNSM process, a compressive residual stress approximately -318 MPa was induced for U1 and approximately -395 MPa for U2. It is obvious that this value increases with the increasing strike number subjecting to the sample's surface. The residual stress on the sample's surface processed with different treatments was induced by different kinds of mechanism. The quenching and tempering treatment processes the samples with a sharp change in the temperature which induces the surface compressive residual stress. For UNSM treatment, a severe plastic deformation is subjected on the materials surface zone and brings large strain in the grains within material surface. So with the process number increasing, larger strain is stored in the crystalline and bigger residual stress is produced.

## **3.3 Fatigue properties**

### **3.3.1 S-N curves**

High-cycle fatigue test was carried out to determine the characters of fatigue properties of S45C with the different surface treatments on a rotating bending fatigue machine. The S-N curves obtained from the test are shown in Figure 3-12. It can be seen that the fatigue life of all kinds of samples was significantly improved after surface treatments, but the degree of improvement is different varying with surface treating methods. The fatigue limit of the un-treated specimen was

464 Mpa, 523 Mpa for U1 and 550 for U2. The base material S45C steel can be calculated the fatigue strength by a simple expression:

$$\sigma = 1.6Hv \quad (3.1)$$

Gradual harden surface layers produced on the S45C steel surface by the UNSM treatments to improve the fatigue strength. After treatments, nano-structured layers with different grain sizes and different depths were produced. As the structure of surface zones changes gradually, the strength of the materials in different depths also decreases with the depth from sample surface. With the hardening surface, the fatigue crack induced by persistent slip bands (PSD) was difficult to form and the fatigue limit stress was improved. Also the fatigue crack initiation model changed with the different surface state.

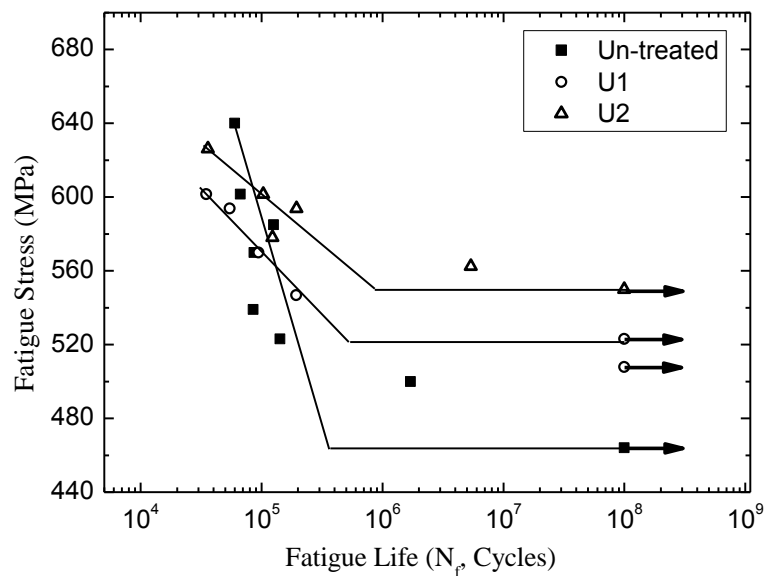


Figure 3-12 S-N curves of un-treated and UNSMed (U1 and U2) specimens.

### 3.3.2 Fatigue fractures

The observations of the fatigue fractures were shown in Figure 3-13 ~15. It can be seen that after surface treatment not only was the fatigue strength enhanced but also the fracture mode was

changed. For un-treated, the persistent slip bands (PSBs) is the main reason inducing the fatigue failure for un-treated S45C sample and in Figure 3-13 no surface defects can be found in the fatigue

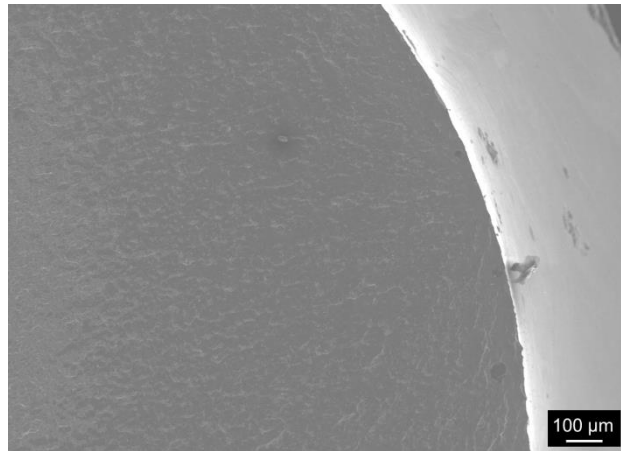


Figure 3-13 The fracture surface of failure un-treated specimen (un-treated, 539 MPa,  $8.51 \times 10^4$ ).

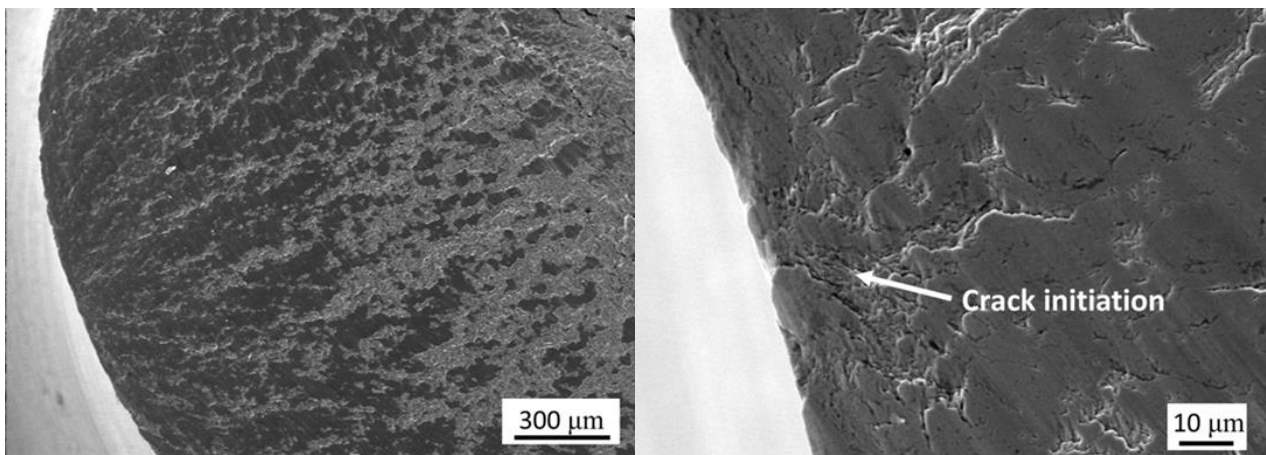


Figure 3-14 The fracture surface of failure U1 specimen (U1, 546.8 MPa,  $1.93 \times 10^5$ )

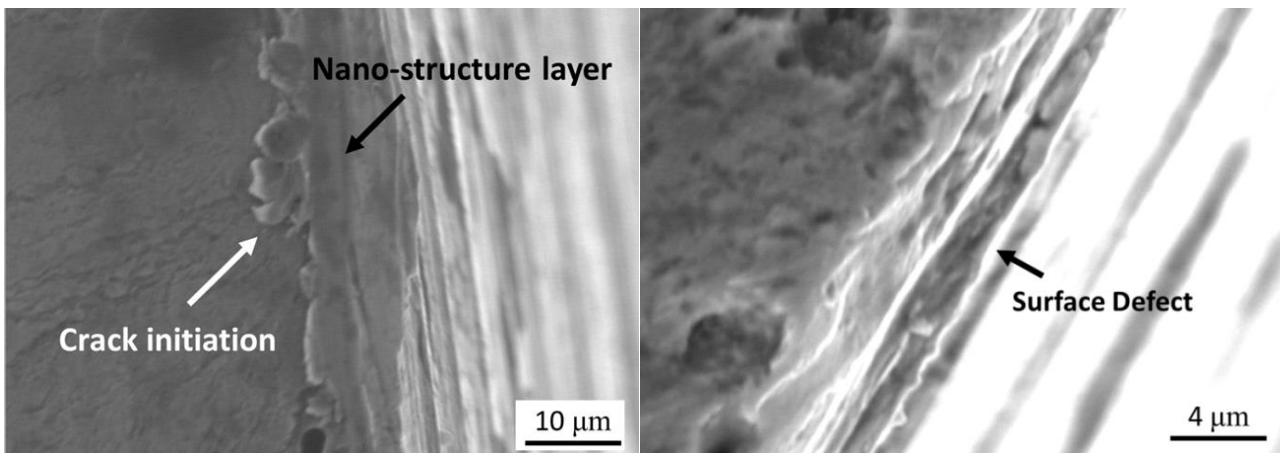


Figure 3-15 The fracture surface of failure U2 specimen (left, U2, 546.8 MPa,  $1.93 \times 10^5$ ; right, U2, 562Mpa,  $5.39$

$\times 10^6$ )

crack source. With above surface morphology results, UNSM process marks were produced on the surface of the UNSMed samples. In Figure 3-14 and 3-15, we can see that for the UNSMed specimens, the fatigue crack sources are the UNSM process defects produced during the UNSM treatment and on the sample surface there are many parallel defects also can be observed. On the edge of cross-sectional micrographs of U2 specimens, there are many small cracks also could be observed (Figure 3-16).

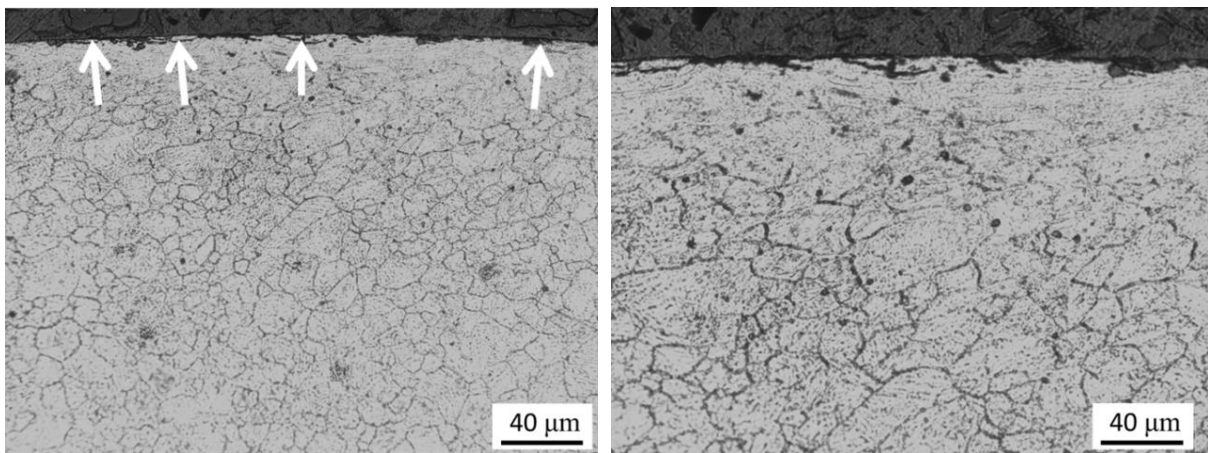


Figure 3-16 The cracks on the edge of cross-sectional micrographs of U2 specimens.

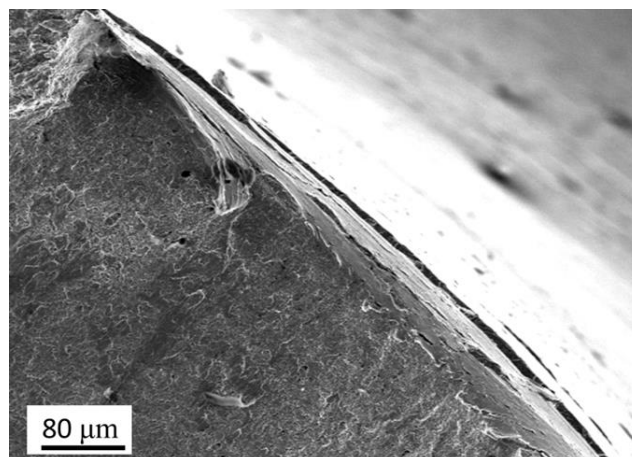


Figure 3-17 The final fracture after fatigue test.

The final fractures of the fatigue crack were also observed (Figure 3-17). When the fatigue crack extended to large enough, the residual zone was broken instantaneously under high load. In these zones some surface cracks along the intersecting boundaries were observed (Figure 3-18) for

U1 and U2 specimens. This means that weakness of the intersecting boundaries for the specimens after UNSM comparing with the other regions in the top surface layers.

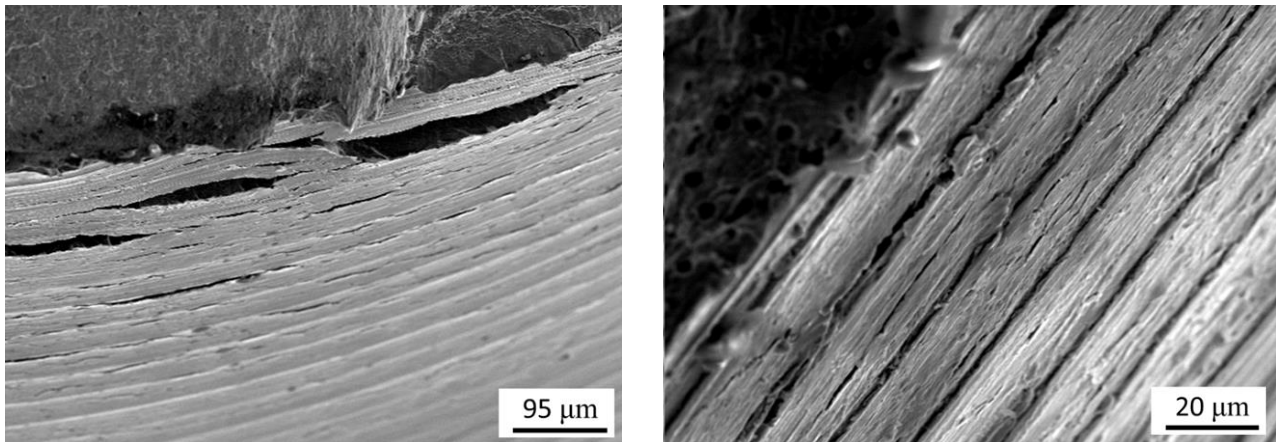


Figure 3-18 Surface cracks along the intersecting boundaries.

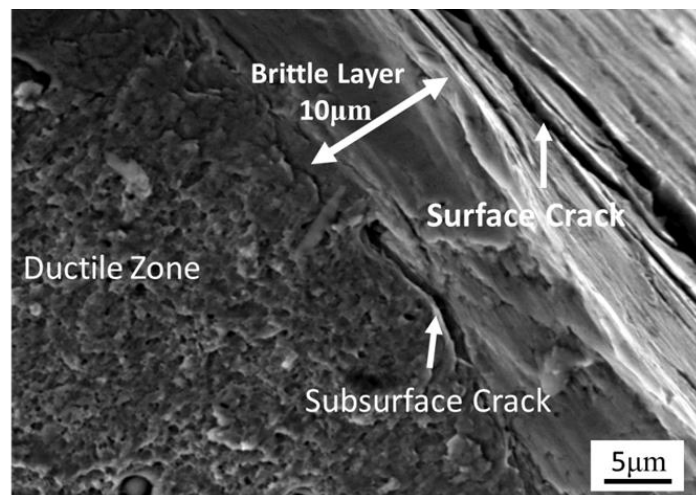


Figure 3-19 An enlarged crack edge of the final fracture zone for U2 specimen

An enlarged zone of U2 specimen was shown in Figure 3-19. Two different kinds of fractures can be observed, one is the ductile zone, in which dimple fracture can be observed and in the fracture edge a brittle layer and thickness about 10 μm was found. Between these two regions, subsurface crack was also found. On the top surface of the brittle layer, some surface cracks were obvious. During UNSM treatment, thousands of strike was carried out on the specimen surface. As the increasing of strike number, the grains in the top surface were refined into nano-size with translation gliding. At the same time the mechanics properties (yield stress and elastic modulus)

were enhanced. During fatigue test, the final fracture was formed with a high stress loading in the final test stage and even the basic materials or the surface layer fractured. Though many researchers have found the super strength of the nano-structured layer, brittle property was found for this layer and the toughness also dropped. With the different mechanics properties between the enhanced top surface and the internal materials, sub-surface cracks were formed during the high loading.

### **3.4 Conclusions**

For the quenched and tempered S45C steel, the maximum static load was 50 N. When the static load exceeded 50 N, as increase of frictional force between strike pin and specimen surface the ultrasonic system could not work in a stable state and surface destroy was observed. Higher hardness and deeper hardening zone can be obtained by the UNSM treatment when the processing density was about 68000 . Though some surface cracks could be found on the U2 specimen surface, higher fatigue limit was obtained for U2 as the reason of high compressive residual stress. The final fractures showed that weakness for the the intersecting boundaries induced by UNSM and sub-surface crack between the surface nanocrystalline layer and base metal were formed as the high loading.

# Chapter 4 Plasma Nitriding S45C steel subjected to ultrasonic nanocrystal surface modification

To improve the fatigue strength of plasma nitrided S45C steel, an ultrasonic nanocrystal surface modification (UNSM) technique with two different strike numbers (34000 times/mm<sup>2</sup> and 68000 times/mm<sup>2</sup>) was employed to modify the surface structure and properties of specimens after plasma nitriding treatment (8 h and 48 h).

## 4.1 Materials Processing

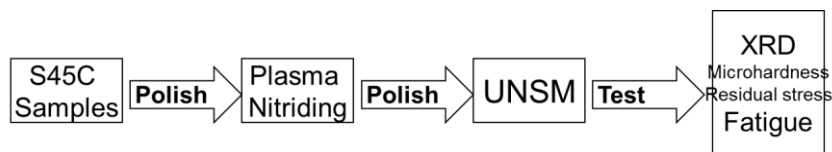


Figure 4-1 Specimens process and test

In this study plasma nitriding was employed to improve the fatigue properties. Because the fish-eye cracks induced by inclusions were observed frequently after nitriding treatment, UNSM was carried out on the nitriding specimens to study the effect of UNSM to the plasma nitriding specimens.

Table 4-1 Condition of specimen's treatment

Specimens	Plasma nitriding (Hr. )	UNSM (mm <sup>-2</sup> )
N8	8	/
N48	48	/
N8U1	8	34000
N8U2	8	68000
N48U1	48	34000
N48U2	48	68000

The plasma nitriding process was performed in a mixture gas (40% N<sub>2</sub>-60% H<sub>2</sub>) at 400 Pa. The specimens were processed at 500 °C with different nitriding time: 8 h (N8) and 48 h (N48). For hybrid surface treatments of UNSM and plasma nitriding, the parameters and process orders were shown in Table 4-1.

## 4.2 Characters of microstructure

### 4.2.1 Surface morphology

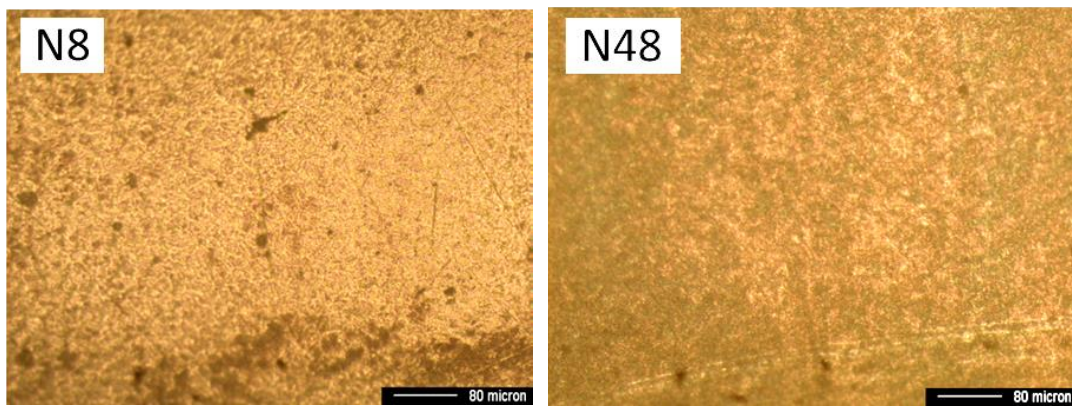


Figure 4-2 Surface morphology of the plasma nitriding specimens.

After plasma nitriding the scratches cannot be found and typical nitriding surface can be observed to replace the polishing marks by the generation of nitrides. During plasma nitriding process the surface kinetics and bulk diffusion occurred at the same time, so the surface state was affected by the growth of surface compound layer obviously. The surface morphology of before and after UNSMed specimens was shown in Figure 4-3. It is obvious that UNSMed processing marks were produced on the specimen surface. As the processing principle, these marks show parallel and as the increase of processing number these marks become more obvious. For the parallel marks, the distance between each other was approximately 70 μm. This value equals to the processing parameter of the feed rate which is 0.07 mm/rev. During surface treatment, only the surface under

the center of the tip can receive most severe plastic deformation as the reason of ball shape of the process tip. As the increase of strike number, a little growth can be observed with the surface roughness. For the nitriding samples, the UNSMed marks show unobvious as the reason of nitrides within top surface region reducing the plastic deformation of sample surface. Compared with the soft un-nitriding sample, better surface roughness can be obtained for the sample surface with higher hardness. It also means fewer surface defects produced on the nitriding sample surface.

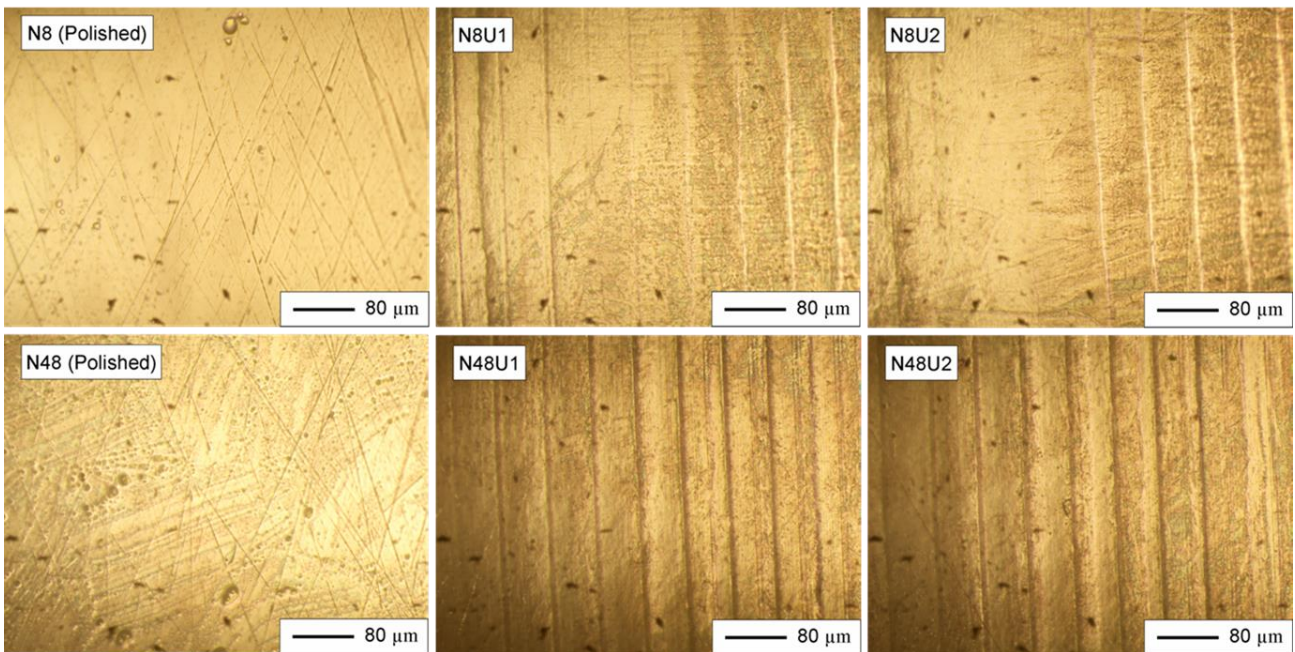


Figure 4-3 Surface morphology of the plasma nitriding specimens before and after UNSM.

The surface roughness of all the samples UNSMed before and after was measured and shown in Table 4-2. Before UNSM treatment the nitriding layer was removed and polished. The roughness of the un-UNSMed sample was about 0.173, for U1 0.150 and U2 0.160~0.165. The surface roughness is improved after UNSM process and as the increment of strike number; the value of surface roughness has a little increasing. Comparing with Suh[25], Lee[48] and Cao[8]' work, it also can be seen that UNSM is one surface treatment which not only refines the surface grain size into nano-size and gets a hard surface but also has little destroy to workpiece surface and even

improve surface roughness. This is different from the conventional surface treatment, shot pinning, which also can obtain a high compressive residual stress but also get destroy and defect on the materials surface. This may be the reason of the short distance of the strike pin about 30  $\mu\text{m}$ , the big size of shot ball and the strict control of the strike number. From the surface roughness test result, it can be conjectured that in spite of little defect brought on the sample surface, with the strike number increasing there are some faults maybe induced by the repeated strike. In the study of S45C subjected to UNSM [8], some small crack and machine mark can be found. But in this study, there is little can be found. This can be explained for the harder surface which hinders the more severe deformation destroys occurring but a larger strain induced for softer surface materials.

Table 4-2 Result of the surface roughness

specimens	Test1	Test2	Test3	Average value Ra ( $\mu\text{m}$ )	Measuring position
Un-treated	0.15	0.18	0.19	0.173	Center R
N8U1	0.17	0.13		0.165	Center R
N8U2	0.14	0.16		0.150	Center R
N48U1	0.17	0.16		0.165	Center R
N48U2	0.15	0.17		0.160	Center R

## 4.2.2 Microstructure

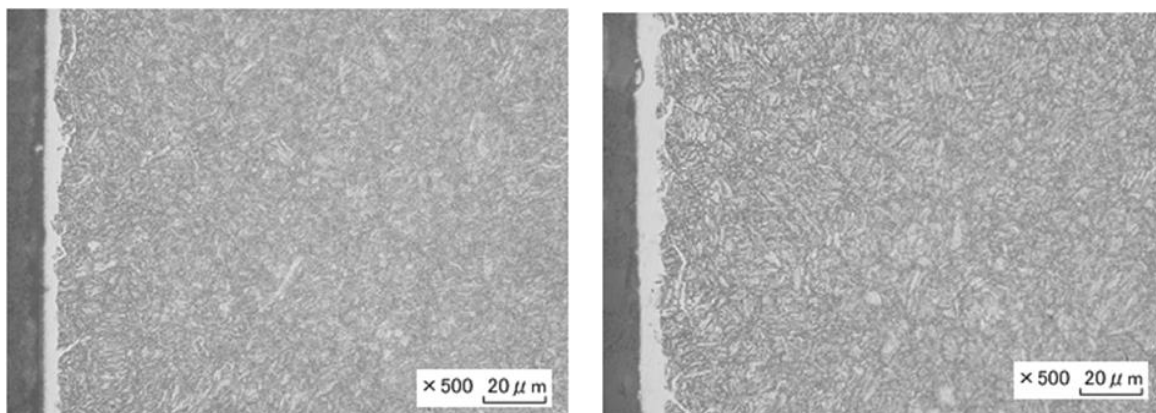


Figure 4-4 The microstructure of cross-section of plasma nitriding specimens.

After plasma nitriding, an obvious compound layer (Figure 4-4), white layer (difficult to be

etched), was produced on the top surface of the nitriding samples. For the nitriding sample, a compound layer can be found on the nitriding sample surface (approximately 3  $\mu\text{m}$  for N8 and approximately 8  $\mu\text{m}$  for N48 sample). All the UNSMed samples can be found a grain refined layer at the edges of the cross-section. However for the pre-nitriding samples (Figure 4-5), this layer is difficult to be distinguished and only some deformed grains can be found and the results show that the deformed layer induced by UNSM decreases with the increase of pre-sample surface hardness.

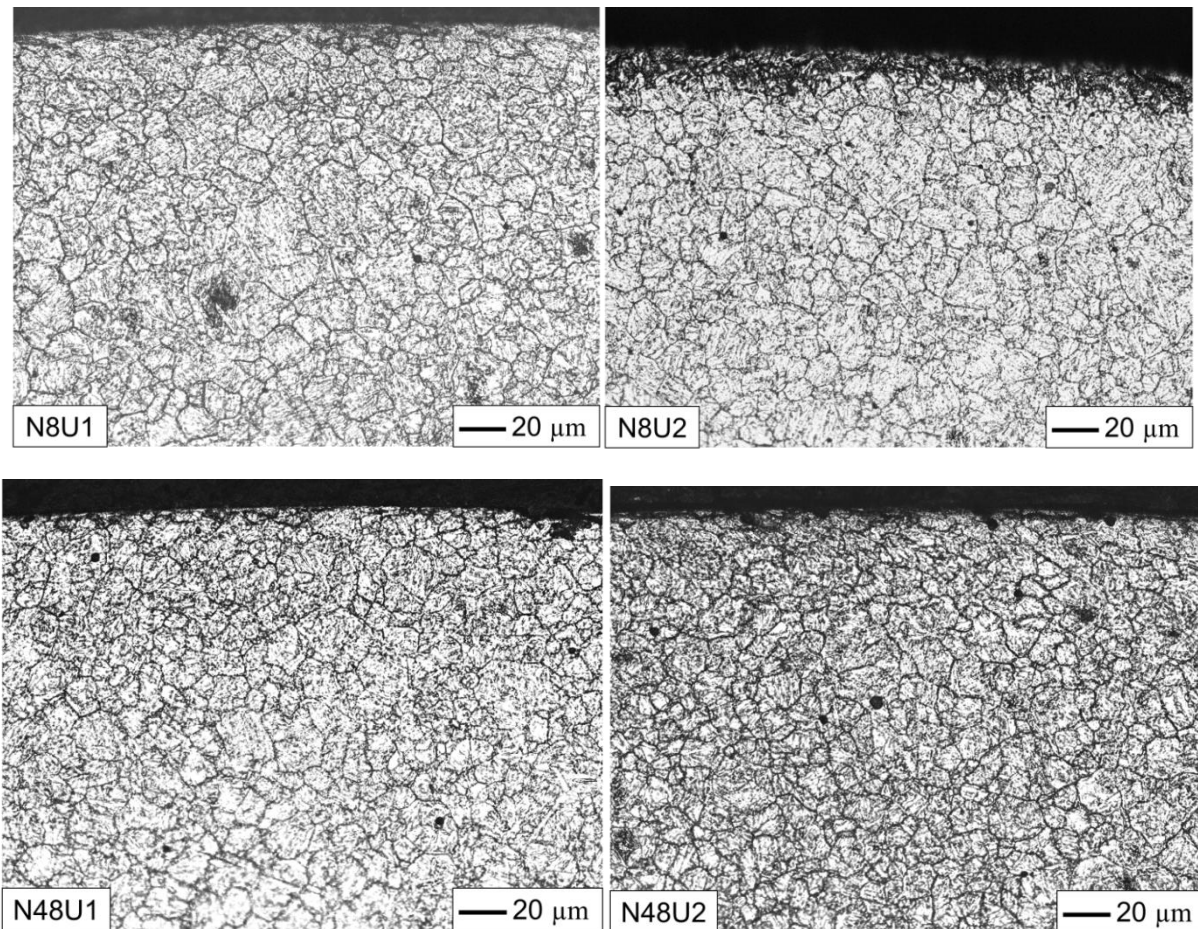


Figure 4-5 The microstructure of cross-section of nitriding specimens after UNSM.

### 4.2.3 XRD results

A compound layer and a diffusion zone were formed on the S45C samples surface zones during plasma nitriding process with the reaction and diffusion of nitrogen. Through the XRD test

(Figure 4-7), it can be seen that the compound was confirmed as  $\gamma'$ -Fe<sub>4</sub>N. The compound layers

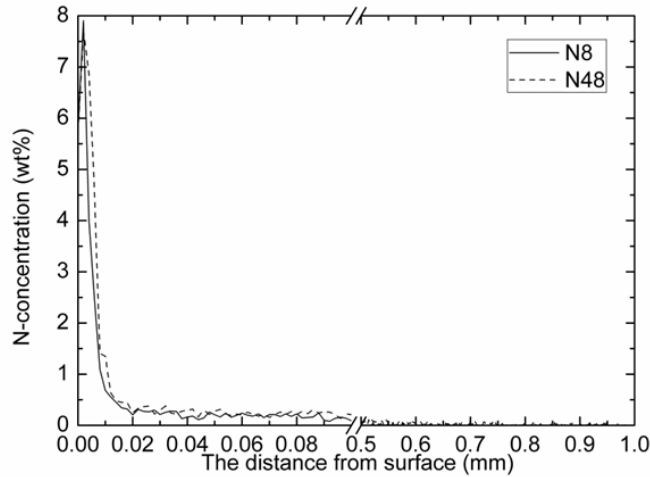


Figure 4-6 N-concentration along the cross-sectional surface of plasma nitriding samples.

were about 5  $\mu\text{m}$  for N8 samples and 10  $\mu\text{m}$  for N48. The content of nitrogen (wt %) of diffusion zones was also detected to find that the depths were about 500  $\mu\text{m}$  for N8 samples and 900  $\mu\text{m}$  for N48 (Figure 4-6). For the brittle properties of the nitrides, the surface layer about 12  $\mu\text{m}$  was removed to receive the plastic deformation easily from the UNSM treatment and so there is less nitrides inside the surface zone compared with the compound layer.

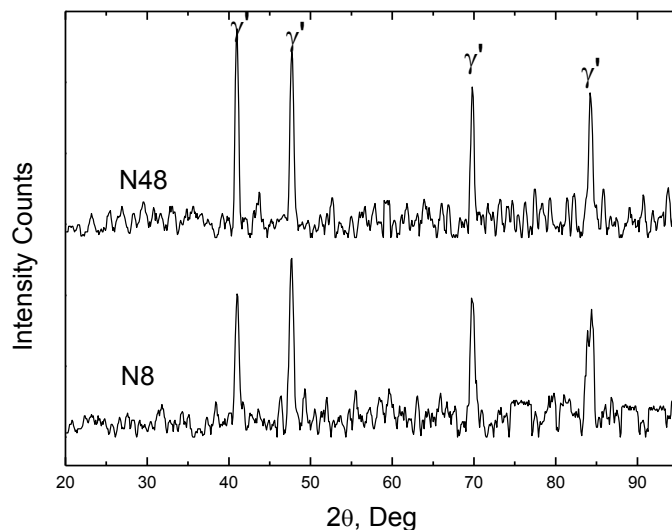


Figure 4-7 XRD patterns of the surface of plasma nitriding S45C samples (N8 and N48).

Figure 4-8 shows the XRD patterns of the samples (N8 and N48) after polishing (removing surface compound layer) and different UNSM treatment (34000 and 68000 times/ $\text{mm}^2$ ) with a quick

scanning speed. It can be seen that it is difficult to find nitrides peaks as the so little content of nitrides on the polished samples surface and only typical diffraction patterns of ferrite, (110), (200), (211), can be observed. At the same time broadened patterns can be get for both nitriding samples after UNSM treatment and broader Bragg deflection patterns can be observed with the increasing strike number. This can be attributed to that the refinement of grain size and internal strain of the crystal lattice both can induce broadening of materials typical XRD peak from which the grain size can be calculated. We can conclude that a grain refinement layer was produced on the UNSMed samples surface. From other researches[8, 25] results a nano-grain size can be get for the materials subjected to UNSM treatment. So it can be inferred that a nano-structured layer also was obtained on the surface of nitriding samples from UNSM treatment in this study.

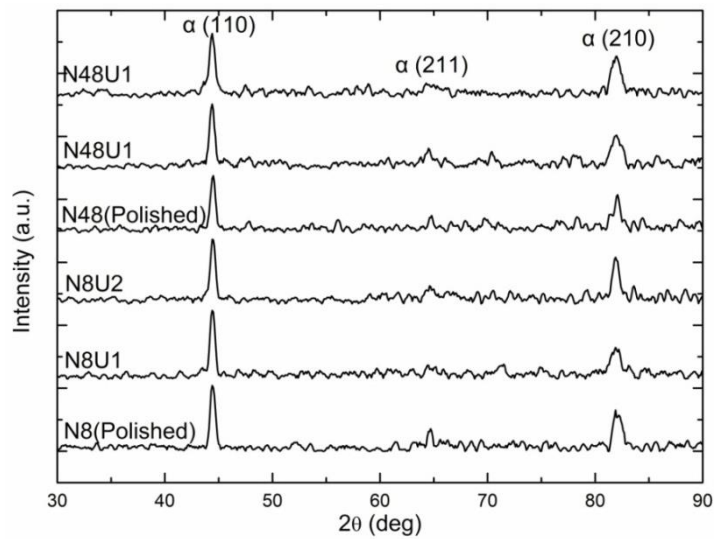


Figure 4-8 XRD patterns of the surface of plasma nitriding S45C samples (N8 and N48) polished and then

UNSMed as a function of the strike number (un-UNSMED, 34000 and 68000 strike number).

To get more information about the surface structure, the peaks were scanned slowly with 0.02 degree and 5 s duration and to get the more precise data about the state of surface nano-structure. Figure 4-9 the result of (211) peak, which was the most affected peak by the UNSM treatment, was shown. It is obvious that the diffracted intensity was affected and decreased with the nitriding time

and the strike number of UNSM treatment. All the N48 samples have a lower diffracted intensity compared with N8 samples. The values of full width at half maximum (FWHM) were also measured and find that the nitriding time have slight affection on the FWHM value of the peak for only nitriding samples. The reason is that in the diffusion zone the nitrogen mainly diffuses along the grain boundaries to react with iron element. So it has little change to the ferrite grain size and for the increasing of nitrides, the XRD patterns intensity of ferrite decreases. However a higher value of FWHM for N48 samples can be obtained after the UNSM treatment which provided severe plastic deformation on the samples surface. It means that a smaller grain size can be obtained for N48 samples. Some researchers have found that the hard second phase can get smaller grain size under the same surface treatment condition as an easier grain refinement method[49].

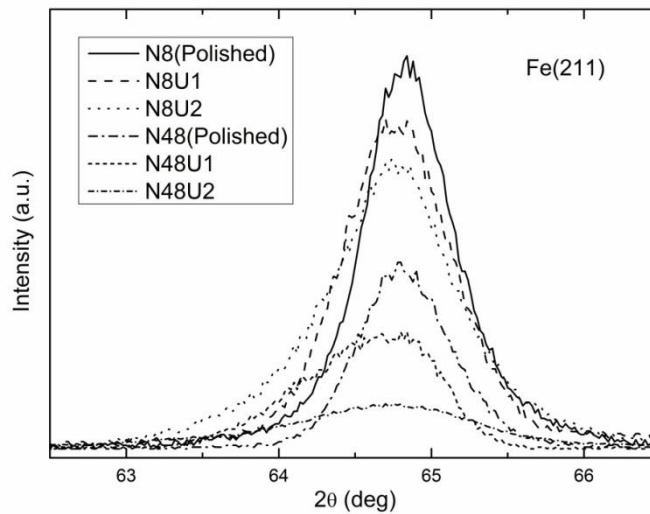


Figure 4-9 The XRD pattern of Fe (211) diffraction angles for plasma nitriding S45C (N8 and N48) samples surface with different strike number.

#### 4.2.4 Microhardness

To study the effect of UNSM on nitriding zone with various process conditions, the micro-Vickers hardness was measured for the cross-sectional samples. Figure 4-10 and 4-11 display

the hardness profile for the un-UNSMed and UNSMed samples. After UNSM treatment, there is a significant increment to the surface hardness for all the UNSMed samples. For the N8 specimens, the surface hardness increases to about 542 HV after U1 treatment and 562 HV after U2 treatment from 443 HV of un-UNSM N8 specimens and these values are higher than the un-UNSMed N48 samples. The surface hardness is also changed into 632 HV after U1 treatment and 653 HV after U2 treatment from 512 HV for N48 specimens after UNSM treatment. From the result it can be seen that increasing of strike number has no significant increment on the subsurface harness and the depth of deformation zone for the same nitriding samples. Only the surface layer about 30  $\mu\text{m}$  have a significant different with the different strike numbers. At the same time, it can be seen that the refined structured layer has different depth for the UNSMed N8 and N48 specimens. Compared with the UNSMed N8, the UNSMed N48 has a thinner refined structured layer. For all nitriding samples, the plastic deformed zone is thinner than the nitriding diffusion zone.

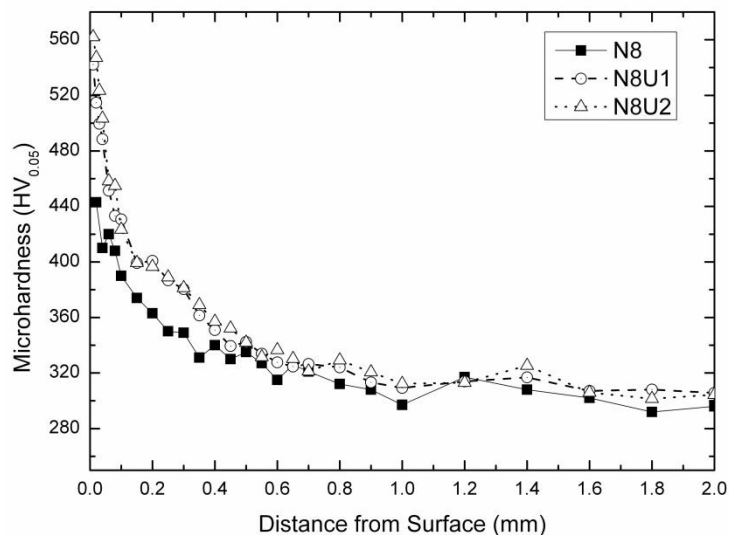


Figure 4-10 Hardness profile of un-UNSMed and UNSMed N8 specimens with different strike numbers.

As we know that there are many ways can be used to improve the materials surface hardness. In this paper, the microhardness gradient layer, called diffusion zone, of nitriding specimens is due

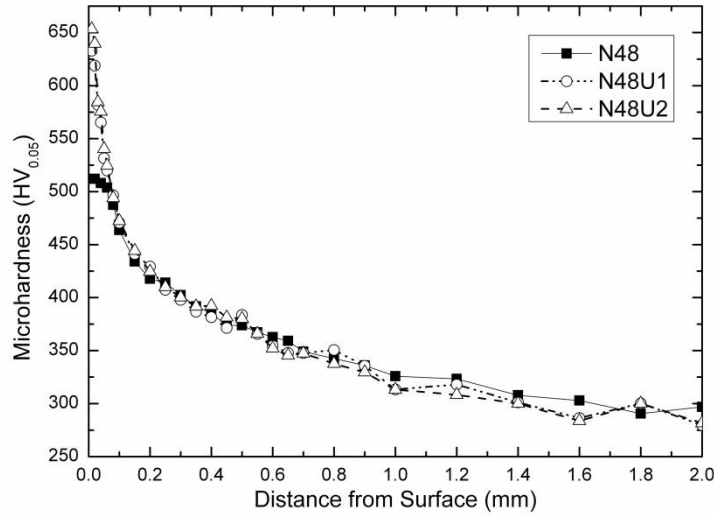


Figure 4-11 Hardness profile of un-UNSMed and UNSMed N48 specimens with different strike numbers.

to the diffused nitrogen along grain boundaries forming nitrides inside materials. The hardness value has a linearly function with N concentration. With the nitriding time increasing, a deeper diffusion zone and a harder surface can be get for more nitrogen ions dissolve into the inside of samples. On the other hand, the grain refinement also can enhance the hardness of materials according to the Hall-Patch equation. From references [47, 48], we can know that for multi-phase alloys the ferrite grain will be easier to change into nano-size because of the hard particles and get a deeper deformation zone at the same time. The ferrite is easy to refine and the dislocations begin at the multi-phase interfaces. This is different with the pure Fe which the grain boundaries are the source of dislocations. For the second phase deformation and refinement occur when the ferrite grains size is smaller than the second phase. So we can deduce that in the nitriding samples the same phenomenon also occurs. The hard nitrides play roles which induce the more dislocations and easier of the ferrite refinement. The microhardness result shows that the hardness of the N48 samples were improved more than the N8 samples after UNSM treatment. The changes for the depths of plastic deformation layer, however, are different. The N8 samples, which contain less nitride, have a deeper plastic deformation zone. This may be the reason of harder for nitrides than

carbides which hinder the plastic deformation energy from reaching the deeper zone.

#### 4.2.5 Residual stress

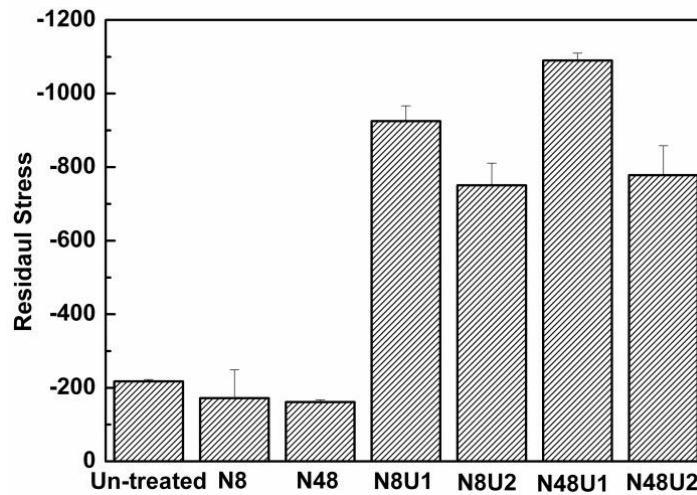


Figure 4-12 The residual stress of all samples (quenched and tempered, N8, N48, plasma nitriding samples with different UNSM treatment) on the surface of specimens was measured by XRD.

The residual stress in the surface zone of all specimens was detected and shown in Figure 4-12. It can be seen that for the untreated specimens about -200MPa residual stress was produced, and the nitriding sample have about -170MPa for nitriding 8h and -160MPa for nitriding 48h respectively. For the UNSMed nitriding specimens, a very high compressive residual stress (-925 MPa for N8U1, -750 MPa for N8U2, -1090 MPa for N48U1 and -778 MPa for N48U2) on the surface zone can be found. It is easy to find that the U1 process can induce a higher compressive residual stress than the U2 process. Whether for N8 specimens or N48, a decrease of compressive residual stress was observed after U2 treatment under the same treating condition. It is different from the result of UNSM subjected to S45C steel without nitriding treatment [8]. Compare the nitriding specimens with different nitriding time, a higher residual stress can be obtained on surface of specimens under

the same UNSM treating condition. The specimens with longer nitriding time can get a higher compressive residual stress through UNSM treatment.

The residual stress of untreated sample surface, which was induced by pre-quenching processing, decreases with the tempering time duration. For the only nitriding samples, the values of residual stress induced by nitrides produced during plasma nitriding was very close. This is the reason of the bigger volume of nitrides than the ferrite and a compressive residual stress, which has a close connection to the elements of materials, was produced. With the S<sup>2</sup>PD process, materials grains suffer large plastic deformation and high strain was produced inside grains. This kind of residual stress increases with the treating time and strike number. The reduction of residual stress of the nitriding materials may be another kind of residual stress formation. From [84], we can know that during nitriding process nitrogen not only has a reaction with iron element, but also dissolves in the ferritic matrix. This nitrogen dissolving into ferritic matrix also called as excess-nitrogen is not stable and easy to get out changing into nitrogen gas. So we can infer that with the severe plastic deformation the excess nitrogen was taken out and gathers along the boundaries or fault and combine to gas. As increasing volume of the gas, the grain receives a compressive stress and show a compressive stress. Long nitriding time will provide more excess nitrogen atoms in the ferrite matrix, so a higher residual stress can be found on the surface of N48U1 specimens. Through UNSM process dislocations and boundaries were produced in the surface zone and induce a gradient grain size along the cross-section direction. The number of dislocation and boundaries relates closely to the strike number. When increase the strike number, a smaller grain size will be produced and more boundaries and more dislocation will be produced. More space was provided for the nitrogen gas induced by severe plastic deformation treatment. So when increase the strike

number, the residual stress will decrease. This residual stress mechanism is different from the residual stress induced by nitrides and the other plastic deformation process.

## 4.3 Fatigue properties

### 4.3.1 S-N curves

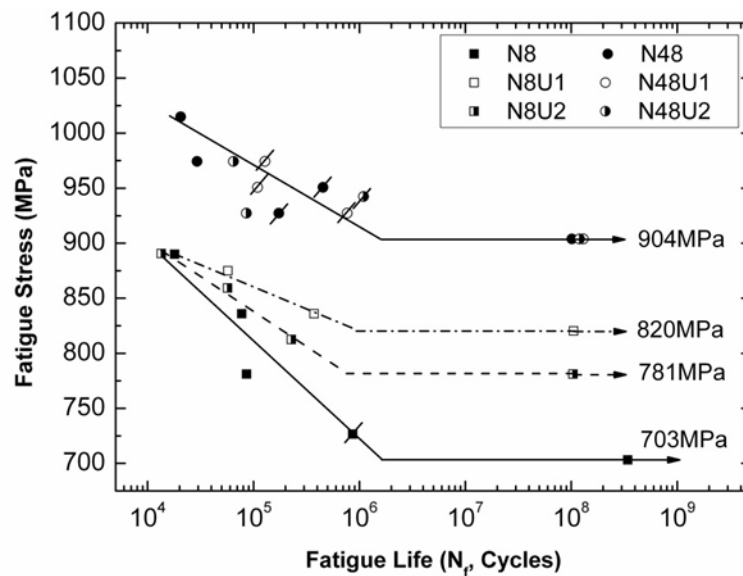


Figure 4-13 S-N curves of rotating-bending fatigue test for plasma nitriding samples before and after the UNSM treatment. (Marked as the internal factors inducing fatigue failure)

Figure 4-13 shows the fatigue test result of only plasma nitriding and post-UNSM plasma nitriding samples. The quenched and tempered S45C samples have been test and the fatigue limit is about 464 MPa with no surface treatment. After plasma nitriding, the fatigue limit has been improved to 700 MPa for N8 samples and 903 MPa for N48 samples. The fatigue strength increases as prolonging nitriding time. About 95% of the fatigue limit strength has been increased maximally by plasma nitriding treatment. For post-UNSM treatment to N8 specimens, fatigue limit was improved to 820 MPa with U1 treatment and 781 MPa with U2. The fatigue strength is still lower than N48 fatigue limit. It is obvious to find that the fatigue limit declines as the increase of strike

number to the surface of nitriding specimens. It is different with the result[8] of S45C samples with no pre-treatment subjected to UNSM and higher fatigue strength can be obtained with increase strike number. For N48 specimens without and with UNSM surface treatment, there is no different for the fatigue limit about 903 MPa and no improvement of the fatigue strength by the UNSM can be found except the crack initiation modes. The effect of UNSM on the fatigue limit weakens for the basic nitriding materials with the high fatigue strength. It is clear that though the fatigue strength can be enhanced by UNSM, the nitriding time plays a main role in improving fatigue properties.

From the S-N curves (marked point: sub-surface crack initiation), there are different performances of the fatigue test for the UNSMed N8 and UNSMed N48 samples. For N8 specimens, the fatigue failure started mainly from the surface crack initiation. Except the applied stress approaching the limit stress for N8 specimens, a sub-surface crack can be found. At the same time, a resistance can be found for the N8 specimens with the same loading for the surface crack initiation after UNSM treatment. Though nano-grains have little resistance to the crack growth [85]. The high compressive residual stress and the zone with twins and high dislocation densities produced during the process of UNSM treatment may be the main reason to hinder the initiation of fatigue crack. So the N8U1 has a higher fatigue limit stress for a higher compressive residual stress in the surface zone. For all N48 specimens, there is no improvement of fatigue strength limit and the fish-eye crack initiation is the main crack initiation mode. Especially for N48U1 all of the specimens failed from the fish-eye crack. Even the applied stress increases to 890 MPa, with the same load the N48 and the N48U2 specimens both failed from the surface crack. It is obvious that U1 treatment holds back the surface crack initiation and increases the applied stress which induces a surface crack for the harder surface and high compressive stress was produced by UNSM treatment. Harder surface

and smaller grain size was possessed for the N48U2 specimens, but a more roughness of surface was produced by U2 treatment from the surface roughness result. It can be inferred that more defects were brought into the smooth surface. From Holzapfel's study[86], we can know that the higher loading will induce high decline of the residual compressive stress and a sharp cutoff appear at the first cycle loading. The residual stress of N48U1 after  $10^3$  cycles with the fatigue limit load was -430 MPa and declines about 60% comparing with the initial residual stress. So it can be inferred that a decline of residual stress in the sub-surface zone also occurred and little effect of the residual stress impacts to the crack initiation resistance for the sub-surface crack initiation under high loading.

### 4.3.2 Fatigue fractures

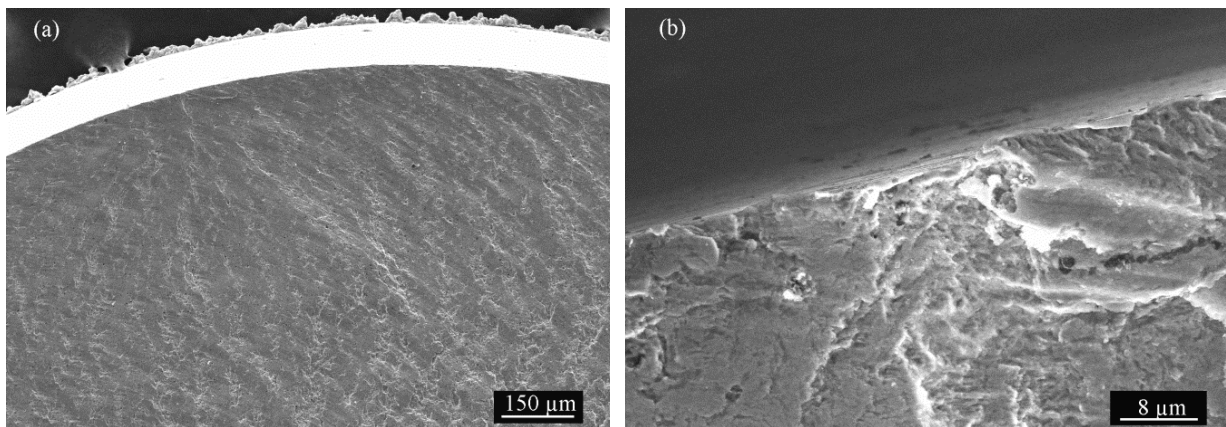


Figure 4-14 (a) The fracture of failure specimen induced by the surface defect (N8U1, 835.9MPa,  $3.7 \times 10^5$ ); (b) enlargement of the surface defect induced by UNSM and obvious machining mark can be found.

To study the reason of the fatigue failure of the specimens under different surface treatment, the fractures of the failure samples were observed by SEM and shown in Figure 4-14 and 4-15. All the fracture surfaces were observed and analyzed to find that the reason that inducing fatigue failure can be classified into three kinds: PSBs, surface defects and sub-surface defects. For post-UNSM

nitriding specimens, the surface defects and inclusions inside materials were the main reasons inducing materials failure. For the post-UNSMed N8 specimens, the surface crack failure all started from the surface defects. In Figure 4-14b, a clear machine mark can be found in the surface defect. The sub-surface crack, named as fish-eye, always starts from a nonmetallic inclusion and propagate around the centre of inclusion, Figure 4-15. To study the composition of the inclusions inducing fatigue failure, the energy-dispersive X-ray spectroscopy (EDX) was employed to detect and analyze. The results show that the inclusions mainly contain Al, Ca, Mg, Si and O elements Figure 4-16. These oxides play the roles in centre inducing stress concentration and the initiation crack of fatigue failure.

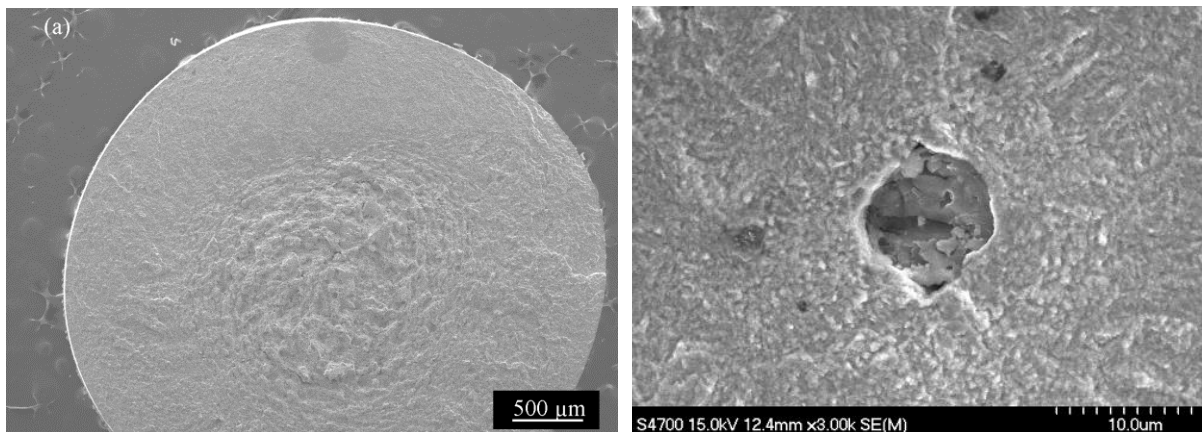


Figure 4-15 (a) The fracture of failure specimen induced by sub-surface defect (N48U1, 974.2MPa,  $1.3 \times 10^5$ ); (b) enlargement of the initiation crack (facet area and inclusion).

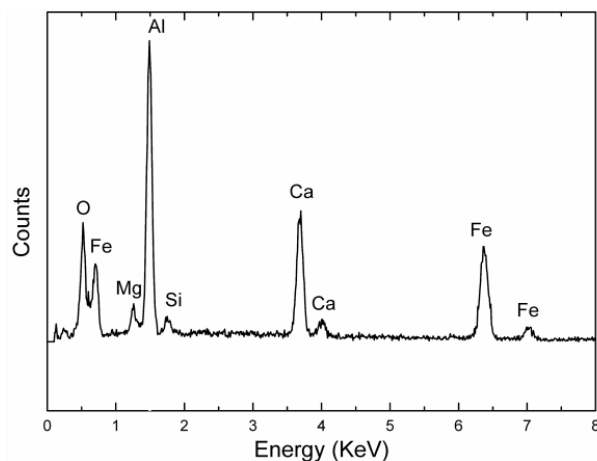


Figure 4-16 Chemical composition of the inclusion.

## 4.4 Effect to the fatigue crack initiations

As high compressive residual stress was produced in the surface region, the effect of UNSM to the fatigue crack initiations were also investigated. The depth of the center of inclusion position from the surface,  $D_{inclusion}$ , was measured from the SEM images. The result is shown in Figure 4-17. It can be found that after UNSM treatment the position of inclusion inducing a fish-eye crack was affected and move to deeper depth for UNSMed N48 samples and for UNSMed N8, there is no fish-eye crack initiation mode inducing samples failure. From the result of micro-hardness, also the plastic deformation layer was measured about 200  $\mu\text{m}$  for UNSMed N48 samples and 500  $\mu\text{m}$  for UNSMed N8. No crack source in the severe plastic deformation layer. It may be the result of the hardness enhancement, the grain refinement of the deformation layer and the residual stress in this layer hinder a fish-eye crack initiation.

According to Murakami [86], a facet area, which has rough propagation surface, is often found in the fish-eye crack. To analyze the effect of UNSM on the internal fractures, the depth and the diameter of the inclusions, facet area, and flat area were measured. The stress intensity factor  $\Delta K$  also can be calculated from Eq.4.1 [86]. The  $\sigma_{at}$  is the nominal stress at the fracture origin and area is the area of inclusion, facet area or flat area. We calculated  $\Delta K_{facet}$  of specimens with the facet area size notch and showed it in Figure 4-18.

$$\Delta K = 0.5 \cdot \sigma_{at} \sqrt{\pi \sqrt{area}} \quad (\text{Sub-surface}) \quad (4.1)$$

It can be found that  $\Delta K_{facet}$  is a constant value about 4.08  $\text{MPa}\cdot\text{m}^{1/2}$ . The nitriding time and UNSM treatment, there is no different for the sub surface crack failure specimens.

The threshold stress intensity factor,  $\Delta K_{th}$ , also can be predicted by Eq.4.2 [86]. The area is

the area of the inclusion inducing a sub-surface crack initiation.  $H_v$ , we choose the hardness value of the position which is the depth of the inclusion from surface. With measurement of the size of all inclusion of the fish-eye crack failure samples, the  $\Delta K_{th}$  can be statistically about  $4.51 \text{ MPa}\cdot\text{m}^{1/2}$ .

$$\Delta K_{th} = 3.3 \times 10^{-3} (H_v + 120) (\sqrt{\text{area}})^{1/3} \quad (4.2)$$

It is clear that the  $\Delta K_{\text{facet}}$  is very close to the  $\Delta K_{th}$  calculated from Murakami equation. So we can use this equation to predict the fatigue limit stress. Also we can infer that there is a small  $\Delta K$  for the sub-surface crack propagation from  $\Delta K_{\text{inclusion}}$  to  $\Delta K_{\text{facet}}$  with a different propagation mechanism which has been explained as hydrogen induced crack. Less effect of residual stress and hardness of surface impact to fish-eye induced fatigue failure for deeper of the position of the inclusion.

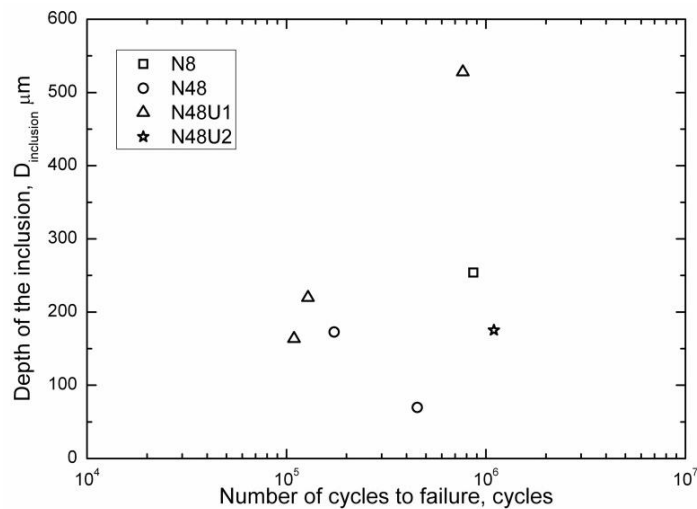


Figure 4-17 The depth of inclusion position affected by UNSM

The  $\Delta K_{th}$  is an important parameter that we can use to predict the fatigue strength. In this study the surface and sub-surface crack initiation is the main fatigue failure reason. The fatigue test result shows that when the applied stress approaching to the fatigue limit stress, the surface crack always induces the sample failure. Even in some papers in ultrahigh cycle fatigue test a very low applied stress also can lead to fatigue failure. As many factors impact on the surface  $\Delta K_{th}$  and it is

difficult to obtain the shape of the surface crack induced by PSBs, but we can infer that these values are bigger than  $\Delta K_{\text{facet}}$  and  $\Delta K_{\text{inclusion}}$ . It is easy to conclude that under same low applied stress, the sub-crack is easy to nucleate than the smooth surface crack. When the applied stress increases, as a long time will be spent from  $\Delta K_{\text{inclusion}}$  to  $\Delta K_{\text{facet}}$  for fish-eye crack propagation[87], the surface crack is easier to nucleate and propagate. It explains the phenomenon that sub-crack initiation always induces fatigue failure with loading stress approaching the fatigue limit stress.

From the fracture observation result, for the post-UNSM nitriding specimens, the defect inducing surface crack on the surface of specimens can be clearly observed. Fernandez pariente' study [9] have shown that with shot peening to nitriding materials surface,  $\Delta K_{\text{th surface crack}}$  can be improved and bigger than  $\Delta K_{\text{th nitriding}}$ . So there is more improvement for  $\Delta K_{\text{th N8U1}}$  than  $\Delta K_{\text{th N8U2}}$ . For post-UNSMed N48 specimens, though, also a harder surface can improve the surface  $\Delta K_{\text{th}}$  to a higher value, the no improvement of sub-surface  $\Delta K_{\text{th}}$  results in no improvement of the fatigue limit. All in all U1 process brought fewer defects and bigger residual stress to the materials surface than U2 process, better fatigue properties can be get for both N8 and N48 specimens.

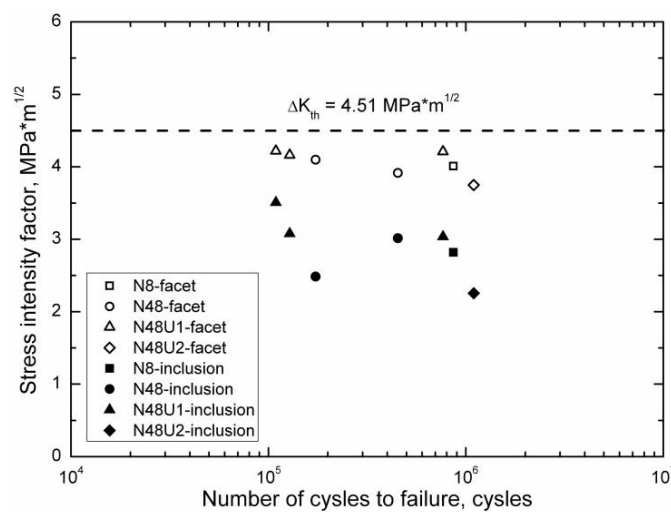


Figure 4-18  $\Delta K$  calculated from facet area and inclusion area.

## 4.5 Conclusions

1. A plastic deformation layer and smooth surface can be produced after UNSM treatment; a smaller grains size can be get with the increasing number of UNSM; for N48 specimens' surface a smaller grain size can be get compared with N8 specimens.
2. The surface microhardness can be effectively enhanced by UNSM treatment and the value increases with the increasing process number; in the same condition a thicker plastic deformation layer can be obtained for N8 sample.
3. High compressive residual stress was produced on the all sample surface zone after the UNSM treatment and a decline of the residual stress was found as the increasing of striking number with the same static loading for both N8 and N48 specimens.
4. For the N8 samples high residual compressive stress hinds the fish-eye crack initiation and slows the growth of fatigue crack. For the N48 samples, UNSM have no improvement to the fatigue limit stress and the increasing process number will induce the more surface crack failure as the increasing of surface roughness.
5. The UNSM treatment deepens inclusion position for the plastic deformation layer, hard surface, and residual stress induced by UNSM treatment.
6. For the failure samples induced by fish-eye crack, the  $\Delta K_{\text{facet}}$  was found as a constant value about  $4.08 \text{ MPa}\cdot\text{m}^{1/2}$  and closed to the value  $4.5 \text{ MPa}\cdot\text{m}^{1/2}$  predicted through the hardness of materials.

# Chapter 5 Effect of pre-ultrasonic nanocrystal surface modification to plasma nitriding S45C steel

In this chapter, the main content is about the effect of pre-ultrasonic nanocrystal surface modification to the result of plasma nitriding. Gradient microstructures with two different grain sizes and depths were produced on the surface layer of S45C steel by ultrasonic nanocrystal surface modification (UNSM). The plasma nitriding at 500 °C for 8 h and 48 h was employed to process the UNSMed sample surface and investigate the surface properties.

## 5.1 Preparation of specimens

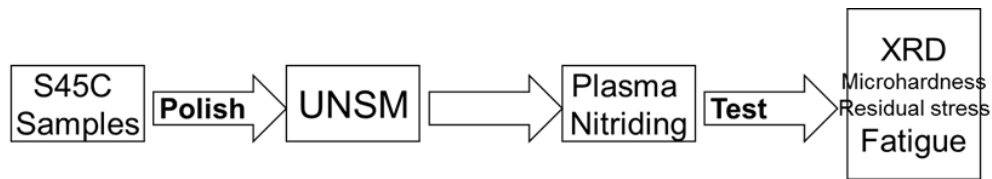


Figure 5-1 Specimens processing

Table 5-1 Condition of specimen's treatment

Specimens	UNSM (mm-2)	Plasma nitriding (hr.)
U1N8	34000	8
U2N8	68000	8
U1N48	34000	48
U2N48	68000	48

Increasing the depth of nitriding diffusion zone can enhance the fatigue obviously. In this study the pre-UNSM was employed to provide more grain boundaries for the nitriding diffusion. The

same plasma nitriding condition was used. The specimens processing orders were shown in Figure 5-1. The UNSM parameters and nitriding time were listed in Table 5-1.

## 5.2 Characters of microstructure

### 5.2.1 Surface morphology

The surface morphology of specimens after pre-UNSM and plasma nitriding was shown in Figure 5-2. During plasma nitriding the surface was changed for the adsorption and the decomposition of nitrides. It can be found that little effect of plasma nitriding to the marks produced by UNSM.

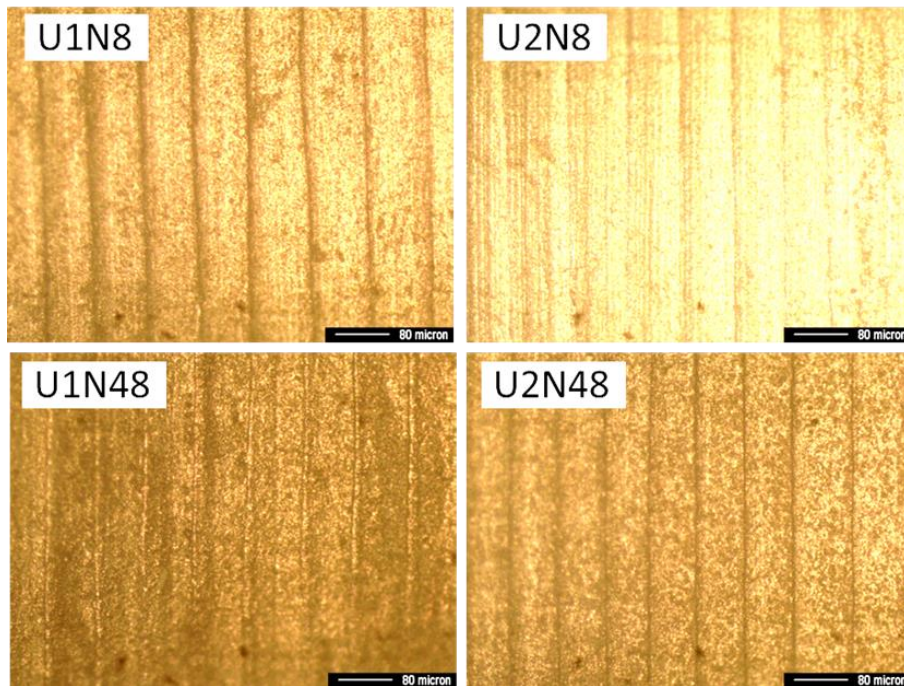


Figure 5-2 Surface morphology of specimens after pre-UNSM and plasma nitriding.

### 5.2.2 Microstructure

After nitriding, both the un-UNSM and UNSM treated samples were cut and polished to

observe the microstructures of the cross-section. The microstructure of the plasma nitriding samples without UNSM and with UNSM (UNSM34000 and UNSM68000) at 500 °C for different nitriding times (8 h and 48 h) are shown in Figure 5-3. The typical white layers of the nitrides compound, which were difficult to etch, can be found in all samples. A grain refined zone, which is significantly different from the untreated nitriding samples, was observed in pre-UNSMed nitriding samples. The surface region can be divided into three zones from the surface to the core: a compound layer, a nitriding refined grains zone and a nitriding coarse grains zone. The grains in the grain-refined zone are stroked into small grains, and the shapes of the grains are difficult to distinguish under an optical microscope. This zone is different from the basic material without the

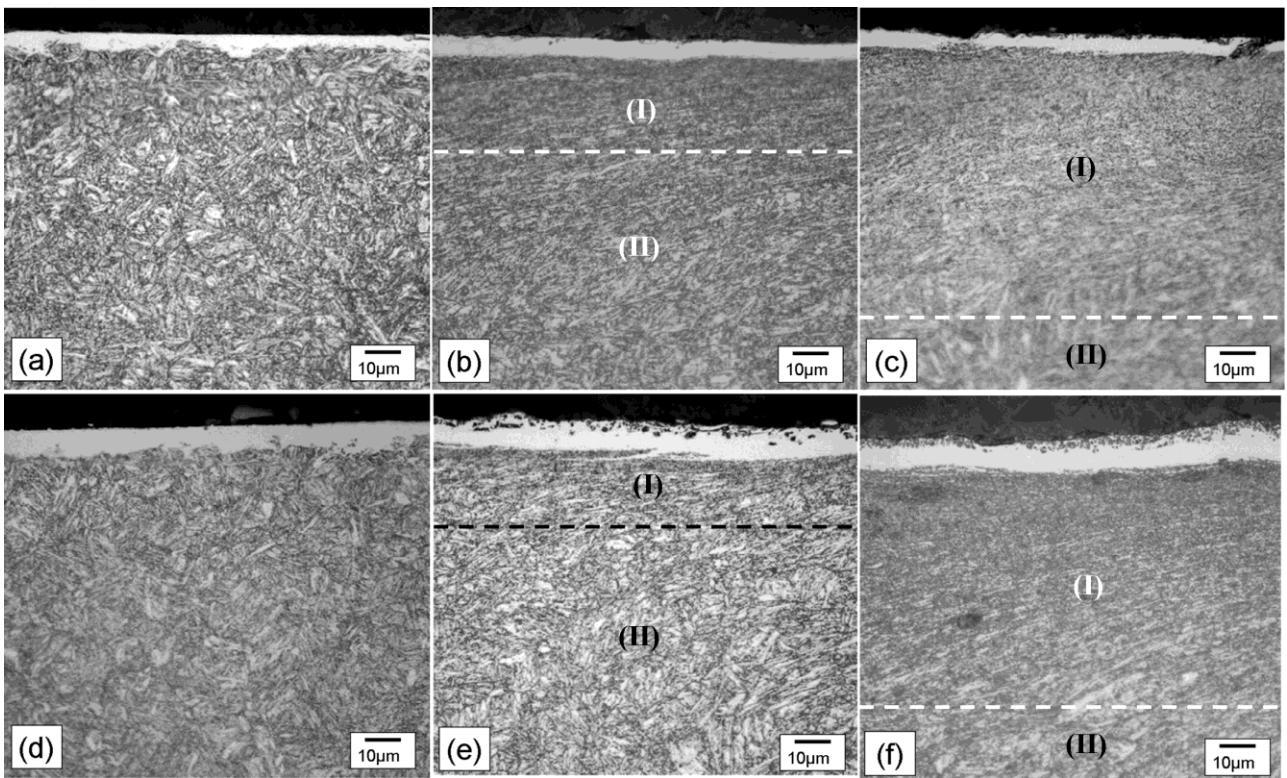


Figure 5-3 Cross-sectional optical images of the plasma nitriding 8 h (a, un-UNSMed; b, UNSM 34000; c, UNSM 68000) and 48 h (d, un-UNSMed; e, UNSM 34000; f, UNSM 68000); zone I was nitriding refined grains zone and

zone II was nitriding coarse grains zone.

pre-UNSM treatments, whose grains are needle-like and have a length of approximately 10 μm. The

depths of this grain-refined zone measured approximately 40  $\mu\text{m}$  for UNSM34000 and approximately 98  $\mu\text{m}$  for UNSM68000 on average. For the top surface layer, the grains have been refined into a nano-size from the XRD results of the UNSMed specimens. From Ref.[8], it can be found that the nano-grains' layer may be approximately 2  $\mu\text{m}$  with UNSM34000 and 30  $\mu\text{m}$  with UNSM68000 for S45C steel for the same UNSM condition. Therefore, not only does the nano-grain layer thickness increase with the strike number, but the depth of the grain-refined zone also increases with a larger strike number.

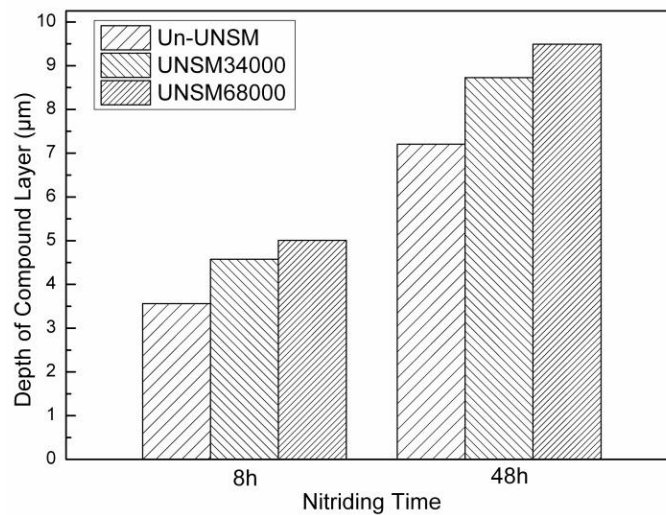


Figure 5-4 The thickness of compound layer was produced for 8 h and 48 h with different pre-treatment (un-UNSMed, UNSM 34000 and UNSM 68000).

A morphology change of the compound layer can also be observed from the micrographs. The un-UNSM samples have a smooth outside surface and an uneven internal face for the compound layer. However, the opposite phenomenon can be found for the nitriding UNSMed sample. The internal compound face is smooth, but the outside surface is uneven, induced by the obvious flaking. During the nitriding process, the nitrogen atoms diffuse not only along the grain boundaries but also into the crystal lattice to form the nitrides. For a large grain, the surface compound layer tends to grow along the direction of the grain boundaries, so the un-smooth internal face was formed as a

serrated shape. When the surface grains were refined into a small size and even nano-size, there were more boundaries to provide more diffusion channels and a reaction face. The grain is too small to impact the growth direction of the compound layer, so the nitriding compound layer can form uniformly. The average thickness of the compound layers was also measured and is presented in Figure 5-4. The surface nano-grain promotes an increase in the nitriding compound thicknesses. However, the nitriding time is still the major parameter that controls the growth of the compound layer. A longer nitriding time induces a thicker nitriding compound layer. Larger strike numbers of UNSM result in a smaller grain size and deepen the grain refinement layer. The samples with the smaller grain size and the deeper nano-grain layer can develop a thicker compound layer for the nitriding 8 h and 48 h samples. At a later stage of the nitriding treatment, the grain refinement zone still contributes to the growth of the compound layer, and there is more growth of the compound layer for the nitriding 48 h samples. Compared with the other nitriding nano-structured surface test [28, 69], there is less of an increase in the compound layer thickness. This may be the reason for the high nitriding temperature, which induces the growth of the nano-grains and causes more nitrides to hinder the growth of the compound layer.

### **5.2.3 XRD results**

The compound layer was analyzed by the XRD and is shown in Figure 5-5. The X-ray patterns show that only  $\gamma'$ -Fe<sub>4</sub>N, which can be found, was the main phase composing the white layer. The test result shows that the  $\gamma'$ -Fe<sub>4</sub>N phase produced on the sample surface with the plasma nitriding process can also be found in many other research results [35, 56, 88]. T. Hirsch [55] has found that in the N<sub>2</sub>-H<sub>2</sub> gas mixture, the  $\gamma'$ -Fe<sub>4</sub>N phase was formed before the nucleation of the  $\epsilon$ -Fe<sub>2-3</sub>N phase,

and a lower temperature was needed to form the  $\epsilon$ -Fe<sub>2-3</sub>N phase with the plasma nitriding process. We can infer that the main phase of the compound layer was  $\gamma'$ -Fe<sub>4</sub>N and that the plasma condition makes the nucleation of the  $\epsilon$ -Fe<sub>2-3</sub>N phase difficult. Because of the curved surface and the thick compound layers of the specimens, the  $\alpha$ -Fe is difficult to detect. Comparing the XRD results of all samples after different treatments, it is difficult to find a significant variation among these peaks. Therefore, it is easy to conclude that the pre-UNSM treatment and the nitriding time have no effect on the formation of the surface nitriding phase and that changing the grain size does not change the composition of the nitriding phase under this nitriding treatment at 500 °C. This result is different from the low temperature nitriding test [28, 69], in which the pre-S<sup>2</sup>PD treatment can impact the composition of the compound layer. The reason may be the high temperature (500 °C), long nitriding time and the method of the plasma nitriding treatment, which induces the growth of the nano-grain on the specimen's surface and weakens the effect of the grain size on nitride formation.

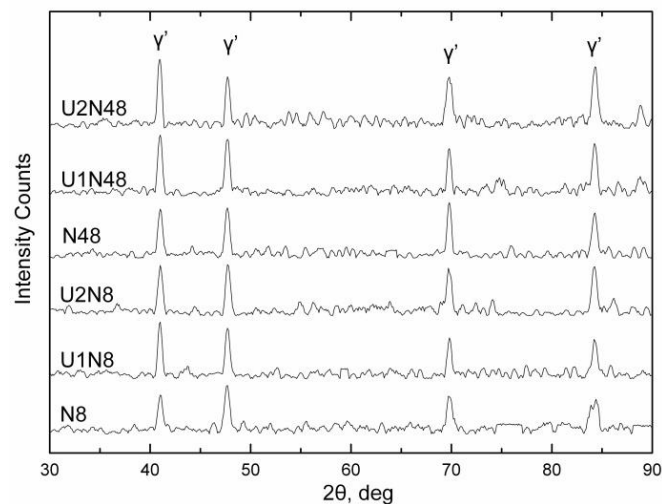


Figure 5-5 X-ray diffraction patterns of the plasma nitriding un-UNSMed, UNSM 34000 and UNSM 68000 S45C specimens (8 h and 48 h).

## 5.2.4 Microhardness

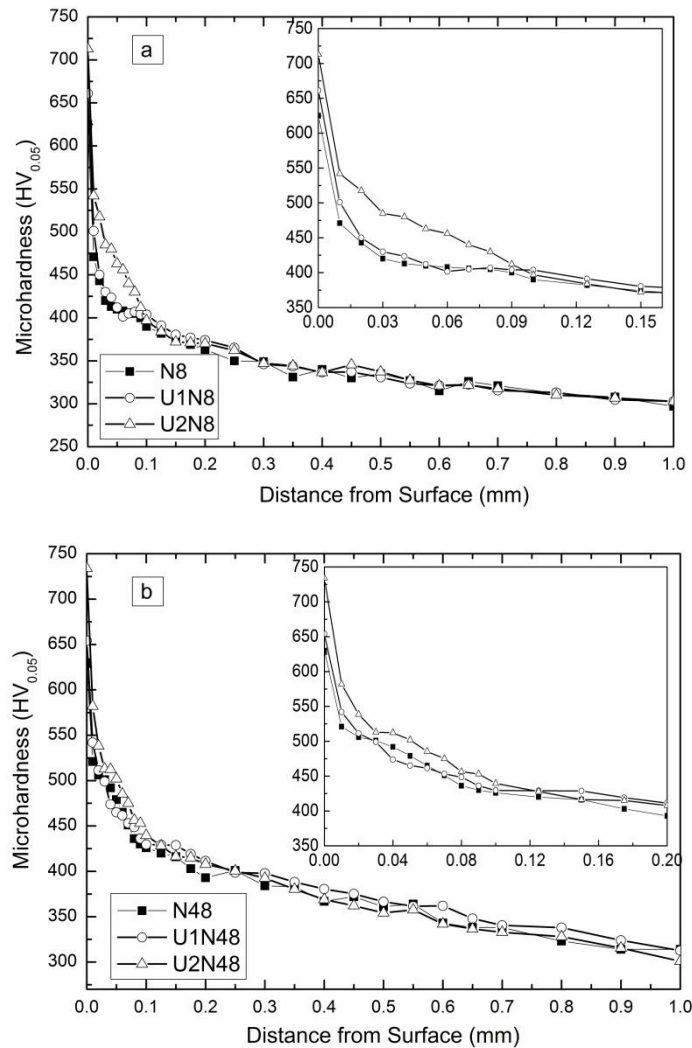


Figure 5-6 The microhardness profiles of plasma nitriding specimens for 8 h (a) and for 48 h (b) specimens.

The micro-hardness of the cross-section of all samples was also measured and is shown in Figure 5-6. There is a certain effect of the pre-UNSM treatment on the plasma nitriding result. The enhanced zones can be divided into two zones: the compound layer zone and the diffusion zone. For the UNSM68000, the nitriding sample surface hardness for nitriding 8 h and 48 h was significantly enhanced to approximately 734 HV and 713 HV, respectively. In Fig. 6a, there is an enhanced zone of approximately 90  $\mu\text{m}$  for the hardness of U2N8, the microhardness value of which is even higher than the N48 sample and significantly higher than the un-UNSMed and the pre-UNSM34000

sample. The hardness value decreases quickly and becomes the same with the un-UNSMed sample at a depth of approximately 90  $\mu\text{m}$ . The same result can also be found for the sample of nitriding 48 h. From the results, it is difficult to distinguish the nitriding refined grains zone and the nitriding coarse grains zone from the hardness test results, especially for the pre-UNSM34000 samples. By the rule of 10% above the core hardness, the depth can be calculated as approximately 0.5 mm for the 8 h samples and 0.9 mm for the 48 h. The pre-treatment has no effect on the depth of the diffusion zone, and only a significant enhancement of the surface zone of approximately 90  $\mu\text{m}$  (UNSM68000), which is close to the grain refinement zone (98  $\mu\text{m}$ ), was obtained from the metallographic results. It was shown that only the nitriding refined grains zone has a higher hardness than the un-UNSMed sample. The reason is that the surface nitride  $\gamma\text{-Fe}_4\text{N}$  was quickly produced in a short time, and more nitrides were obtained in this zone.

### **5.3 Effect to nitrogen diffusion**

To study the effects of the grain-refined layer on the plasma nitriding of samples, the N-concentration along the cross-section of the nitriding samples was measured and is shown in Figure 5-7. The results show that the N-concentration of all samples from the highest surface gradually dropped from approximately 7 %-8 % (wt.%) to 0 % at a depth of 500  $\mu\text{m}$  for nitriding 8 h and 800  $\mu\text{m}$  for 48 h. The depth of the diffusion zone can be concluded to be approximately 500  $\mu\text{m}$  for 8 h and 800  $\mu\text{m}$  for 48 h. The same diffusion depths can be found for all samples with the same nitriding time. This result is also obtained from the microhardness results. The only difference between the un-UNSMed and UNSMed samples was the zone in the top surface, where more nitrogen was absent for the UNSMed samples. A decrease of the top surface nitrogen concentration

was observed for the nitriding 48 UNSMed samples, a larger decrease was found for the N48U2

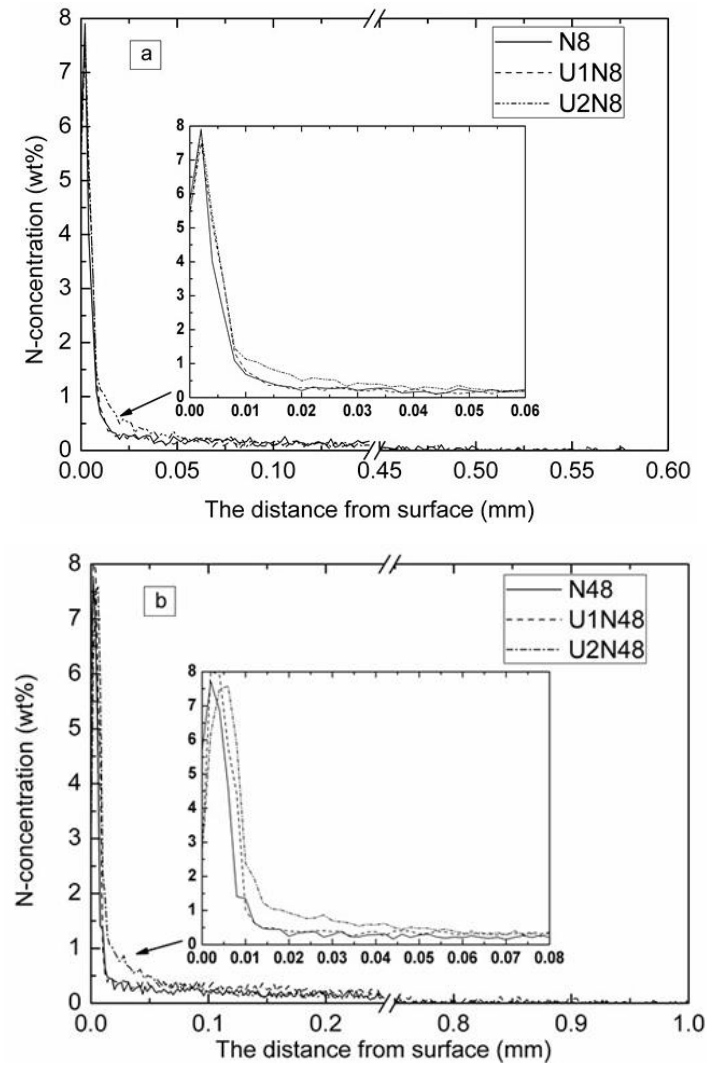


Figure 5-7 N-concentration along the cross-sectional surface of plasma nitriding specimens for 8 h (a) and for 48 h (b).

sample and the N-concentration in top surface is dropped to approximately 3 %. In Figure 5-7a, we can see that the compound layer of the UNSMed sample is a little thicker than that of the un-UNSMed sample, and a region (50  $\mu\text{m}$ ) where more nitrogen was detected than for the pre-UNSM 34000 and the un-UNSMed sample was found for the pre-UNSM 68000 sample beneath the compound layer, even more than was found for the nitriding 48 h sample. However, beneath the 50  $\mu\text{m}$  zone, the nitrogen concentration becomes less than that of the N48 samples and has the same

value compared with the other N8 samples. Between the pre-UNSM 34000 sample and the un-UNSMed sample, it is difficult to find this difference in the nitriding 8 h condition. For all the nitriding 48 h samples, the same result is also found. The nitrogen enrichment zone of nitriding 48 h pre-UNSM68000, however, is deeper (approximately 80  $\mu\text{m}$ ) than the nitriding 8 h samples (approximately 50  $\mu\text{m}$ ). For nitriding 48 h pre-UNSM34000, an inconspicuous zone approximately 30  $\mu\text{m}$  was also found.

The results above show that the gradual grain-refined layer with a nano-structured surface produced by UNSM enhances the nitrogen diffusion only near the top surface zone and has little effect on deep diffusion even with a long nitriding time at 500 °C. On the top surface, the highest nitrogen concentration of all samples was detected and similar concentrations of approximately 7~8 % were found. This result is lower than that reported in other research [28, 71], which was approximately 10~12 %. The reason is that the compound layer only contains the  $\text{Fe}_4\text{N}$  phase and little or no  $\text{Fe}_{2-3}\text{N}$  phase. For the nitriding 48 h UNSMed samples, a decrease of the nitrogen concentration on the top surface may be the reason for the defects (Figure 5-3e, f and Figure 5-11b, c) induced by the plasma nitriding. For microstructure from the UNSMed sample surface, the grain size increases as the depth increases. For the nano-sized grain, the nitrogen reaction is very easy and has a quick reaction with the ferrite even at a low nitriding temperature (300 ~ 400 °C) [28, 64, 66, 69-71]. When the grain size grows, it is difficult to nitride these grains in a short time. From the test result, we find that the UNSMed layers promoted the formation of compound layers and the diffusion of nitrogen in the surface zone, and as nitriding time increases, this phenomenon becomes more visible. It can also be found that with the refined grain, the distribution of the nitrogen concentration in the surface zone is smooth, and a wave line was used to obtain the nitrogen content

distributed within the N48 samples. The UNSMed grain refined layer can also produce a stable gradual distribution of the nitrogen concentration.

We conclude that the grain-refined layer produced by UNSM has a great effect on the diffusion of nitrogen, and the reaction with iron for a small grain size provides more boundaries and a larger reaction surface for the plasma nitriding treatment. However, when only the grain size in the surface zone is comparable to a nano-grain, the diffusion and permeation of nitrogen depend mainly on the nitriding time. Therefore, obtaining a smaller grain size and a deeper grain-refined layer is good for the nitriding process.

## 5.4 Fatigue behavior

### 5.4.1 S-N curves

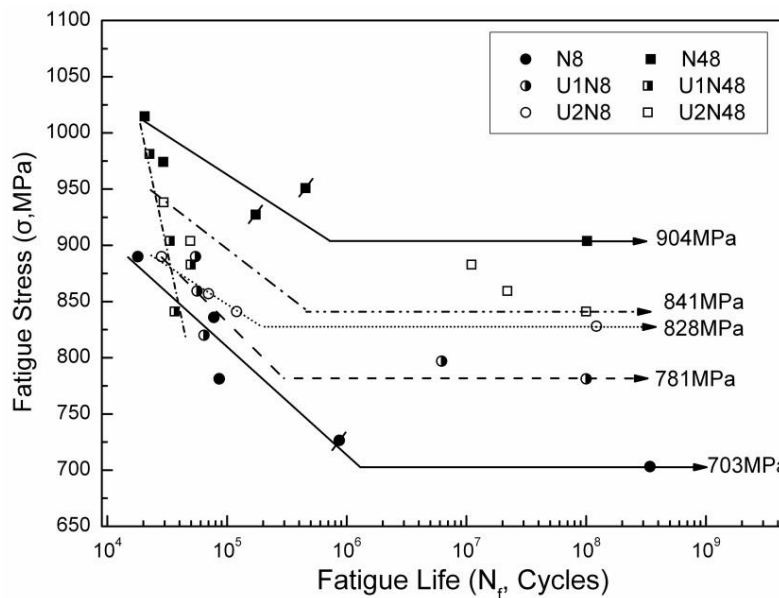


Figure 5-8 S-N curves of rotating-bending fatigue test for plasma nitriding samples with different pre-surface treatment: un-UNSMed; UNSM 34000; UNSM 68000 (Marked as the internal factors inducing fatigue failure).

The fatigue test was employed to test the fatigue properties, and the typical S-N curves are

presented in Figure 5-8. The nitriding 8 h and 48 h samples were tested, and the limit strengths were approximately 703 MPa and 904 MPa, respectively. With the pre-UNSM treatment, the U1N8 fatigue limit increased to 781 MPa, and the fatigue limit increased to 828 MPa for U2N8. For the nitriding 48 h, however, all the fatigue limit strengths decreased. The fatigue limit of the U2N48 samples dropped to approximately 841 MPa, which is almost the same as U2N8. It is difficult to confirm the limit strength for U1N48 because of the small number of specimens. Only the U1N48 sample quickly fractured and failed during the fatigue test.

## 5.4.2 Fatigue fracture

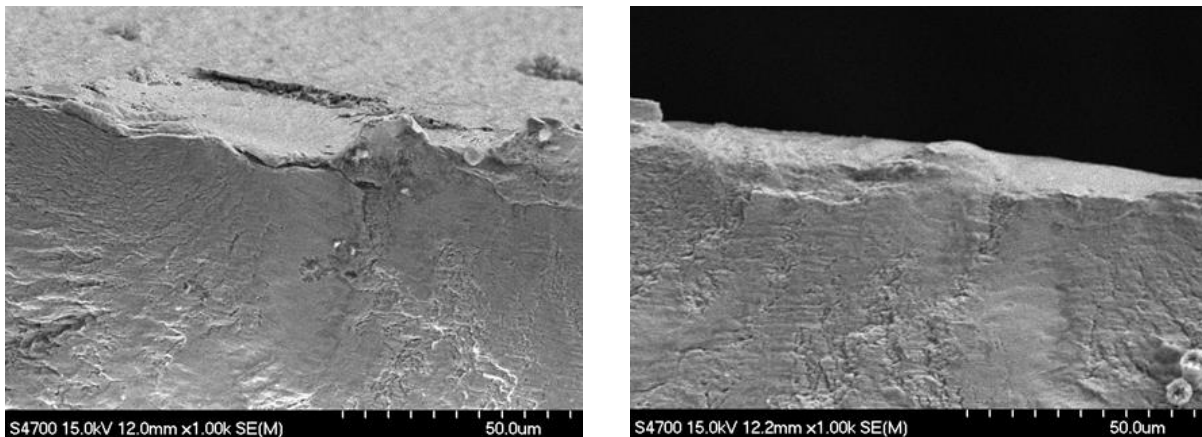


Figure 5-9 (Left) The fracture surface of failure specimen induced by surface defect (U1N48, 974.2 MPa,  $3.32 \times 10^4$ ); (Right) fatigue crack induced by the surface spalling.

For the only nitriding samples, the failure of the fatigue sample can be separated into two types: one is the crack initiation from the surface and the other is the sub-surface crack induced by inclusion, as shown in Figure 5-10, such as aluminum oxide, calcium oxide or other oxides detected by EDX (shown in Figure 5-10, right). All of these inclusions have different properties than the basic material, iron, and induce a stress concentration to produce a sub-surface crack. For the nitriding 48 h of the UNSMed specimens, the fatigue failure began at the specimen's surface, as

shown in Figure 5-9. From the enlargement of the surface defect, it can be observed that there is surface layer flaking, and some small voids can be found where the flaking occurs, as shown in Figure 5-9 left. For the nitriding 8 h of the UNSMed specimens, it was difficult to find a defect from the fracture surface that induces the fatigue failure. From the fatigue result, the enhancement of the fatigue strength may be the reason for the enrichment of nitrogen at the surface region, which has more nitrides compared with the un-UNSMed specimens and exerts a higher hardness.

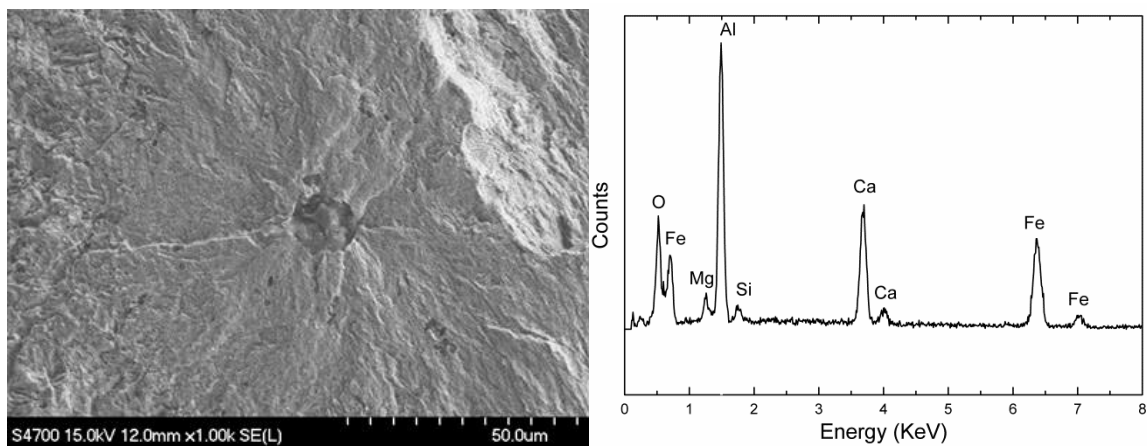


Figure 5-10 (Left) The fracture surface of failure specimen induced by the sub-surface inclusion (U1N48, 841 MPa,  $3.64 \times 10^4$ ); (Right) EDX data on the inclusion.

## 5.5 Voids induced by plasma nitriding in nanocrystal surface

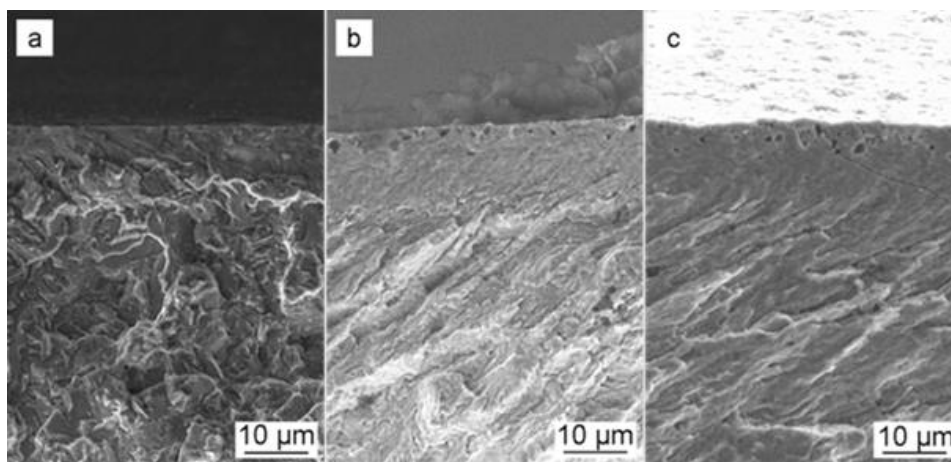


Figure 5-11 The fracture surface edges of all plasma nitriding 48 specimens (a, un-UNSMed; b, UNSM

34000 and c, UNSM68000) and small voids were produced in the zone near the top surface only for nitriding 48 h UNSMed specimens.

The fracture edges of all nitriding 48 h with and without the UNSM treatment were scanned by SEM and are shown in Figure 5-11. From the results, we can see that with the pre-UNSM treatment, a few voids can be produced in the surface compound layer, which cannot be found in all nitriding 8 h samples. By increasing the strike number and decreasing the grain size, the amount of voids increases and their location grows to a deeper position, approximately 5  $\mu\text{m}$  for U1N48 and approximately 7  $\mu\text{m}$  for U2N48. Even a crack initiating from the surface voids can be observed, as shown in Figure 5-11c. The U2N48 surface was also scanned by SEM (Figure 5-12). Some voids in

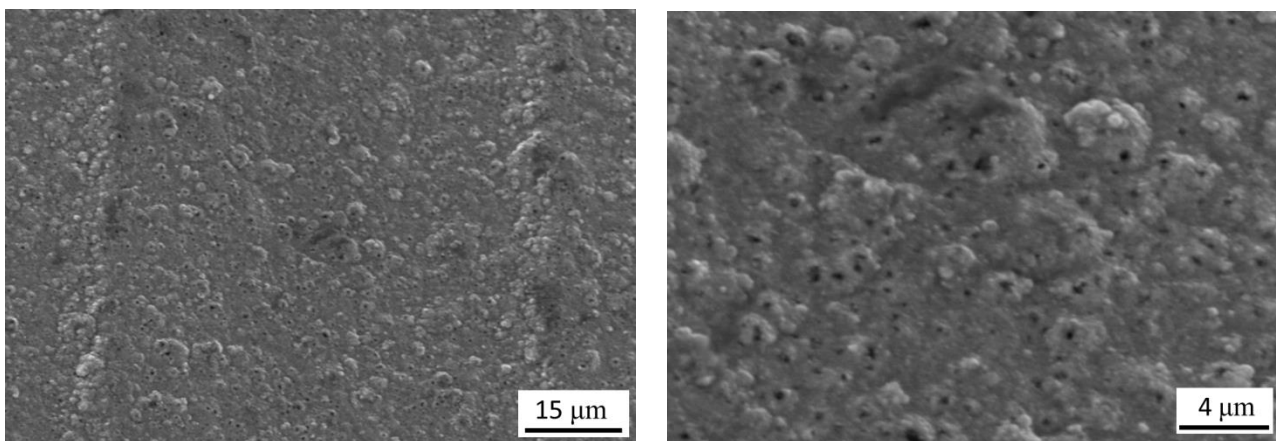


Figure 5-12 SEM images of surface voids in the top surface of U2N48 specimen.

the top surface layer can be observed. During plasma nitriding, many nitrogen and hydrogen atoms are produced to impact the workpiece surface in an accelerating field. However, as the nitriding time increases, the nitrogen and hydrogen atoms diffusing through the nitriding compound layer decrease because of the increase of the thick compound layer. As the nonidentity between ion production and diffusion, excess nitrogen and hydrogen atoms can be induced easily and easily coagulate to molecular nitrogen and hydrogen gas within the compound layer to produce small voids. With the excess gas, the prolonged nitriding (>100 h) treatment [84] and the thicker

compound layer [57], it can be easy to find a defect within the compound layer zone. At the same time it can be seen in Figure 5-13, more defects (grain boundaries and defects as the nanocrystalline surface layer induced by UNSM), the defects are easy to gather during the adsorption and the decomposition of nitrides.

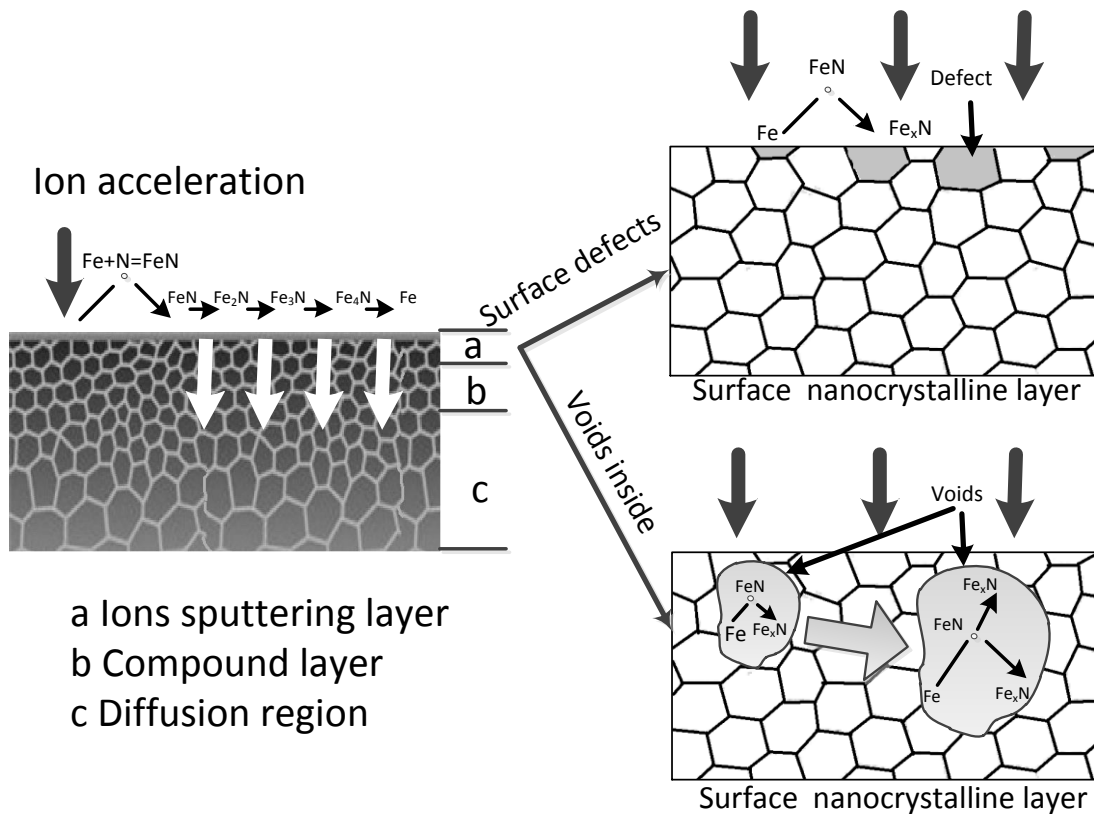


Figure 5-13 Mechanism of the formation of voids during plasma nitriding nanocrystalline surface layer.

From the results above, we find that the compound layer is the main reason for hindering nitrogen from diffusing into the material sub-surface. With pre-UNSM treatment, a decrease of the grain size on the sample surface introduced more boundaries and faults and promoted the reaction of nitrogen with the elements in the materials. It becomes easier to form a thicker compound layer, and too thick of a compound layer will hinder more nitrogen ions and induce more excess nitrogen within the compound layer. Using pre-UNSM 68000, a larger number of deeper voids can be

induced than using the pre-UNSM 34000 treatment. Even flaking of the compound layer can be found, and no void can be found for the un-UNSMed samples at the same nitriding time. Although there are a larger number of deeper voids in the nitriding UNSM68000 specimen surface, for the fatigue test, the enrichment of the nitrogen diffusion region makes the U2N48 have a higher fatigue limit than the U1N48 specimens because the compound layer does not determine the fatigue strength [89].

## 5.6 Conclusions

(1) The UNSM treatment was employed to obtain two different grain sizes and depths of a grain refined layer on the S45C specimen's surface.

(2) As the surface grain became refined, the thickness of the compound layer was improved and thickened with the increase of the UNSM strike number. There was no effect of the pre-UNSM treatment on the nitriding phase, and the entire nitriding compound layers were  $\gamma'$ -Fe<sub>4</sub>N mainly.

(3) A nitrogen enrichment region was formed in the pre-UNSM68000 specimens after nitriding treatment for a short time. The grain refined layer had little effect on the deeper region diffusion of nitrogen atoms.

(4) The fatigue limit of the pre-UNSM samples for nitriding increased slightly, but for nitriding 48 h, it decreased as surface defects developed (small voids inducing surface layer flaking).

(5) During the 48 h nitriding treatment, some defects (small voids) can be produced within the compound layer as the reason of nanocrystalline surface and too thick compound layer for the nitriding pre-UNSMed sample.

# Chapter 6 Conclusions

## 6.1 Main conclusions

As presented in previous chapters, the surface treatments of UNSM, plasma nitriding, and the hybrid surface treatments of these two treatments. The effect of UNSM parameters to microhardness, residual stress, surface morphology and microstructure were investigated. For the hybrid surface treatments, effect of UNSM to plasma nitriding specimens and pre-UNSM to the results of plasma nitriding were studied. In this chapter, a brief summary of the whole research and major conclusions obtained in the study are given.

1. For the quenched and tempered S45C steel, the maximum static load was 50 N. When the static load exceeded 50 N, as increase of frictional force between strike pin and specimen surface the ultrasonic system could not work in a stable state and surface destroy was observed. Smaller surface nanocrystalline, higher hardness and deeper hardening zone, and higher compressive residual stress can be obtained by the UNSM treatment when the processing density was about 68000. Though some surface cracks could be found on the U2 specimen surface, higher fatigue limit was obtained for U2 as the reason of high compressive residual stress. The final fractures showed that weakness for the intersecting boundaries induced by UNSM and sub-surface crack between the surface nanocrystalline layer and base metal were formed as the high loading.

2. A plastic deformation layer and smooth surface can be produced after UNSM treatment; a smaller grains size can be get with the increasing number of UNSM; for N48 specimens' surface a smaller grain size can be get compared with N8 specimens. The surface microhardness can be effectively enhanced by UNSM treatment and the value increases with the increasing process

number; in the same condition a thicker plastic deformation layer can be obtained for N8 sample. High compressive residual stress was produced on the all sample surface zone after the UNSM treatment and a decline of the residual stress was found as the increasing of striking number with the same static loading for both N8 and N48 specimens. For the N8 samples high residual compressive stress hinders the fish-eye crack initiation and slows the growth of fatigue crack. For the N48 samples, however, UNSM has no improvement to the fatigue limit stress and the increasing process number will induce the more surface crack failure as the increasing of surface roughness. The UNSM treatment deepens inclusion position for the plastic deformation layer, hard surface, and residual stress induced by UNSM treatment. For the failure samples induced by fish-eye crack, the  $\Delta K_{\text{facet}}$  was found as a constant value about  $4.08 \text{ MPa}\cdot\text{m}^{1/2}$  and closed to the value  $4.5 \text{ MPa}\cdot\text{m}^{1/2}$  predicted through the hardness.

3. The UNSM treatment was employed to obtain two different grain sizes and depths of a grain refined layer on the S45C specimen's surface. As the surface grain became refined, the thickness of the compound layer was improved and thickened with the increase of the UNSM strike number. There was no effect of the pre-UNSM treatment on the nitriding phase, and the entire nitriding compound layers were  $\gamma'$ -Fe<sub>4</sub>N mainly. A nitrogen enrichment region was formed in the pre-U2 specimens after nitriding treatment for a short time. The grain refined layer had little effect on the deeper region diffusion of nitrogen atoms. The fatigue limit of the pre-UNSM samples for nitriding increased slightly, but for nitriding 48 h, it decreased as surface defects developed (small voids inducing surface layer flaking). During the 48 h nitriding treatment, some defects (small voids) can be produced within the compound layer as the reason of nanocrystalline surface and too thick compound layer for the nitriding pre-UNSMed sample.

## 6.2 Future work

Although some work have been done on the hybrid surface treatments of ultrasonic nanocrystal surface modification and plasma nitriding, it is complex for the surface layers produced by the hybrid surface treatments. Much further work is required for realizing the relation between nanocrystalline and thermal diffusion. With this technology more hybrid surface treatments can be

The future work can be focused on the following aspects of the hybrid surface treatments.

1) In our research, high compressive residual stress could be obtained for plasma nitriding specimens subjected to UNSM as the reason of the enhancement of surface layer strength by nitride phase. Though a thin grain refined layer could be produced, a higher residual stress can provide certain advantages, for example, fatigue life and surface corrosion. The UNSM also can be combined with the surface hardening technology to obtain a high compressive residual stress in a short time.

2) In this work we found that at high nitriding time only dozens of micron diffusion can be enhanced and after the long nitriding time surface defects were found. Thermal diffusion at low temperature and nitriding with short time should be studied. Now there are many studies about the effect of surface nanocrystalline to the nitrogen potential with gas nitriding. Little research can be found for the role of surface nanocrystalline during plasma nitriding and the effect to the phase.

# References

- [1] Fang TH, Li WL, Tao NR, Lu K. Revealing Extraordinary Intrinsic Tensile Plasticity in Gradient Nano-Grained Copper. *Science* 2011; 331:1587-1590
- [2] Wang YM, Wang K, Pan D *et al.* Microsample tensile testing of nanocrystalline copper. *Scripta Materialia* 2003; 48:1581–1586.
- [3] Wang ZB, Lu J, Lu K. Wear and corrosion properties of a low carbon steel processed by means of SMAT followed by lower temperature chromizing treatment. *Surface and Coatings Technology* 2006; 201:2796-2801.
- [4] Mordyuk BN, Prokopenko GI, Vasylyev MA, Iefimov MO. Effect of structure evolution induced by ultrasonic peening on the corrosion behavior of AISI-321 stainless steel. *Materials Science and Engineering A* 2007; 458:253–261.
- [5] Tao N, Tong W, Wang Z *et al.* Mechanical and Wear Properties of Nanostructured Surface Layer in Iron Induced by Surface Mechanical Attrition Treatment. *Journal of Materials Science & Technology* 2003; 19:563-566.
- [6] Ting W, Dongpo W, Gang L *et al.* Investigations on the nanocrystallization of 40Cr using ultrasonic surface rolling processing. *Applied Surface Science* 2008; 255:1824–1829.
- [7] Webster GA, Ezeilo AN. Residual stress distributions and their influence on fatigue lifetimes. *International Journal of Fatigue* 2001; 23:S375–S383.
- [8] Cao XJ, Pyoun YS, Murakami R. Fatigue properties of a S45C steel subjected to ultrasonic nanocrystal surface modification. *Applied Surface Science* 2010; 256:6297-6303.
- [9] Fernandez pariente I, Guagliano M. About the role of residual stresses and surface work hardening on fatigue  $\Delta K_{th}$  of a nitrided and shot peened low-alloy steel. *Surface and Coatings Technology* 2008; 202:3072-3080.
- [10] Cao XJ, Yang F, Murakami R. Fatigue properties of a S45C steel with plasma nitriding. Auckland (New Zealand), International Conference on Structural Integrity and Failure SIF 2010; 7.
- [11] Sirin SY, Sirin K, Kaluc E. Effect of the ion nitriding surface hardening process on fatigue behavior of AISI 4340 steel. *Materials Characterization* 2008; 59:351-358.
- [12] Zhang JW, Lu LT, Shiozawa K *et al.* Effects of nitrocarburizing on fatigue property of medium carbon steel in very high cycle regime. *Materials Science and Engineering A* 2011; 528:7060-7067.
- [13] Soleimani SMY, Mashreghi AR, Ghasemi SS, Moshrefifar M. The effect of plasma nitriding on the fatigue behavior of DIN 1.2210 cold work tool steel. *Materials & Design* 2012; 35:87-92.
- [14] GOLGEL B, GENEL K. Fatigue strength improvement of a hard chromium plated AISI 4140 steel using a plasma nitriding pre-treatment. *Fatigue and Fracture of Engineering Materials and Structures* 2005; 29:105–111.
- [15] Cruz PDI, Ode'n M, Ericsson T. Influence of plasma nitriding on fatigue strength and fracture of a B-Mn steel. *Materials Science and Engineering A* 1998; 242:181 – 194.
- [16] Wang Z, Jiang C, Gan X *et al.* Influence of shot peening on the fatigue life of laser hardened 17-4PH steel. *International Journal of Fatigue* 2011; 33:549–556.
- [17] Chan KS. Roles of microstructure in fatigue crack initiation. *International Journal of Fatigue* 2010; 32:1428-1447.
- [18] Murakami Y, Yokoyama NN, Nagata J. Mechanism of fatigue failure in ultralong life regime. *Fatigue and Fracture of Engineering Materials and Structures* 2002; 25:735-746.
- [19] Shiozawa K, Morii Y, Nishino S, L.Lu. Subsurface crack initiation and propagation mechanism in high-strength steel in a very high cycle fatigue regime. *International Journal of Fatigue* 2006; 28:1521–1532.
- [20] Grad P, Reuscher B, Brodyanski A *et al.* Mechanism of fatigue crack initiation and propagation in the very high cycle fatigue regime of high-strength steels. *Scripta Materialia* 2012; 67:838–841.
- [21] Ashrafzadeh F. Influence of plasma and gas nitriding on fatigue resistance of plain carbon (Ck45) steel. *Surface*

and Coatings Technology 2003; 173-174:1196-1200.

- [22] Holzapfel H, Schulze V, Vohringer O, Macherauch E. Residual stress relaxation in an AISI 4140 steel due to quasistatic and cyclic loading at higher temperatures. *Materials Science and Engineering A* 1998; 248 9 – 18.
- [23] Zhuang WZ, Halford GR. Investigation of residual stress relaxation under cyclic load. *International Journal of Fatigue* 2001; 23:S31–S37.
- [24] Torres MAS, Voorwald HJC. An evaluation of shot peening, residual stress and stress relaxation on the fatigue life of AISI 4340 steel. *International Journal of Fatigue* 2002; 24:877–886.
- [25] Suh C, Song G, Suh M, Pyoun Y. Fatigue and mechanical characteristics of nano-structured tool steel by ultrasonic cold forging technology. *Materials Science and Engineering: A* 2007; 443:101-106.
- [26] Tian JW, Villegas JC, Yuan W *et al.* A study of the effect of nanostructured surface layers on the fatigue behaviors of a C-2000 superalloy. *Materials Science and Engineering: A* 2007; 468-470:164-170.
- [27] Lu K, J.Lu. Nanostructured surface layer on metallic materials induced by surface mechanical attrition treatment. *Materials Science and Engineering A* 2004; 375–377:38–45.
- [28] Tong WP, Tao NR, Wang ZB *et al.* Nitriding Iron at Lower Temperatures. *Science* 2003; 299:686-688.
- [29] Ke L, Jian L. Surface Nanocrystallization (SNC) of Metallic Materials-Presentation of the Concept behind a New Approach. *Journal of Materials Science & Technology* 1999; 15:193-197.
- [30] Mordyuk B, Milman Y, Iefimov M *et al.* Characterization of ultrasonically peened and laser-shock peened surface layers of AISI 321 stainless steel. *Surface and Coatings Technology* 2008; 202:4875-4883.
- [31] Tao NR, Sui ML, Lu J, Lu K. Surface Nanocrystallization of Iron Induced by Ultrasonic Shot Peening. *NanoStructured Materials* 1999; 11:433-440.
- [32] Tao NR, Wang ZB, Tong WP *et al.* An investigation of surface nanocrystallization mechanism in Fe induced by surface mechanical attrition treatment. *Acta Materialia* 2002; 50:4603-4616.
- [33] Wu X, Tao N, Hong Y *et al.* Microstructure and evolution of mechanically-induced ultrafine grain in surface layer of AL-alloy subjected to USSP. *Acta Materialia* 2002; 50:2075-2084.
- [34] Li WL, Tao NR, Lu K. Fabrication of a gradient nano-micro-structured surface layer on bulk copper by means of a surface mechanical grinding treatment. *Scripta Materialia* 2008; 59:546–549.
- [35] Cao XJ, Yang F, Murakami R. Fatigue properties of a S45C steel with plasma nitriding. Auckland (New Zealand), *International Conference on Structural Integrity and Failure* 2010; 7.
- [36] Dai K, Shaw L. Comparison between shot peening and surface nanocrystallization and hardening processes. *Materials Science and Engineering: A* 2007; 463:46-53.
- [37] Arifvianto B, Suyitno, Mahardika M. Effects of surface mechanical attrition treatment (SMAT) on a rough surface of AISI 316L stainless steel. *Applied Surface Science* 2012; 258:4538–4543.
- [38] Villegas JC, Dai K, Shaw LL, Liaw PK. Nanocrystallization of a nickel alloy subjected to surface severe plastic deformation. *Materials Science and Engineering A* 2005; 410–411:257–260.
- [39] Umemoto M. Nanocrystallization of Steels by Severe Plastic Deformation. *Materials Transactions* 2003; 44:1900-1911.
- [40] Umemoto M, Todaka Y, Tsuchiya K. Formation of Nanocrystalline Structure in Steels by Air Blast Shot Peening. *Materials Transactions* 2003; 44:1488-1493.
- [41] Todaka Y, Umemoto M, Tsuchiya K. Comparison of Nanocrystalline Surface Layer in Steels Formed by Air Blast and Ultrasonic Shot Peening. *Materials Transactions* 2004; 45:376-379.
- [42] Todaka Y, Umemoto M, Tanaka S, Tsuchiya K. Formation of Nanocrystalline Structure at the Surface of Drill Hole in Steel. *Materials Transactions* 2004; 45:2209-2213.
- [43] Tao NR, Sui ML, J.Lu, Lu K. Surface Nanocrystallization of Iron Induced by Ultrasonic Shot Peening. *NanoStructured Materials* 1999; 11:433-440.

- [44] Tao NR, Wang ZB, Tong WP *et al.* An investigation of surface nanocrystallization mechanism in Fe induced by surface mechanical attrition treatment. *Acta Materialia* 2002; 50:4603–4616.
- [45] Wang K, Tao NR, Liu G *et al.* Plastic strain-induced grain refinement at the nanometer scale in copper. *Acta Materialia* 2006; 54:5281–5291.
- [46] Prakash NA, Gnanamoorthy R, Kamaraj M. Surface nanocrystallization of aluminium alloy by controlled ball impact technique. *Surface & Coatings Technology* 2012; 210:78–89.
- [47] Zhou L, Liu G, Ma XL, Lu K. Strain-induced refinement in a steel with spheroidal cementite subjected to surface mechanical attrition treatment. *Acta Materialia* 2008; 56:78-87.
- [48] Lee WB, Cho KT, Kim KH *et al.* The effect of the cementite phase on the surface hardening of carbon steels by shot peening. *Materials Science and Engineering: A* 2010; 527:5852-5857.
- [49] Cho KT, Yoo S, Lim KM *et al.* Effect of Si content on surface hardening of Al–Si alloy by shot peening treatment. *Journal of Alloys and Compounds* 2011; 509:S265-S270.
- [50] Zhang HW, Hei ZK, Liu G *et al.* Formation of nanostructured surface layer on AISI 304 stainless steel by means of surface mechanical attrition treatment. *Acta Materialia* 2003; 51:1871–1881.
- [51] Dai K, Shaw L. Analysis of fatigue resistance improvements via surface severe plastic deformation. *International Journal of Fatigue* 2008; 30:1398-1408.
- [52] Liu XC, Zhang HW, Lu K. Strain-Induced Ultrahard and Ultrastable Nanolaminated Structure in Nickel. *Science* 2013; 342:337-340.
- [53] Wang ZB, Tao NR, Tong WP *et al.* Diffusion of chromium in nanocrystalline iron produced by means of surface mechanical attrition treatment. *Acta Materialia* 2003; 51:4319–4329.
- [54] Chang H-W, Kelly PM, Shi Y-N, Zhang M-X. Thermal stability of nanocrystallized surface produced by surface mechanical attrition treatment in aluminum alloys. *Surface & Coatings Technology* 2012; 206:3970–3980.
- [55] Hirsch T, Clarke TGR, Rocha AdS. An in-situ study of plasma nitriding. *Surface & Coatings Technology* 2007; 201:6380–6386.
- [56] Keddad M. Characterization of the nitrided layers of XC38 carbon steel obtained by R.F. plasma nitriding. *Applied Surface Science* 2008; 254:2276-2280.
- [57] Wang L, Ji S, Sun J. Effect of nitriding time on the nitrided layer of AISI 304 austenitic stainless steel. *Surface & Coatings Technology* 2006; 200:5067-5070.
- [58] Camps E, Muhl S, Romero S, Garcí'a JL. Microwave plasma nitrided austenitic AISI-304 stainless steel. *Surface and Coatings Technology* 1998; 106:121-128.
- [59] Wang L, Xu X, Yu Z, Hei Z. Low pressure plasma arc source ion nitriding of austenitic stainless steel. *Surface and Coatings Technology* 2000; 124:93-96.
- [60] Baranowska J, Kusior E, Amigo V, Szczeciński K. Surface modification of austenitic steel by low-temperature plasma. *Vacuum* 2005; 78:389-394.
- [61] Wang J, Zhang G, Sun J *et al.* Low temperature nitriding of iron by alternating current pretreatment. *Surface and Coatings Technology* 2006; 200:6666-6670.
- [62] Wang J, Zhang G, Sun J *et al.* Low temperature nitriding of medium carbon steel. *Vacuum* 2006; 80:855-859.
- [63] Asgari M, Barnoush A, Johnsen R, Hoel R. Microstructural characterization of pulsed plasma nitrided 316L stainless steel. *Materials Science and Engineering: A* 2011; 529:425-434.
- [64] Ferkel H, Glatzer M, Estrin Y, Valiev RZ. RF plasma nitriding of a severely deformed high alloyed steel. *Scripta Materialia* 2002; 46:623-628.
- [65] Tong WP, He CS, He JC *et al.* Strongly enhanced nitriding kinetics by means of grain refinement. *Applied Physics Letters* 2006; 89:021918.
- [66] Tong WP, Tao NR, Wang ZB *et al.* The formation of  $\epsilon$ -Fe<sub>3</sub>N phase in a nanocrystalline Fe. *Scripta Materialia* 2004;

50:647–650.

- [67] Tong WP, Liu CZ, Wang W *et al.* Gaseous nitriding of iron with a nanostructured surface layer. *Scripta Materialia* 2007; 57:533–536.
- [68] Tong WP, Han Z, Wang LM *et al.* Low-temperature nitriding of 38CrMoAl steel with a nanostructured surface layer induced by surface mechanical attrition treatment. *Surface & Coatings Technology* 2008; 202:4957–4963.
- [69] Li Y, Wang L, Zhang D, Shen L. The effect of surface nanocrystallization on plasma nitriding behaviour of AISI 4140 steel. *Applied Surface Science* 2010; 257:979-984.
- [70] Shen L, Wang L, Wang Y, Wang C. Plasma nitriding of AISI 304 austenitic stainless steel with pre-shot peening. *Surface & Coatings Technology* 2010; 204:3222–3227.
- [71] Panicaud B, Chemkhi M, Roos A, Reira D. Theoretical modelling of iron nitriding coupled with a nanocrystallisation treatment. Application to numerical predictions for ferritic stainless steels. *Applied Surface Science* 2012; 258:6611-6620.
- [72] Gu JF, Bei DH, Pan JS *et al.* Improved nitrogen transport in surface nanocrystallized low-carbon steels during gaseous nitridation. *Materials Letters* 2002; 55:340-343.
- [73] Tong WP, He CS, He JC, Zuo L. Strongly enhanced nitriding kinetics by means of grain refinement. *APPLIED PHYSICS LETTERS* 2006; 89:021918.
- [74] She D, Yue W, Fu Z *et al.* The effect of nitriding temperature on hardness and microstructure of die steel pre-treated by ultrasonic cold forging technology. *Materials & Design* 2013; 49:392-399.
- [75] Lu SD, Z.B.Wang, K.Lu. Enhanced chromizing kinetics of tool steel by means of surface mechanical attrition treatment. *Materials Science and Engineering A* 2010; 527:995–1002.
- [76] Xiang ZD, Datta PK. Shot peening effect on aluminate diffusion coating formation on alloy steels at low temperatures. *Scripta Materialia* 2006; 55:1151–1154.
- [77] Si X, Lu B, Wang Z. Aluminizing Low Carbon Steel at Lower Temperatures. *JOURNAL OF MATERIALS SCIENCE & TECHNOLOGY* 2009; 25:433-436.
- [78] Balusamy T, Narayanan TSNS, Ravichandran K. Effect of surface mechanical attrition treatment (SMAT) on boronizing of EN8 steel. *Surface & Coatings Technology* 2012; 213:221-228.
- [79] Amanov A, Cho IS, Pyoun YS *et al.* Micro-dimpled surface by ultrasonic nanocrystal surface modification and its tribological effects. *Wear* 2012; 286–287:136–144.
- [80] Amanov A, Penkov OV, Pyun Y-S, Kim D-E. Effects of ultrasonic nanocrystalline surface modification on the tribological properties of AZ91D magnesium alloy. *Tribology International* 2012; 54:106-113.
- [81] Yasuoka M, Wang P, Zhang K *et al.* Improvement of the fatigue strength of SUS304 austenite stainless steel using ultrasonic nanocrystal surface modification. *Surface and Coatings Technology* 2013; 218:93-98.
- [82] Zhou L, Liu G, Ma XL, Lu K. Strain-induced refinement in a steel with spheroidal cementite subjected to surface mechanical attrition treatment. *Acta Materialia* 2008; 56:78–87.
- [83] Dai K, Shaw L. Comparison between shot peening and surface nanocrystallization and hardening processes. *Materials Science and Engineering A* 2007; 463:46–53.
- [84] Wiggen PCV, Rozendaal HCF, Mittemeijer EJ. The nitriding behaviour of iron-chromium-carbon alloys. *Journal of Material Science* 1985; 20:4561-4582.
- [85] Hanlon T Y-NK, S. Suresh. Grain size effects on the fatigue response of nanocrystalline metals. *Scripta Materialia* 2003; 49:675-680.
- [86] H.Holzapfel, V.Schulze, O.Vohringer, E.Macherauch. Residual stress relaxation in an AISI 4140 steel due to quasistatic and cyclic loading at higher temperatures. *Materials Science and Engineering: A* 1998; 248:9-18.
- [87] Ranc N, Wagner D, Paris PC. Study of thermal effects associated with crack propagation during very high cycle fatigue tests. *Acta Materialia* 2008; 56:4012-4021.

- [88] Berg M, Budtz-Jørgensen CV, Reitz H *et al.* On plasma nitriding of steels. *Surface and Coatings Technology* 2000; 124:25-31.
- [89] Zhang JW, Lu LT, Shiozawa K *et al.* Effects of nitrocarburizing on fatigue property of medium carbon steel in very high cycle regime. *Materials Science and Engineering A* 2011; 528:7060–7067.

# Acknowledgement

During the past years of my Ph.D study, I was lucky to receive a lot of help and cooperate with such excellent colleagues. Here, I would like to take this opportunity to thank all of the people who have supported me and helped me.

First of all, I would like to express my appreciation to my supervisors Prof. Dr. Ri-ichi Murakami from the University of Tokushima and Prof. Dr. Jianxun Zhang from Xi'an Jiaotong University. With their support, encouragement, and guidance, I could take part in the Double Degree Program between the University of Tokushima and Xi'an Jiaotong University. It provides a good chance for me to study abroad and offers a financial support for my study. Also I would like thank Prof. Dr. Linjie Zhang and lecturer Kazuya Kusaka for the guidance of XRD experiments.

Secondly, I would like to thank Dr. Pangpang Wang, Dr. Dongyan Zhang, and Dr. Xiaojian Cao for their guidance in experiment and helpful suggestion in writing papers.

Thirdly, thanks all the members in CICEE, Dr. Pankaj Koinka, Dr. Walter Carpenter, and Asada San.

Then, I would like to thank my Japanese teacher, Nayoko Kohno and her husband Kiyoshi Kohno. Thanks for a truly enjoyable experience in Japan. Thanks to my friends: Dr. Xiaojing Yu, Dr. Chuncai Kong, Dr. Jingxiang Li, Dr. Junhang Guo, Mr. Kaiyue Zhang, Mr. Fan Yang, Mr. Yongjie Xu and Ms. Yuexia Sun.

Finally, I wish to express my deepest appreciation to my family for their support and encouragement. Especially, thanks my wife for her love and accompanying.

# Publications

## Journals

1. Bo Wu, Pangpang Wang, Young-Shik Pyoun, Jianxun Zhang, and Ri-ichi Murakami, Effect of ultrasonic nanocrystal surface modification on the fatigue behaviors of plasma-nitrided S45C steel. *Surface & Coatings Technology*, 2012, 213: 271–277.
2. Bo Wu, Pangpang Wang, Young-Shik Pyoun, Jianxun Zhang, and Ri-ichi Murakami, Study on the fatigue properties of plasma nitriding S45C with a pre-ultrasonic nanocrystal surface modification process, *Surface & Coatings Technology*, 2013, 216: 191–198.

## International Conferences

1. Bo Wu, Jianxun Zhang, Ri-ichi Murakami, An investigation of fatigue properties of pre-quenched-tempered S34C steel with plasma nitriding treatment, *International Journal of Modern Physics: Conference Series* vol. 6, pp. 233-238, 2012. (oral)
2. Bo Wu, Jianxun Zhang, Young-Shik Pyoun, Ri-ichi Murakami, Effect of Ultrasonic Nanocrystal Surface Modification to the Fatigue Properties of S45C with Different Surface Hardness, 13th International Conference on Fracture, June 16–21, 2013, Beijing, China. (oral)